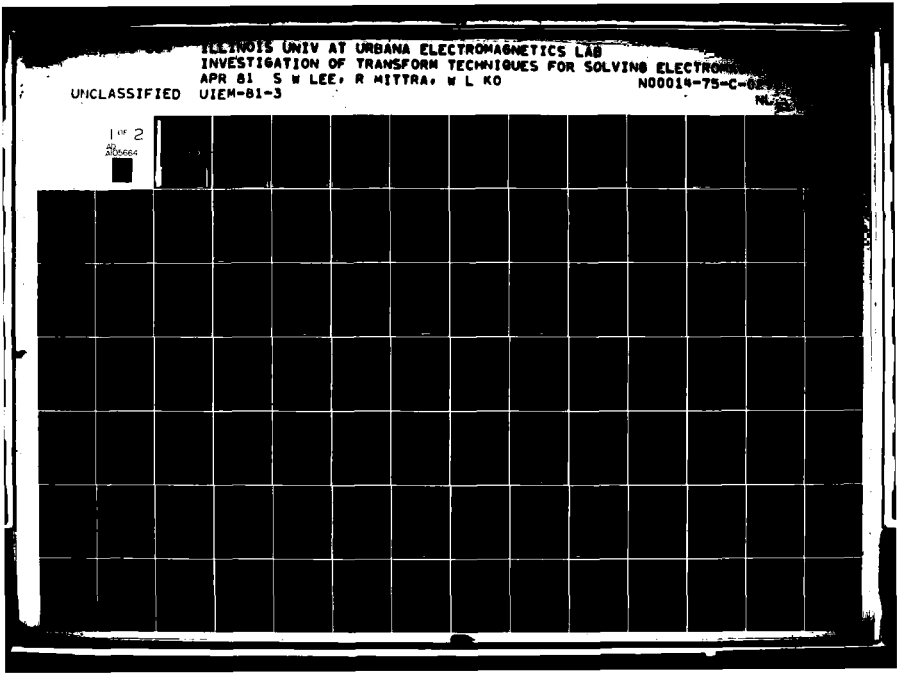
ILLINOIS UNIV AT URBANA ELECTROMAGNETICS LAB
INVESTIGATION OF TRANSFORM TECHNIQUES FOR SOLVING ELECTRO
APR 81 S W LEE, R MITTRA, W L KO
N00014-75-C-0
UNCLASSIFIED UIEM-81-3
NL
1 OF 2
AD A105664

ELECTROMAGNETICS LABORATORY
TECHNICAL REPORT NO. 81-3

April 1981

LEVEL II

(2)

Accession

INVESTIGATION OF TRANSFORM TECHNIQUES FOR SOLVING ELECTROMAGNETIC RADIATION AND SCATTERING PROBLEMS

Final Report

S. W. Lee
R. Mittra
W. L. Ko

ELECTROMAGNETICS LABORATORY
DEPARTMENT OF ELECTRICAL ENGINEERING
ENGINEERING EXPERIMENT STATION
UNIVERSITY OF ILLINOIS AT URBANA-CHAMPAIGN
URBANA, ILLINOIS 61801

SUPPORTED BY
CONTRACT NO. N00014-75-C-0293
OFFICE OF NAVAL RESEARCH
DEPARTMENT OF THE NAVY
ARLINGTON, VIRGINIA 22217

(14 UILU-ENG-81-2544
UILU-ENG-81-2544

UNCLASSIFIED
SECURITY CLASSIFICATION OF THIS PAGE (When Data Entered)

REPORT DOCUMENTATION PAGE	READ INSTRUCTIONS BEFORE COMPLETING FORM
1. REPORT NUMBER (6) 2. GOVT ACCESSION NO. AD-A105664	3. RECIPIENT'S CATALOG NUMBER (9)
4. TITLE (and Subtitle) INVESTIGATION OF TRANSFORM TECHNIQUES FOR SOLVING ELECTROMAGNETIC RADIATION AND SCATTERING PROBLEMS.	5. TYPE OF REPORT & PERIOD COVERED FINAL REPORT, 1 Mar 79 - 31 Dec 80
	6. PERFORMING ORG. REPORT NUMBER EM 81-3; UILU-ENG-81-2544
7. AUTHOR(s) S. W. Lee, R. Mittra, W. L. Ko (15)	8. CONTRACT OR GRANT NUMBER(s) N00014-75-C-0293
9. PERFORMING ORGANIZATION NAME AND ADDRESS Electromagnetics Laboratory Department of Electrical Engineering University of Illinois, Urbana, IL 61801	10. PROGRAM ELEMENT, PROJECT, TASK AREA & WORK UNIT NUMBERS Project No. N.A.
11. CONTROLLING OFFICE NAME AND ADDRESS (11) Office of Naval Research Department of the Navy Arlington, Virginia 22217	12. REPORT DATE Apr 81 13. NUMBER OF PAGES 130
14. MONITORING AGENCY NAME & ADDRESS (if different from Controlling Office) (12) 131	15. SECURITY CLASS. (of this report) UNCLASSIFIED 15a. DECLASSIFICATION DOWNGRADING SCHEDULE

16. DISTRIBUTION STATEMENT (of this Report)

Distribution Unlimited. Reproduction in whole or in part is permitted for any purpose of the United States Government.

17. DISTRIBUTION STATEMENT (of the abstract entered in Block 20, if different from Report)

18. SUPPLEMENTARY NOTES

19. KEY WORDS (Continue on reverse side if necessary and identify by block number)

Spectral domain techniques; fast Fourier transform; frequency selectric surfaces; leaky-wave antennas; radar scattering

20. ABSTRACT (Continue on reverse side if necessary and identify by block number)

In this report we summarize the research performed under the ONR Grant N00014-75-C-0293 during the calendar years 1979 and 1980. We describe a number of electromagnetic scattering problems which we have solved using the spectral domain methods. Among these are the frequency selective surfaces, leaky-wave antennas on dielectric waveguides and arbitrarily shaped conducting or dielectric scatterers.

DD FORM 1 JAN 73 1473 EDITION OF 1 NOV 65 IS OBSOLETE UNCLASSIFIED
SECURITY CLASSIFICATION OF THIS PAGE (When Data Entered)

408102

UILU-ENG-81-2544

Electromagnetics Laboratory Report No. 81-3

INVESTIGATION OF TRANSFORM TECHNIQUES FOR SOLVING ELECTROMAGNETIC RADIATION AND SCATTERING PROBLEMS

Final Report

S. W. Lee
R. Mittra
W. L. Ko

April 1981

Office of Naval Research
Department of the Navy
Arlington, Virginia 22217

Contract No. N00014-75-C-0293

Electromagnetics Laboratory
Department of Electrical Engineering
Engineering Experiment Station
University of Illinois at Urbana-Champaign
Urbana, Illinois 61801

ABSTRACT

In this report we summarize the research performed under the ONR Grant N00014-75-C-0293 during the calendar years 1979 and 1980. We describe a number of electromagnetic scattering problems which we have solved using the spectral domain methods. Among these are the frequency selective surfaces, leaky-wave antennas on dielectric waveguides and arbitrarily shaped conducting or dielectric scatterers.

TABLE OF CONTENTS

I. INTRODUCTION

This research effort was to develop new approaches to solving electromagnetic and acoustic scattering problems in frequency regimes and for geometrical configurations, for which the conventional numerical or asymptotic techniques are found to be inadequate, inefficient and/or inaccurate. Rather than employ either the matrix methods or the ray techniques, which are typically valid in the low- and high-frequency regimes respectively, we investigate the application of the FFT algorithm in the spectral or transform domain. Two different variations of the method have been studied. The first of these employed asymptotic solutions, such as those based on the Physical Optics or GTD methods, as initial approximations for an iterative procedure for constructing the solution to the scattering problem. The second version of the spectral technique utilized the variational principle and developed a procedure called the spectral-Galerkin method. The end result of the application of the latter method is a matrix equation for the coefficients of the expansion functions used to represent the unknown field. Typically, the size of this matrix is much smaller than the one obtained via conventional procedures. Our objectives were to investigate these spectral domain techniques in great detail and to evaluate the scope and limitations of the two approaches.

II. SUMMARY OF TECHNICAL ACCOMPLISHMENTS

During the last grant period, we have carried out an extensive investigation of the spectral-Galerkin and spectral iteration techniques and have applied them to the problem of analyzing a number of electromagnetic radiation and scattering problems. We have applied the spectral approach to the problem of scattering by frequency selective surfaces (FSS) which find widespread use in radomes, reflector antennas, and optical filters. The spectral iteration technique has been found useful in the low and intermediate frequency ranges where the cell size or the period of the FSS, which comprises a screen with periodic perforations, is on the order of two wavelengths or less. Beyond this limit, the spectral-iteration technique is more efficient as it avoids matrix inversion altogether and derives the solution to the integral equation using an iterative procedure. Using these two methods, we have successfully analyzed several different versions of FSS and have compared the results with theoretical and experimental data published elsewhere. The results derived with the spectral approach have not only been found to be accurate and efficient, but are also applicable in a frequency range which is considerably wider than that of the conventional method.

The spectral iteration approach has also been found useful for analyzing other stuctures, such as conducting and dielectric scatterers of arbitrary shape. To-date, only a preliminary investigation of this problem has been carried out but the results appear to be quite encouraging. An invited paper describing the spectral technique was recently presented at the Method of Moments Workshop held in St. Cloud, Florida, under the auspices of Rome Air Development Center. A paper describing this

presentation is appended herewith (Appendix I). Other manuscripts accepted for journal publication and describing the work carried out with partial support from this grant are also attached.

APPENDIX A

SOLVING ELECTROMAGNETIC SCATTERING PROBLEMS WITHOUT MATRIX INVERSION

R. Mittra, C. H. Tsao and R. Kastner
Electromagnetics Laboratory
University of Illinois
Urbana, IL 61801

Abstract - The applications of the Moment Method a la Harrington to the solution of electromagnetic scattering and radiation problems are well known, and the method has revolutionized the way boundary-value problems are being solved today on modern computers. However, as the frequency becomes higher and the body size becomes comparable to the wavelength of the incident field, the CPU time on the computer becomes large and the storage requirements also become large - if not prohibitive. It is therefore useful to look for alternative approaches to the moment method for attacking the radiation and scattering problems in the so-called resonance region and above.

In this paper, we introduce an iterative technique in the spectral domain which circumvents the limitations of the moment method alluded to above. The method is computationally efficient because it makes extensive use of the FFT algorithm to perform the Fourier transformation, which is an integral part of the spectral domain approach. The procedure also has the unique feature that it has built-in convergence and accuracy checks, features which are not typically found in other methods. The paper illustrates the application of the spectral-iteration technique using scattering from periodic structures and arbitrary bodies as examples.

The work was supported by the Office of Naval Research, Contract N00014-75-C-0293.

I. INTRODUCTION

The purpose of this paper is to describe an approach called the spectral-iteration technique for solving electromagnetic scattering problems without the need for matrix inversion. The method is especially suited in the high frequency range where the dimensions of structure are large compared to the wavelength. If the moment method were applied in this range, the matrix size that would be required to handle such structures would be large, and the matrix inversion time as well as the storage cost would be prohibitive. Also, there are geometries such as grating structures which we will be discussing shortly, for which no asymptotic solutions are available because the ray solutions based on GTD, or physical optics approximations, are entirely inadequate.

Although the spectral-iteration technique has recently been applied to a wide class of problems,* for the sake of illustrating the principles of the method we will use the example of periodic structures such as arrays of conducting strips or periodically perforated screens which can be either free-standing or printed on dielectric substrates (see Figure 1). These gratings have frequency selective properties, and find many applications as artificial dielectrics, optical and quasi-optical devices, and dichroic surfaces for antenna reflectors and radomes.

Conventionally, the problem of electromagnetic scattering from these periodic structures is attacked using the mode-matching procedure employed in conjunction with the method of moments. A description of this procedure can be found in a number of papers on the subject by Chen [1], Lee [2], and McPhedran and Maystre [3]. Though this method works quite well in the low-frequency region, it becomes prohibitively costly if not impractical at the high frequency region where the aperture size is one to two wavelengths, or larger, because

*For a bibliography on Spectral Domain Methods refer to the Appendix.

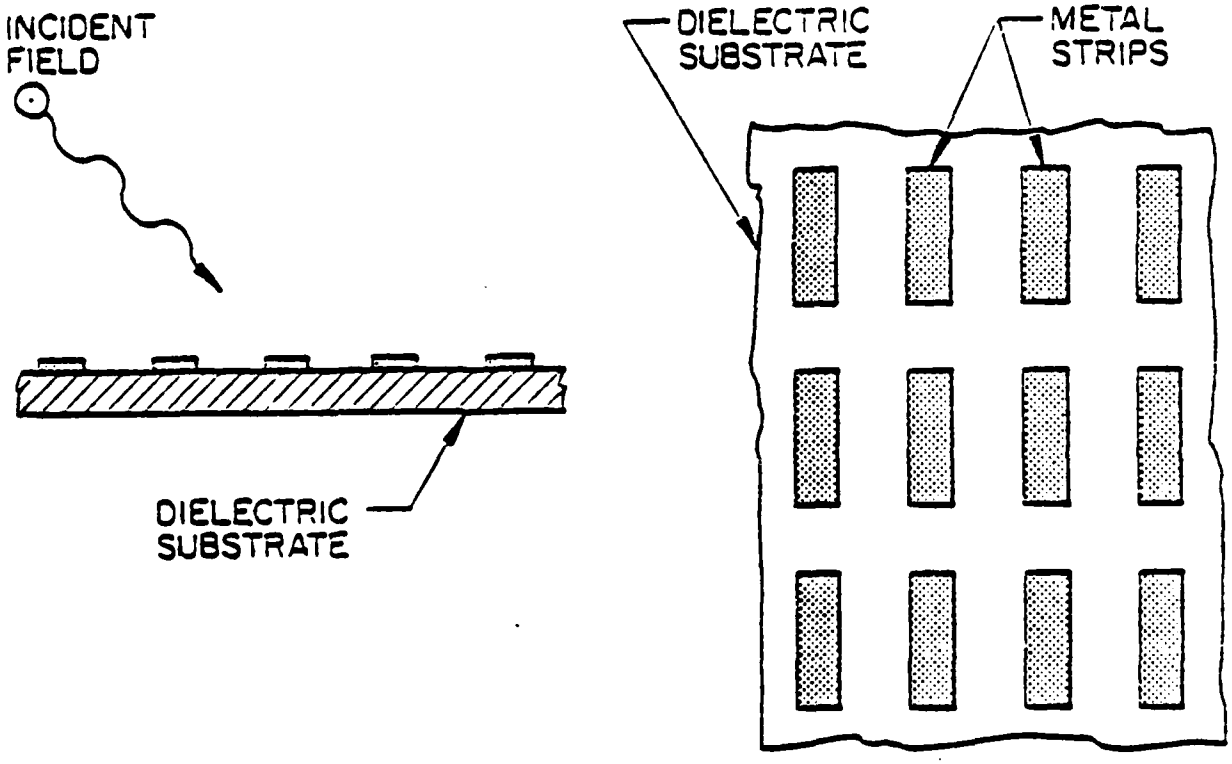

(a) Side view

(b) Top view

Figure 1. Frequency selective surface.

the matrix size required for an accurate solution becomes prohibitively large and the numerical computation becomes extremely time-consuming and costly. As mentioned earlier, the high frequency techniques, e.g., GTD, cannot be applied to circumvent the above difficulty either, because the complex geometrical configuration of the structure does not lend itself to the ray formalism of GTD. In this paper we introduce a new technique based on the spectral domain approach which provides an efficient and accurate solution to the grating problems described in this paper.

As a first step, the new approach begins with the formulation of the problem in terms of an integral equation in the transform domain. The standard procedure for deriving the integral equation for the unknown aperture field (or the induced current) is still followed; however, in the transform domain the convolution form of the integral equation becomes an algebraic one. Furthermore, because of the periodic nature of the structure, the transform naturally takes the form of DFT (discrete Fourier transform) which can, in turn, be efficiently evaluated using the FFT (fast Fourier transform) algorithm. The transformed integral equation is subsequently solved, using an iterative procedure, simultaneously for the aperture field and the induced current. It is evident that the method avoids the time-consuming steps of evaluating the matrix elements and their subsequent inversion. More importantly, the problem of storing and handling over-sized matrices is circumvented even at high frequencies, where the number of unknowns can exceed the figure 2000. An added feature of the method is that a built-in step in the iterative procedure provides a convenient measure for the boundary condition check, a feature not readily available in conventional

problem. The above authors have used the GTD solution as the zeroth order approximate solution and have also employed an iterative procedure to generate the final solution. However, to-date this procedure has not been applied to the grating problems being considered in this paper.

In the next section, we present the formulation of the periodic grating problem. In section III, we describe the iterative procedure. In section IV we illustrate the application of the technique to a number of practical geometries. Finally, we demonstrate in section V that the approach is useful for a class of closed-region problems, e.g., waveguide discontinuities. A brief summary of the paper is included in section VI and some conclusions are presented.

II. FORMULATION

For the sake of illustrating the spectral approach, we consider the problem of a uniform plane wave scattered from a free-standing periodically perforated conducting screen shown in Figure 2. However, the method of solution is easily and conveniently extendable to the case of a screen on a dielectric substrate.

Due to the periodicity of the structure, the electric field on either side of the screen can be expanded in terms of the Floquet space harmonics. Using the $e^{j\omega t}$ time convention (suppressed), we can write

$$\begin{bmatrix} E_x \\ E_y \end{bmatrix} = \begin{bmatrix} E_x^i \\ E_y^i \end{bmatrix} + \sum_{m=-\infty}^{\infty} \sum_{n=-\infty}^{\infty} \begin{bmatrix} X_{mn}^+ \\ Y_{mn}^+ \end{bmatrix} \psi_{mn} e^{\gamma_{mn} z} \quad \text{for } z > 0$$

and (1)

$$\begin{bmatrix} E_x \\ E_y \end{bmatrix} = \sum_{m=-\infty}^{\infty} \sum_{n=-\infty}^{\infty} \begin{bmatrix} X_{mn}^- \\ Y_{mn}^- \end{bmatrix} \psi_{mn} e^{-\gamma_{mn} z} \quad \text{for } z < 0$$

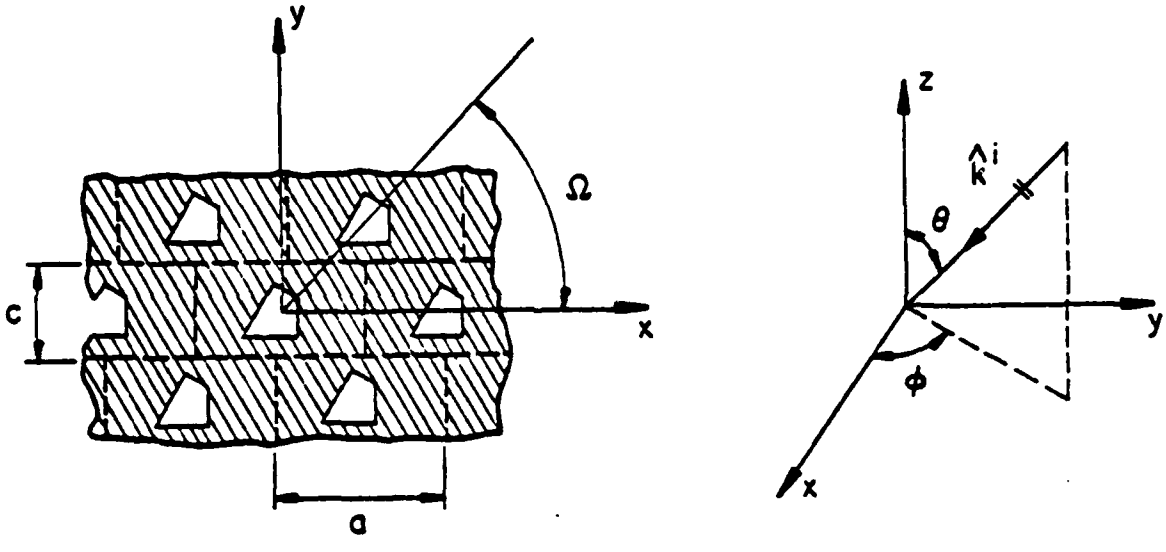

Figure 2. Free-standing, periodically perforated screen illuminated by a plane wave propagating in $\hat{k}_i$ direction.

where $\bar{E}^i$ represents the incident field, (X^+_{mn}, Y^+_{mn}) and (X^-_{mn}, Y^-_{mn}) are the reflection and the transmission coefficients of the Floquet's harmonic modes, respectively and ψ_{mn}'s stand for the Floquet mode functions, given by

$$\psi_{mn} = \exp[j(u_{mo}x + v_{mn}y)]$$

where

$$u_{mo} = \frac{2\pi m}{a} - k \sin\theta \cos\phi$$

$$m,n = 0,\pm1,\pm2,\ldots$$

$$v_{mn} = \frac{2\pi n}{c} - \frac{2\pi m}{a} \cot\Omega - k \sin\theta \sin\phi$$

and

$$\gamma_{mn} = \begin{cases} -j[k^2 - (u^2_{mo} + v^2_{mn})]^{1/2} & \text{if } k^2 > (u^2_{mo} + v^2_{mn}) \\ -[(u^2_{mo} + v^2_{mn}) - k^2]^{1/2} & \text{if } k^2 < (u^2_{mo} + v^2_{mo}) \end{cases}$$

The z-component of the E-field can be derived from (1) using the divergence theorem.

Enforcing the condition that the tangential field is continuous across the interface, we obtain

$$X^+_{mn} = X^-_{mn}\,, \quad Y^+_{mn} = Y^-_{mn} \quad \text{when } m \neq 0 \text{ or } n \neq 0$$

and

$$X^+_{oo} + E^i_x = X^-_{oo}\,, \quad Y^+_{oo} + E^i_y = Y^-_{oo}$$

The H-field in the region $z > 0$ and $z < 0$ can be derived from (1). Evaluating the H-field at $z = 0^-$ and $z = 0^+$, subtracting the expression for one from the other, and making use of the requirement that the tangential components be continuous across the aperture, one arrives at the equation:

$$\frac{1}{-j\omega\mu}\sum_{m=-\infty}^{\infty}\sum_{n=-\infty}^{\infty}\begin{bmatrix} A_{mn} & B_{mn} \\ C_{mn} & -A_{mn} \end{bmatrix}\begin{bmatrix} X_{mn}^{-} \\ Y_{mn}^{-} \end{bmatrix}\psi_{mn} = \begin{bmatrix} -H_x^i + \hat{\theta}[\frac{1}{2} J_y] \\ -H_y^i + \hat{\theta}[\frac{1}{-2} J_x] \end{bmatrix} \text{ for } z = 0 \qquad (2)$$

ere $\bar{H}^i$ is the incident H-field,

$\bar{J}$ is the induced current on the surface,

$A_{mn} = u_{mo} \cdot v_{mn}/\gamma_{mn}$,

$B_{mn} = v_{mn}^2/\gamma_{mn} - \gamma_{mn}$,

$C_{mn} = \gamma_{mn} - u_{mo}^2/\gamma_{mn}$.

In (2) we have used the notation that for a function $f(\bar{r})$ defined on the $z = 0$ plane, where $\bar{r}$ is the position vector on that plane, the truncation operator θ is defined by

$$\theta(f(\bar{r})) = f(\bar{r}) \quad \text{for } \bar{r} \text{ on the conducting surface}$$

$$= 0 \quad \text{for } \bar{r} \text{ in the aperture}$$

and

$$\hat{\theta}(f(\bar{r})) = f(\bar{r}) - (f(\bar{r}))$$

The obvious identity $\hat{\theta}(\bar{J}) = \bar{J}$ and that $\hat{z} \times [\bar{H}(z = 0^+) - \bar{H}(z = 0^-)] = \bar{J}$ have also been used in deriving (2).

Unlike the integro-differential equation in the conventional method, which applies only in the aperture (or strip) region, (2) is valid over the entire surface. The price paid for extending the equation to the full range is the introduction of an extra unknown $\bar{J}$. However, as we will soon see, the additional unknown $\bar{J}$ can be solved for along with the aperture field using the iterative procedure discussed in the next section.

III. ITERATIVE PROCEDURE

The summation involved in (1) and (2) can be readily identified as the DFT operation. Let F be the operator representing the DFT, and let $\bar{E}_t$

represent the tangential electric field in the transformed domain. Identifying $(\bar{X}_{mn}, \bar{Y}_{mn})$ in (2) as the Fourier coefficients $\tilde{\bar{E}}_t$, and writing $\tilde{G}$ for the matrix

$$\begin{bmatrix} A_{mn} & B_{mn} \\ C_{mn} & -A_{mn} \end{bmatrix}$$

we can write (2) symbolically as

$$F(\tilde{G} \cdot \tilde{\bar{E}}_t) = -\tilde{\bar{H}}_t^i + \hat{\theta}(\bar{J}) \tag{3}$$

where the subscript t indicates the tangential components, and it is understood that all the quantities are evaluated at $z = 0$.

If the induced current were available, the solution for $\bar{E}_t$ could be immediately obtained by invoking (3) and by using

$$\tilde{\bar{E}}_t = \tilde{G}^{-1}(F^{-1}(-\tilde{\bar{H}}_t^i + \hat{\theta}(\bar{J}))) \tag{4}$$

In practice, however, $\bar{J}$ is the unknown to be solved for, together with $\bar{E}_t$ and hence (4) cannot be used directly. Instead of using (4), a recursive relation between the (n+1)th approximate solution $\tilde{\bar{E}}_t^{(n+1)}$ and the nth approximation $\tilde{\bar{E}}_t^{(n)}$ is now derived and the two unknowns $\bar{E}_t$ and $\bar{J}$ are solved for simultaneously using an iterative procedure.

To derive the recursion formula for $\tilde{\bar{E}}_t^{(n)}$, we begin with (3), which relates $\bar{J}^{(n)}$ and $\bar{E}^{(n)}$, and write

$$\hat{\theta}(\bar{J}^{(n)}) = F(\tilde{G} \cdot \tilde{\bar{E}}_t^{(n)}) + \tilde{\bar{H}}_t^i \tag{5}$$

Substituting (5) into (4), one obtains

$$\tilde{\bar{E}}_t^{(n+1)} = \tilde{G}^{-1}(F^{-1}(-\tilde{\bar{H}}_t^i + \hat{\theta}(F(\tilde{G} \cdot \tilde{\bar{E}}_t^{(n)}) + \tilde{\bar{H}}_t^i))) \tag{6}$$

Equation (6) is the desired recursive formula. Before inserting $\tilde{\bar{E}}_t^{(n)}$ into (5), we adjust its amplitude by multiplying with a scale

factor K, computed according to the variation expression

$$K = \frac{\langle \bar{E}_t^{(n)}, -\bar{H}_t^i \rangle}{\langle \bar{E}_t^{(n)}, F(\tilde{G} \cdot \tilde{\bar{E}}_t^{(n)}) \rangle} \tag{7}$$

where $\langle f, g \rangle = \int_{\text{aperture}} f \cdot g \cdot da$.

Equation (7) is obtained by applying the one-term Galerkin's method to (3) using $\bar{E}_t^{(n)}$ as the testing function. It is apparent that K = 1 when $\bar{E}_t^{(n)}$ is the exact solution. K, therefore, also provides an indication of the accuracy of the nth iterated result in a weighted-average sense.

In the following we proceed to outline an iterative procedure for solving (6):

1. Begin with an initial estimate $\bar{E}_t^{(0)}$. The amplitude of $\bar{E}_t^{(0)}$ is to be properly adjusted using the scale factor K determined from (7).
2. Compute $\tilde{\bar{E}}_t^{(0)}$, the discrete Fourier transform of $\bar{E}_t^{(0)}$. This step can be carried out efficiently using the FFT algorithm.
3. Compute $\tilde{G} \cdot \tilde{\bar{E}}_t^{(0)}$.
4. Obtain the DFT of $\tilde{G} \cdot \tilde{\bar{E}}_t^{(0)}$ using FFT.
5. Subtract $-\bar{H}_t^i$ from the result obtained from step 4. This gives the zeroth-order approximate solution $\bar{J}^{(0)}$. Generally, the approximate solution for $\bar{J}$ obtained in this step has non-zero values extending beyond the conducting surface. The satisfaction of the boundary condition for the induced current can thus be verified by checking how well the nth approximation for the current $\bar{J}^{(n)}$ is confined to the conducting surface.
6. Add $-\bar{H}_t^i$ to $\bar{J}^{(0)}$ obtained in the last step, and take the inverse DFT of the result using FFT.

7. Multiply $\tilde{G}^{-1}$ by the result obtained from step 6, obtaining $\tilde{\bar{E}}_t^{(1)}$
8. Take the inverse transform of $\tilde{\bar{E}}_t^{(1)}$ to get $\bar{E}_t^{(1)}$. The exact solution for $\bar{E}_t$ should have zero value on the conducting surface. This criterion serves as a boundary condition check for the approximate solution $\bar{E}_t^{(n)}$ obtained in this step.
9. Repeat the whole procedure, as necessary, using $\theta(\bar{E}_t^{(1)})$ to generate the next higher-order solutions $\bar{J}^{(1)}$ and $\bar{E}_t^{(2)}$ until convergence is achieved.

In the following two sections several examples are presented to illustrate the application of the technique described above.

IV. SCATTERING FROM GRATINGS AND GRIDS

Let us consider a free-standing, strip grating structure illuminated by a normally incident uniform plane wave as shown in Figure 3. Let the incident E-field be polarized parallel to the edges of the strip (an H-wave).

The formulation for this problem is given by (2). The iterative procedure discussed in section III is applied to solve for the tangential aperture E-field, $\bar{E}_t$, and the induced current density, $\bar{J}$.

Figure 4a shows the incident E-field truncated in the aperture, which is used as the zeroth-order approximation for $\bar{E}_t$, i.e., $\bar{E}_t^{(0)} = \theta(\bar{E}_t^i)$. The $\bar{J}^{(0)}$ derived from $\bar{E}_t^{(0)}$ is shown in Figure 5a. $\bar{J}^{(0)}$ has significant non-zero values extending into the aperture region. This could be expected because of the crude initial estimate made for $\bar{E}_t^{(0)}$. Figure 5b shows $\bar{J}^{(1)}$ obtained after one iteration. Observe the significant improvement achieved with just a single iteration even though the zeroth-order approximation for $\bar{E}_t^{(0)}$ was rather crude. Higher-order solutions for $\bar{E}_t^{(n)}$ and $\bar{J}^{(n)}$, obtained via further iterations, are shown, respectively, in Figures 4b to 4d and Figures 5b to 5d. The

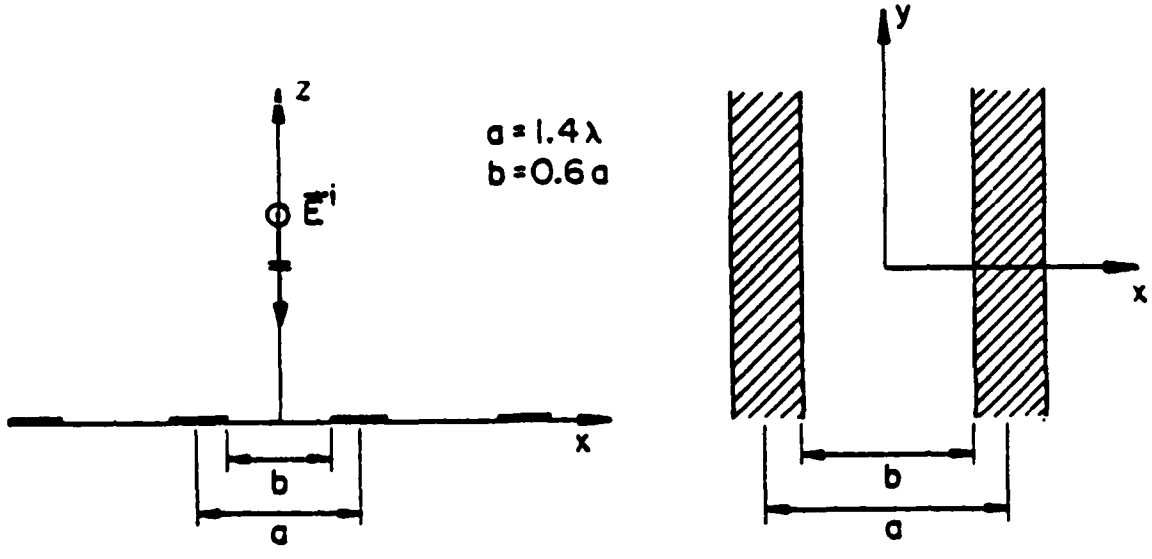

Figure 3. Free-standing grating illuminated by a normally incident H-wave.

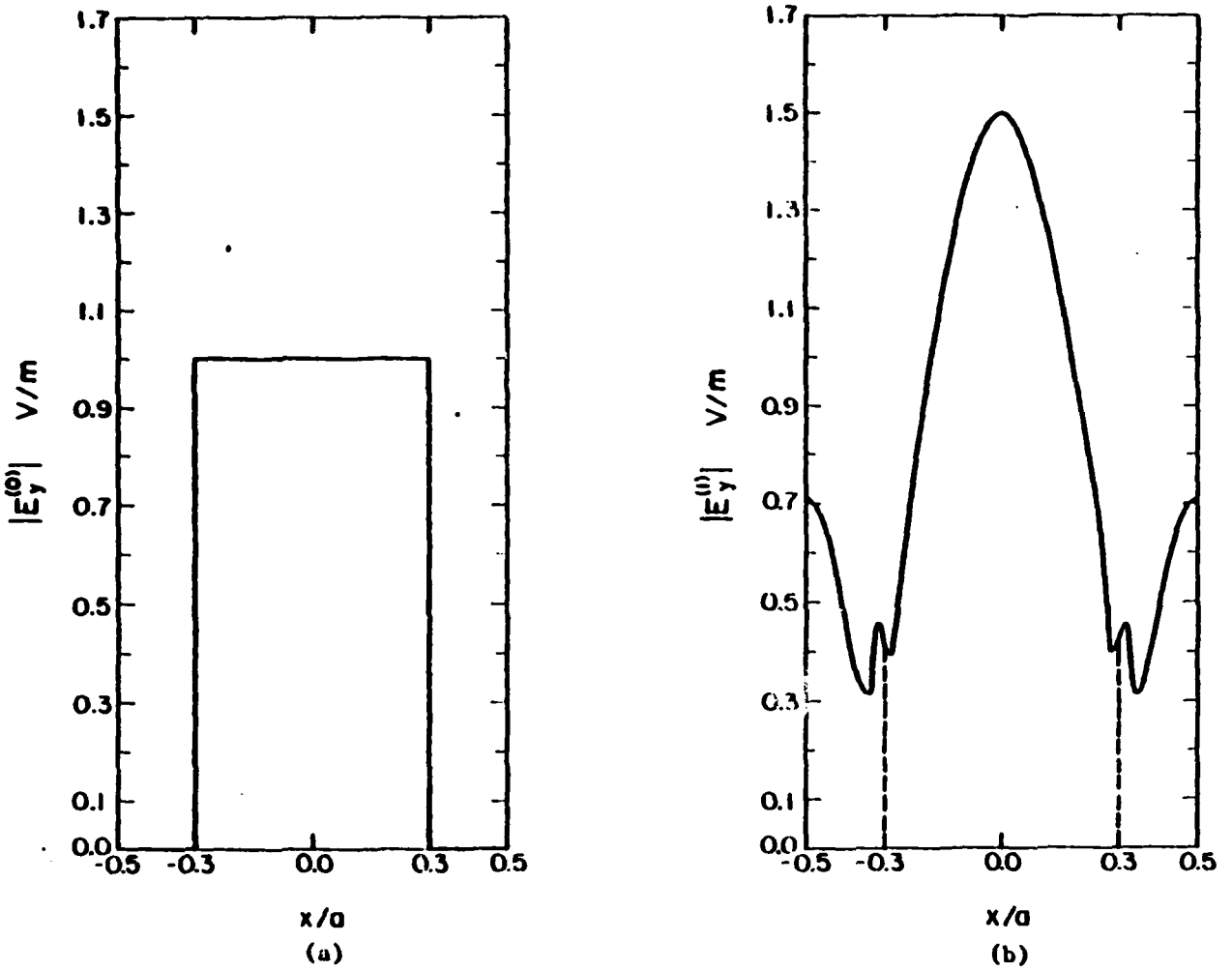

Figure 4. Magnitude of the aperture E-field distribution for the geometry shown in Figure 3, obtained via four consecutive iterations.

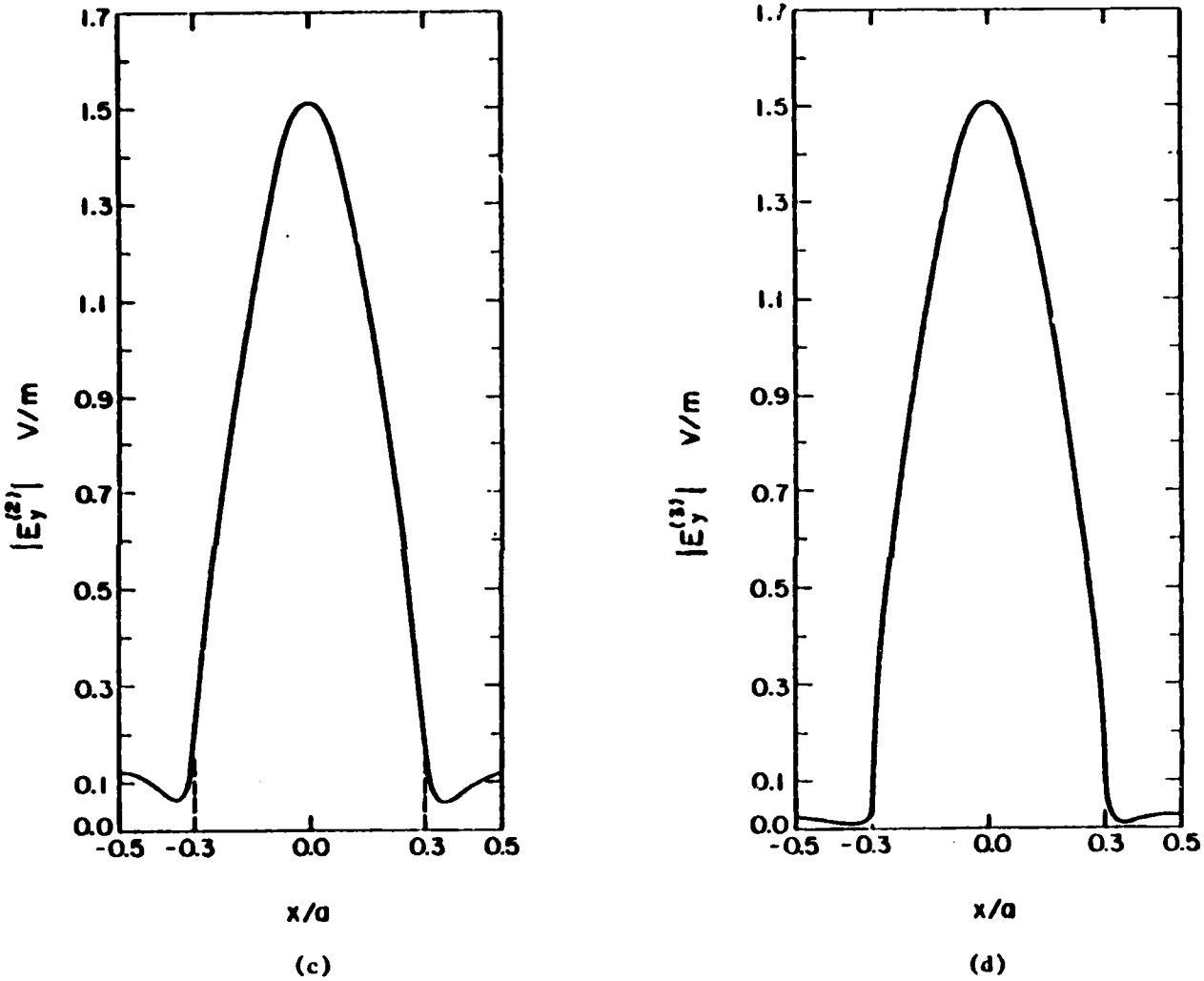

Figure 4. Magnitude of the aperture E-field distribution for the geometry shown in Figure 3, obtained via four consecutive iterations.

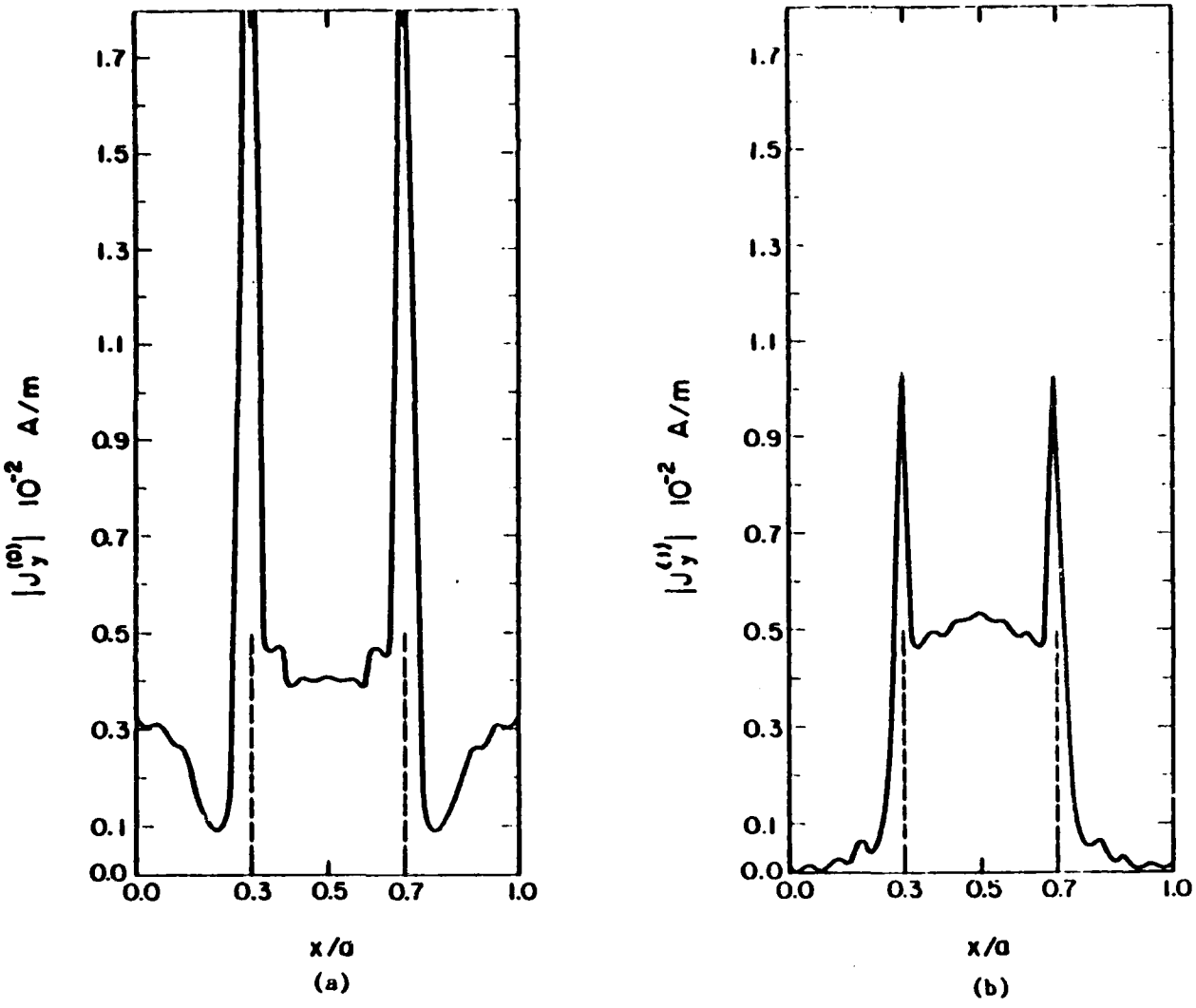

Figure 5. Magnitude of the induced current density distribution on the strip for the geometry in Figure 3, obtained via four consecutive iterations.

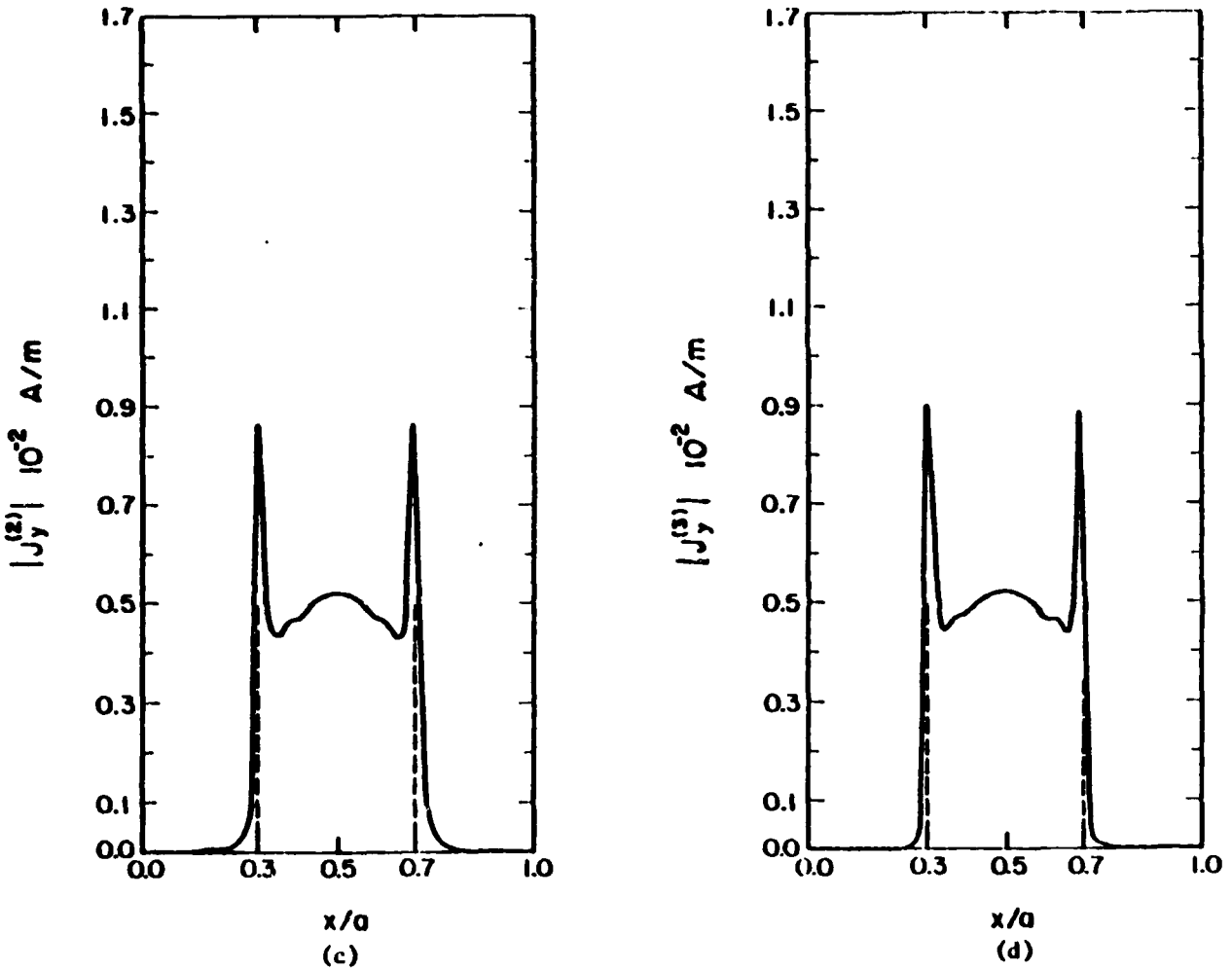

Figure 5. Magnitude of the induced current density distribution on the strip for the geometry in Figure 3, obtained via four consecutive iterations.

rapid convergence and the accuracy, which is verified by the boundary condition check of the solutions, are well-demonstrated in these figures. The induced current density $\bar{J}$ also shows the expected edge behavior, i.e., it becomes large at the edges as it should for the incident H-wave.

Figures 6 and 7 show the solutions for $\bar{E}_t$ and $\bar{J}$ obtained after four iterations when the gratings are illuminated by an obliquely incident plane wave with an incident angle $\theta = 30°$ and with the H-field polarized parallel to the edges of the strip (in the E-wave case). Again, the boundary conditions are satisfied extremely well by the results, and the aperture E-field also shows the expected edge behavior for the incident E-wave.

Next we consider the scattering from a free-standing conducting grid illuminated by a normally incident plane wave. The geometry of the problem is shown in Figure 8. The aperture area is approximately $10\lambda^2$ whereas the cell area is about $44\lambda^2$. The initial approximation for $\bar{E}_t$ is still chosen to be the truncated incident field, and the dominant component of the tangential aperture E-field is shown when the incident E-field is polarized in the y-direction.

For all the computations in this section, 32 terms in the Floquet expansion functions are used in representing the unknown fields along each of the two dimensions. This leads to 2^{11} equivalent unknowns to be solved for. The computation time, however, required for deriving the solution is quite moderate (5 ~ 6 secs. of CPU time on the CDC Cyber 175 System). Clearly, any matrix method dealing with such a large number of unknowns will be totally impractical.

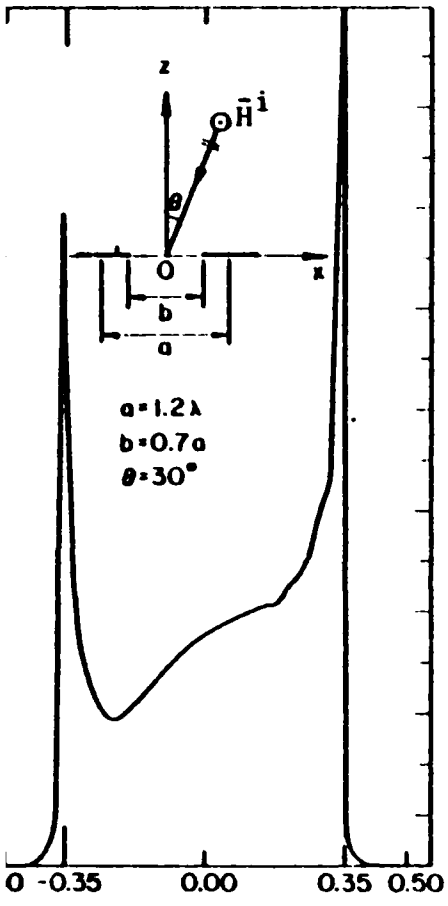

Magnitude of the aperture E-field distribution for a free-standing grating illuminated by an obliquely incident E-wave.

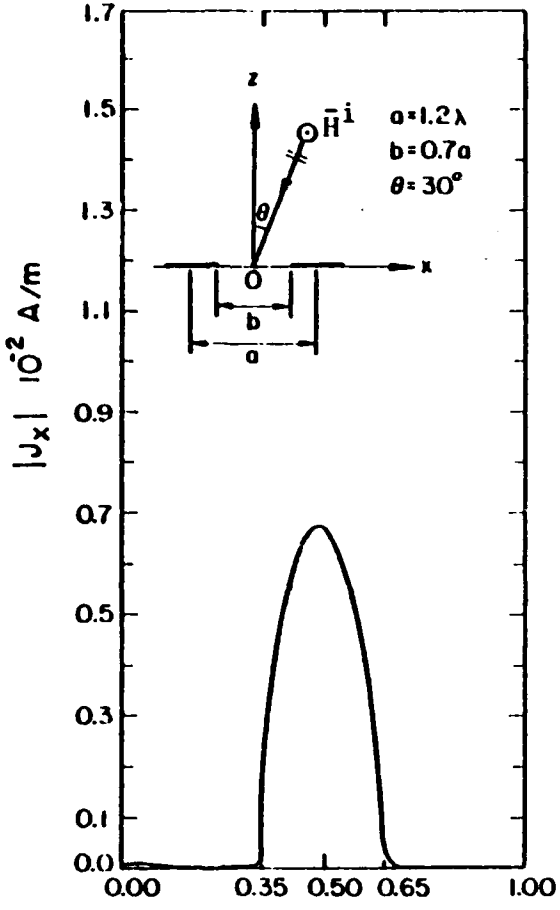

Figure 7. Magnitude of the induced current density distribution on the strips of a free-standing grating illuminated by an obliquely incident E-wave.

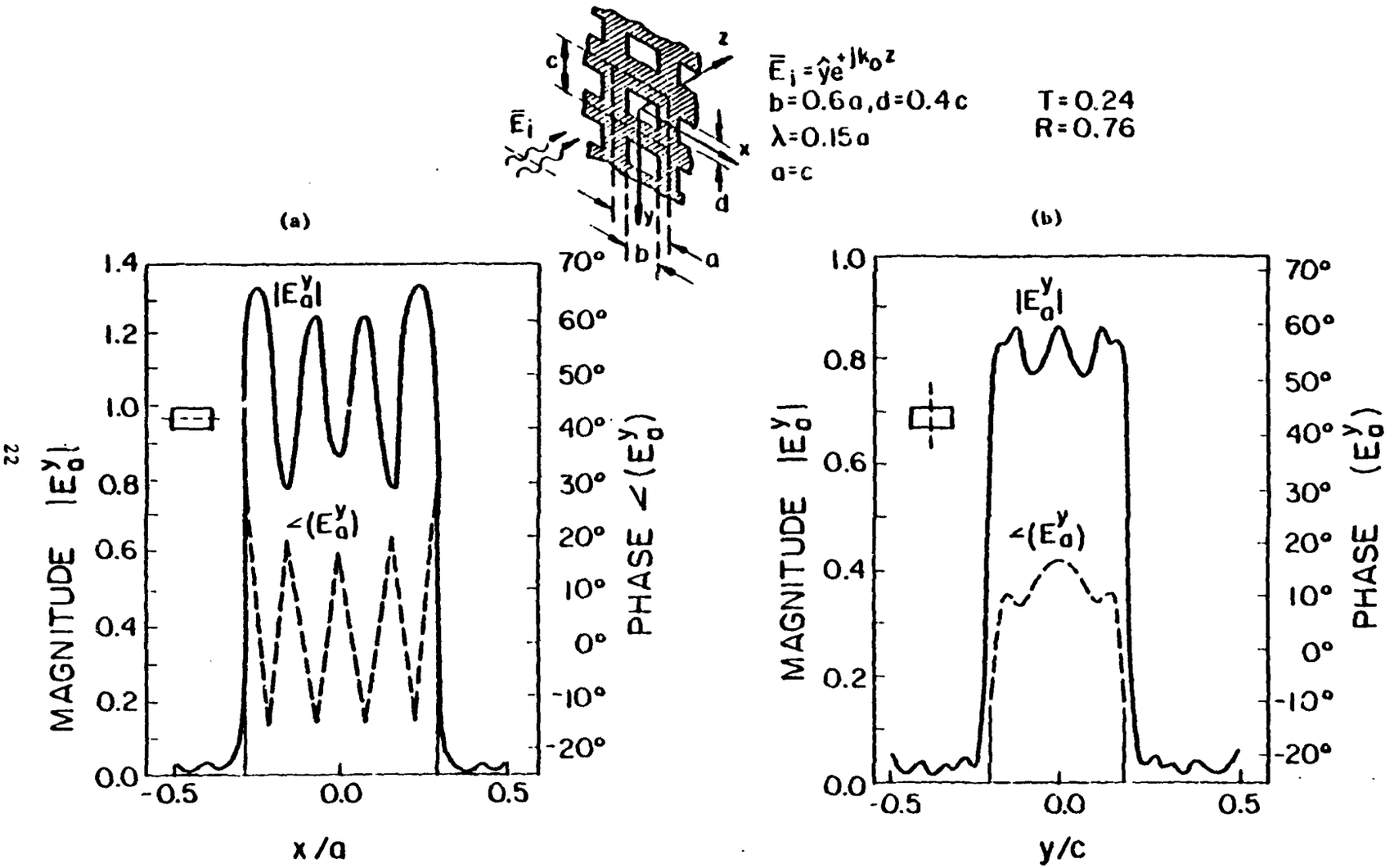

Figure 8. Distribution of the dominant component of E-field in the plane of a perforated screen with rectangular apertures. (a) E_y-field sampled along the x-axis; (b) E_y-field sampled along the y-axis.

regions of dissimilar dimensions. An open-region type example is a corrugated surface which can be thought of as a junction of two regions, viz., the infinite half-space and a periodic array of short-circuited waveguides. For the sake of simplicity, a closed-region type problem - a step discontinuity in a parallel-plate waveguide - is considered in this section. The geometry is shown in Figure 9. The incident field is a TE mode wave. The formulation of this problem can be found in the literature. The integral equation is given by

$$\int_0^b E_y(x')K^-(x,x')dx' = \int_0^b E_y(x')K^+(x,x')dx' - 2H_x^i \qquad (8)$$

$$\text{for } 0 < x < b, \quad z = 0$$

where E_y is the unknown aperture E-field,

H_x^i is the incident H-field,

$$K^-(x,x') = \frac{1}{j\omega\mu} \sum_{m=-\infty}^{\infty} \Gamma_m^- \sin\frac{m\pi}{a}x \sin\frac{m\pi}{a}x'$$

$$K^+(x,x') = \frac{1}{j\omega\mu} \sum_{m=-\infty}^{\infty} \Gamma_m^+ \sin\frac{m\pi}{b}x \sin\frac{m\pi}{b}x'$$

$$\Gamma_m^- = \begin{cases} j(k^2 - (\frac{m\pi}{a})^2)^{1/2} & \text{if } k^2 > (\frac{m\pi}{a})^2 \\ ((\frac{m\pi}{a})^2 - k^2)^{1/2} & \text{if } k^2 < (\frac{m\pi}{a})^2 \end{cases}$$

and

$$\Gamma_m^+ = \begin{cases} -j(k^2 - (\frac{m\pi}{b})^2)^{1/2} & \text{if } k^2 > (\frac{m\pi}{b})^2 \\ ((\frac{m\pi}{b})^2 - k^2)^{1/2} & \text{if } k^2 < (\frac{m\pi}{b})^2 \end{cases}$$

Note that (8) is defined in the region $0 < x < b$. To apply the iterative technique, it has to be extended to the full range

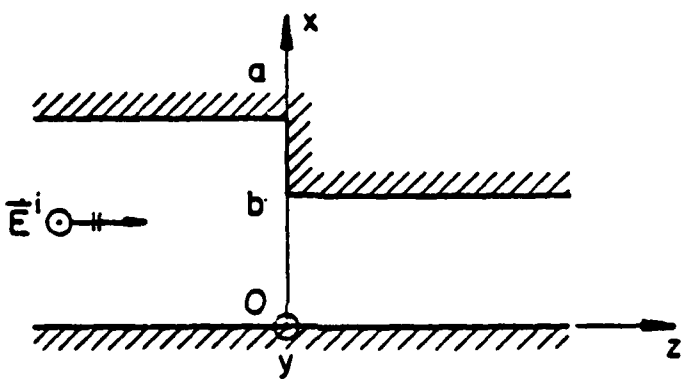

Figure 9. Step discontinuity in a parallel-plate waveguide with a TE incident wave.

$0 < x < a$. This is achieved by introducing an extra unknown function $J(x)$, and the extended equation takes the form

$$\int_0^a E_y(x')K^-(x,x')dx' = \int_0^a E_y(x')K^+(x,x')dx' + \theta(-2H_x^i) + \hat{\theta}(J(x)) \quad (9)$$

for $0 < x < a$

where for any function $f(x)$

$$\theta(f(x)) = f(x) \quad \text{if } 0 < x < b$$

$$= 0 \quad \text{if } b < x < a$$

and

$$\hat{\theta}(f(x)) = f(x) - \theta(f(x))$$

A recursion formula relating the $(n+1)$th order solution $E_y^{(n+1)}$ to the nth solution $E_y^{(n)}$ can be derived via a procedure similar to that developed in section III. The formula is

$$\int_0^a E_y^{(n+1)} \cdot K^- = \int_0^a E_y^{(n)}K^+ + \theta(-2H_x^i) + \hat{\theta}\left(\int_0^a E_y^{(n)}K^- - \int_0^a E_y^{(n)}K^+ - \theta(-2H_x^i)\right) \quad (10)$$

Equation (10) is now solved using an iterative procedure similar to that developed in section III. The integrations in (10) can again be carried out using the FFT because of the characteristic nature of the kernels. Figure 10 shows the aperture E-field distribution at the discontinuity. The initial approximation for E_y is taken to be the incident field truncated in the aperture.

The result is obtained in three iterations with 32 expansion functions used in representing the unknown field. We note that the boundary condition on E_y, viz., that it vanishes at the edges, is satisfied by the iterated solution.

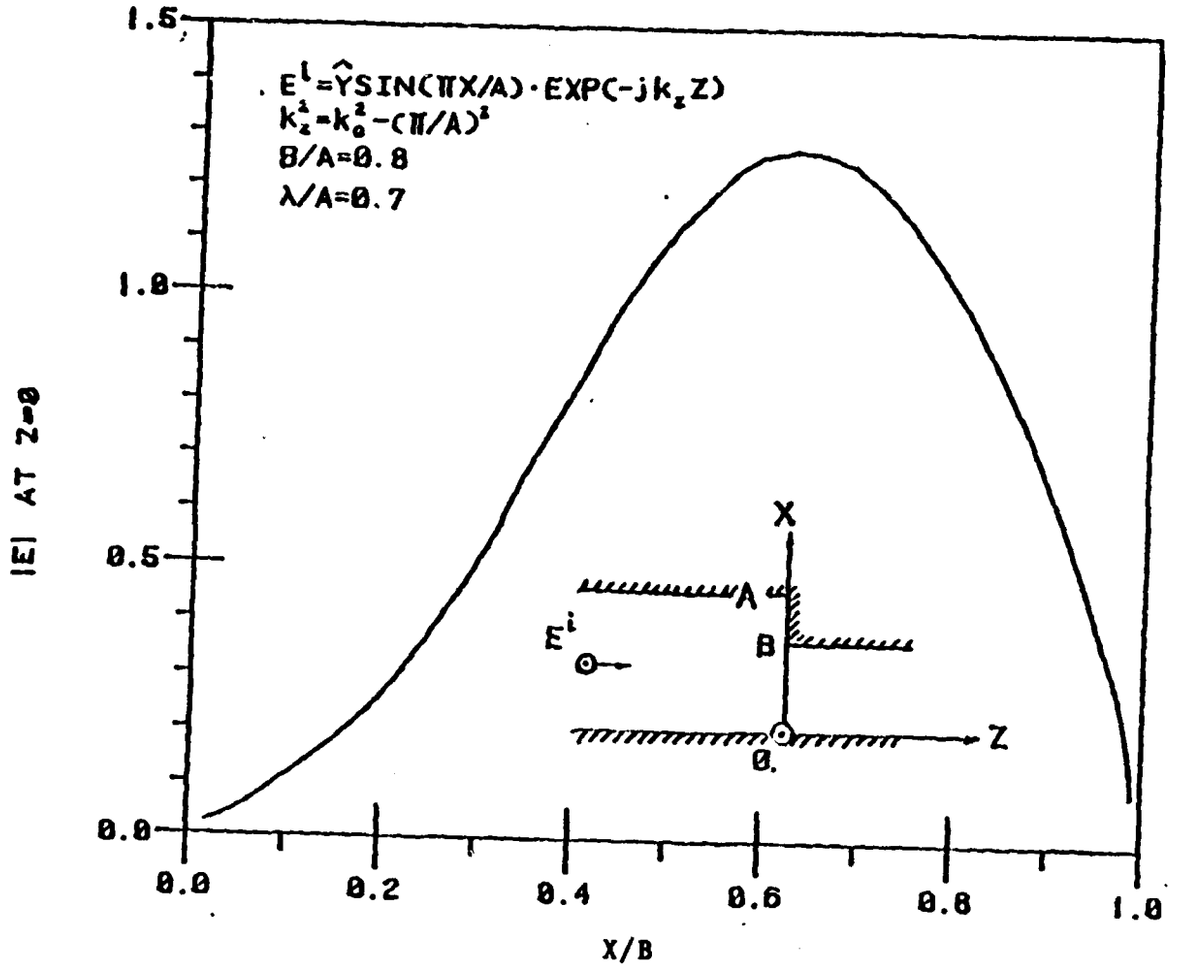

Figure 10. Magnitude of the E-field distribution at the step-discontinuity in a parallel-plate waveguide.

VI. AN EXTENSION OF THE SPECTRAL-ITERATION TECHNIQUE FOR ANALYZING SCATTERING FROM BODIES OF ARBITRARY SHAPE

In the past, the application of the spectral technique has been largely restricted to scatterers with two-dimensional geometries and with planar facets.

A new extension of the method, outlined below, allows one to analyze the problem of scattering from bodies with arbitrary shape and size. The method has wide application since it is capable of handling body shapes which are not conveniently treated either with the low- or the high-frequency techniques, an example being a long and narrow cylinder of finite length. Moreover, the range of application of the spectral-iteration approach encompasses both the low-frequency region, where it can provide faster and more efficient solution than the conventional moment methods, and to the high-frequency range where it yields both the surface current and the near fields. In addition, the method has a built-in boundary condition check, a unique feature not present in asymptotic techniques, e.g., the ray methods.

The first step in the spectral-iteration method is to represent the scatterer via an array of flat slices. The current on each such slice is sampled by a thin ring on the left side of the slice as shown in Figure 11. The iteration begins with an initial guess for the current distribution on the scatterer on the basis of, say, the physical optics (PO) approximation or the GTD. Next, we evaluate the field at the first plane which is farthest to the left of the scatterer. A process of improving the assumption for the current then starts. It is done one slice at a time from left to right, as explained below. Once the whole body has been scanned in this way, the first iteration is over, and the process is repeated until a convergence is attained and the boundary conditions are satisfied.

The manner in which the current rings are updated is described as

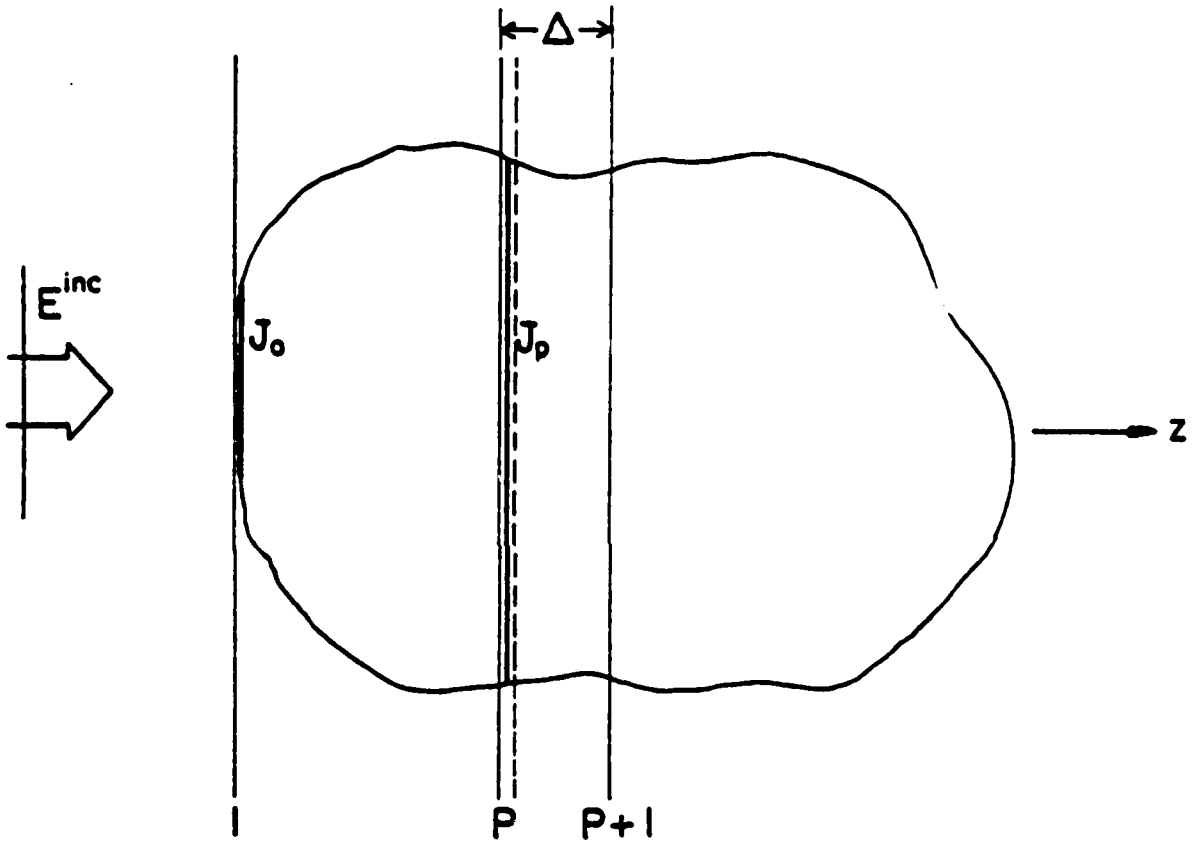

Figure 11. Current slices on 3-dimensional scatterer.

follows. Consider the pth slice, one which is bounded by the pth plane on the left and the p+1th plane on the right, and contains the thin current ring J_p at its left immediately to the right of the pth plane (Figure 11). At the pth-plane the scattered field consists of two components, viz., $\vec{\tilde{E}}_p^-$ and $\vec{\tilde{E}}_p^-$. $\vec{\tilde{E}}_p^-$ is the aggregate of the contribution from all of the sources to the left of the pth plane. Its spectrum is thus propagating to the right and, consequently, the radiation condition dictates the choice of the propagator $e^{-jk_z z}$ for any of its plane-wave spectral components. The second contributor to the scattered field is $\vec{\tilde{E}}_p^-$, which is the contribution of all the currents to the right of the pth plane and is thus propagating to the left. We assume that in the process of scanning the body from the left to right all the currents to the left of the pth plane have been updated, implying the $\vec{\tilde{E}}_p^-$ has been updated as well.

We next proceed to update the current in the pth slice, i.e., J_p. To do this, we look at the plane immediately to the right of J_p. This plane is shown by the dashed line in Figure 5.1. $\vec{\tilde{E}}_p$ can be transformed to this plane simply by adding the contribution of J_p. In the spectral domain we have the expression

$$\vec{\tilde{E}}_p^+ = \vec{\tilde{E}}_p^- + G \cdot \tilde{J}_p \tag{11}$$

where G is the Green's function in the spectral domain, the - superscript denotes the plane immediately to the left of J_p, and the + superscript is associated with the plane immediately to the right of J_p. Since $\vec{\tilde{E}}_p^-$ is known, we are now able to use the assumed J_p in conjunction with (11) to compute $\vec{\tilde{E}}^+$ and then the total scattered field

$$\tilde{E}_p = (\vec{\tilde{E}}^+ + \vec{\tilde{E}}^+)_p$$

Next, inverse transforming $\tilde{E}_p$ yields the scattered electric field in the spatial domain and the application of the boundary condition

allows one to replace the total scattered field E_p inside the body by $-E^{inc}$. A Fourier transform is then taken and the following equation is used to obtain the updated $\vec{E}_p^+$

$$\vec{E}_p^+ = E_p^+ \text{ (updated)} - \vec{E}_p^+ \tag{12}$$

Finally, the updated J_p is derived from (11) and the updated $\vec{E}_p^+$. Also, $\vec{E}_{p+1}^-$ is obtained from $\vec{E}_p^+$ via the equation

$$\vec{E}_{p+1}^- = \vec{E}_p^+ \, e^{-jk_z\Delta} \tag{13}$$

This completes the operation on the pth slice and we move to the (p+1)th slice to repeat the process in order to obtain a new value for J_{p+1}. We continue in the same manner, proceeding to the successive slices toward the right until we are finished with all the slices and have covered the entire body. The end result of this series of steps is a complete, updated version of the current on the entire scatterer. Having obtained this, the first iteration is completed, and the whole process can be repeated.

The iteration process is continued until convergence is achieved, as indicated by the satisfaction of the boundary condition on and in the interior of the scatterer.

It should be noted that since the two-dimensional FFT is used, even for a three-dimensional scatterer, the method is computationally efficient and its storage requirement is low. Furthermore, since the boundary-condition check is applied at each stage of the iteration, the accuracy of the final (convergent) result is guaranteed.

Preliminary studies have indicated that the arbitrary body scheme, though originally conceived in connection with perfectly conducting scatterers, may prove useful for handling dielectric scatterers as well. It appears that the method may be generalizable to inhomogeneous dielectric bodies as well, although more work remains to be done to determine the scope and limitations of this approach.

VII. REFERENCES

[1] C. C. Chen, "Transmission through a Conducting Screen Perforated Periodically with Apertures," Microwave Theory and Techniques, vol. 18, No. 9, pp. 627-632, 1970.

[2] S. W. Lee, "Scattering by Dielectric-Loaded Screen," IEEE Transactions on Antennas and Propagation, vol. 19, No. 5, pp. 656-665, 1971.

[3] R. C. McPhedran and D. Maystre, "On the Theory and Solar Applications of Inductive Guides," Appl. Phys., vol. 14, pp. 1-20, 1977.

[4] W. L. Ko and R. Mittra, "A New Approach Based on a Combination of Integral Equation and Asymptotic Techniques for Solving Electromagnetic Scattering Problems," IEEE Transactions on Antennas and Propagation, vol. 25, No. 2, 1977.

VIII. BIBLIOGRAPHY ON SPECTRAL DOMAIN METHODS

Books

1. R. Mittra and Y. Rahmat-Samii, "A Spectral Domain Approach for Solving High Frequency Scattering Problems," in P.L.E. Uslenghi (Editor), Electromagnetic Scattering, Academic Press, N.Y. 1978.

2. R. Mittra, W. L. Ko and Y. Rahmat-Samii, "Transform Approach to Electromagnetic Scattering I," Proceedings of NATO Advanced Institute, Norwich, England, 1980.

3. R. Mittra and Mark Tew, Accuracy Tests and Iterative Procedures for High Frequency Asymptotic Solutions -- A Spectral Domain Approach, Pergamon Press, 1980.

Journal Articles

1. N. N. Bojarski, "K-Space Formulation of the Electromagnetic Scattering Problem," Technical Report AFAL-TR-71-75, March 1971.

2. T. Itoh and R. Mittra, "Spectral Domain Approach for Calculating the Dispersion Characteristics of Microstrip Lines," IEEE Trans. Microwave Theory Tech., vol. MTT-21, pp. 496-499, July 1973.

3. Y. Rahmat-Samii, T. Itoh and R. Mittra, "A Spectral Domain Technique for Solving Microstrip Line Problems," AEÜ Electronics and Communications, Band 27, pp. 69-71, 1973.

4. Y. Rahmat-Samii, T. Itoh and R. Mittra, "A Spectral Domain Analysis for Solving Discontinuity Problems," IEEE Trans. Microwave Theory Tech., vol. MTT-22, pp. 372-378, April 1974.

5. R. Mittra and T. S. Li, "A Spectral Domain Approach to the Numerical Solution of Electromagnetic Scattering Problems," AEÜ Electronics and Communications, Band 29, pp. 217-222, 1975.

6. R. Mittra, Y. Rahmat-Samii and W. L. Ko, "Spectral Theory of Diffraction," Appl. Phys., vol. 10, pp. 1-13, January 1976.

7. Y. Rahmat-Samii and R. Mittra, "A Spectral Domain Interpretation of High Frequency Diffraction Phenomena," IEEE Transactions on Antennas and Propagation, vol. 25, pp. 676-687, September 1977.

8. Y. Rahmat-Samii and R. Mittra, "On the Investigation of Diffracted Fields at the Shadow Boundaries of Staggered Parallel Plates -- A Spectral Domain Approach," Radio Science, vol. 12, pp. 659-670, September/October 1977.

9. R. Mittra and W. L. Ko, "An Approach to High-Frequency Scattering from Smooth Convex Surfaces," IEEE Transactions on Antennas and Propagation, vol. 25, pp. 781-788, November 1977.

10. W. L. Ko and R. Mittra, "A New Look at the Scattering of a Plane Wave by a Rectangular Cylinder," AEÜ Electronics and Communications, pp. 494-500, December 1977.

11. Y. Rahmat-Samii and R. Mittra, "Spectral Analysis of High Frequency Diffraction of an Arbitrary Incident Field by a Half Plane -- Comparison with Four Asymptotic Techniques," Radio Science, vol. 13, pp. 31-48, January/February 1978.

12. R. Mittra and M. Tew, "Accuracy Test for High-Frequency Asymptotic Solutions," IEEE Transactions on Antennas and Propagation, vol. AP-27, No. 1, pp. 62-67, January 1979.

13. R. Mittra, W. L. Ko and Y. Rahmat-Samii, "Solution of Electromagnetic Scattering and Radiation Problems Using a Spectral Domain Approach -- A Review," Wave Motion J., vol. 1, No. 2, pp. 95-106, April 1979.

14. R. Mittra and S. Safavi-Naini, "Source Radiation in the Presence of Smooth Convex Bodies," Radio Science, vol. 14, No. 2, pp. 217-237, March-April 1979.

15. R. Mittra, W. L. Ko and Y. Rahmat-Samii, "Transform Approach to Electromagnetic Scattering," Proc. IEEE, vol. 67, No. 11, pp. 1486-1503, November 1979.

16. M. Tew and R. Mittra, "An Integral E-Field Accuracy Test for High Frequency Asymptotic Solutions," IEEE Transactions on Antennas and Propagation, vol. AP-28, No. 4, pp. 513-518, July 1980.

17. R. Mittra and R. Kastner, "A Spectral Domain Approach for Computing the Radiation Characteristics of a Leaky-Wave Antenna for Millimeter Waves," AP-S Trans., (to appear) 1980.

18. S. Savavi-Naini and R. Mittra, "High Frequency Radiation from Electromagnetic Source Located on a Finite Cylinder -- A Spectral Dcmain Approach," AP-S Trans., (to appear) 1980.

APPENDIX B

A SPECTRAL DOMAIN APPROACH FOR COMPUTING THE RADIATION CHARACTERISTICS OF A LEAKY-WAVE ANTENNA FOR MILLIMETER WAVES

R. Mittra and R. Kastner

ELECTRICAL ENGINEERING DEPARTMENT
UNIVERSITY OF ILLINOIS
URBANA, ILLINOIS 61801

ABSTRACT

This paper deals with a new method for evaluating the complex propagation constant β in a leaky-wave structure comprising of thin, metallic rectangular strips etched on a dielectric rod of rectangular cross section. The radiation pattern of the leaky wave antenna can be determined once β is known, since $Re(\beta)$ governs the direction of the main beam and $Im(\beta)$ accounts for the beamwidth and aperture efficiency. In addition, the knowledge of the dependence of β on frequency allows one to design the antenna for frequency-scanning applications. The method employed in this paper is based on the spectral domain approach which formulates the eigenvalue problem in the Fourier transform domain. Computed results are shown to be in very good agreement with experimental measurements.

1. Introduction

In this paper we describe a novel method for evaluating the complex propagation constant β in a leaky-wave structure comprised of an array of thin, metallic, rectangular strips etched on a dielectric rod of rectangular cross section. The geometry of the problem is shown in Figure 1. This configuration finds useful applications as a frequency scannable antenna, particularly at millimeter waves where the antenna can be conveniently integrated with dielectric-based planar integrated circuits [1,2,3].

The complex propagation constant β along a leaky-wave antenna determines the radiation pattern of the antenna. Specifically, $\mathrm{Re}(\beta)$ governs the direction of the main beam, and $\mathrm{Im}(\beta)$ accounts for the beam width and aperture efficiency. In addition, when the dependence of β on frequency is known, it is possible to design the antenna for frequency-scanning applications.

In the past, the determination of β has often been accomplished via experimental means, mostly by near-field probing techniques. Analytical evaluation of β has been carried out for structures for which the leaky wave is generated from guiding structure which supports a fast wave, e.g., a slotted waveguide [4]. For such a structure, β differs only slightly from the guided-wave propagation constant in the absence of the slots as

sets of networks are required for every hybrid mode. In addition, the discontinuities must be incorporated into the equivalent network by lump-element representation, which by themselves may require the solution of some involved boundary-value problems.

In this paper we employ a method based on the spectral approach which formulates the eigenvalue problem in the Fourier transform domain. A description of this method appears below.

2. Formulation of the Problem

The formulation of the problem is based on the spectral domain approach which has the following advantageous feature. The Green's function for the dielectric substrate region is conveniently expressible in the transform or spectral domain in a closed form, whereas it takes a complicated form in the conventional space domain approach.

Referring to Figure 1, let us consider a y-polarized wave traveling along the z-direction. Because of the periodic nature of the geometry, we can express the fields propagating along the structure in terms of Floquet space harmonics with wave numbers β_n $(=\beta + 2n\pi/\Delta)$, where β is the complex wave number we are seeking. It is evident that only a finite number of β_n are in the visible region, i.e., satisfy the criterion $|\text{Re } \beta_n| < k$, where k is the free-space wave number, and only these β_n contribute to the leaky-wave radiation. Typically, these leaky-wave antennas are designed such that $n = \pm 1$. As alluded to earlier, the real part of $\beta_{\pm 1}$ determines the direction of the main beam and its scanning properties, whereas the imaginary part determines the beamwidth and efficiency of the antenna.

As a first step toward attacking this problem, we replace the dielectric rod with a slab using the well-know effective dielectric constant method [6], [7]. The effective dielectric constant is given by

$$\varepsilon_{eff} = \varepsilon - \left(\frac{k_y}{k}\right)^2$$

where k is the free-space wave number and k_y is the fundamental mode with spatial frequency corresponding to the cosine variation in the y-direction inside the dielectric. Next, the Green's function for the geometry is constructed in the spectral domain, because the expression for the Green's function in the transform domain is considerably simpler than the corresponding one in the space domain. The expression for $\tilde{G}$, the two-dimensional Fourier transform of the spatial-domain Green's function for the E-field of y-directed point source located at a distance d above the dielectric surface (Figure 2), is formulated in a fashion similar to Collin's [8]. It is given by

$$\tilde{G}(x,u,v) = -j\omega_o(1-u^2)\,\frac{(k_{x1}+k_{x2})e^{jk_{x2}T} - (k_{x1}-k_{x2})e^{-jk_{x2}T}}{(k_{x1}+k_{x2})^2 e^{jk_{x2}T} - (k_{x1}-k_{x2})^2 e^{-jk_{x2}T}}\, e^{-jk_{x1}|x-d|} \qquad (2)$$

where

$$k_{x1} = \sqrt{1-u^2-v^2}$$

$$k_{x2} = \sqrt{\varepsilon_{eff}-u^2-v^2}$$

and u and v are the transform variables corresponding to the y and z directions, respectively. These are normalized with respect to k; hence, all the dimensions are expressed in terms of electric length (radians). In our case, d=0. The tedious Fourier inversion of (2) is avoided by keeping the rest of the development in the transform domain. The representation for the electric field in terms of the current distribution on a strip takes then a simple form of algebraic product (as opposed to convolution in the space domain). We have

$$\tilde{E} = \tilde{G}(o,u,v) \cdot \tilde{J}(o,u,v) \tag{3}$$

where $\tilde{J}$ is the transform of the assumed current distribution on the strip. Since $w << L$, it is reasonable to assume a cosine variation in the y direction and uniform distribution in the z direction. $\tilde{J}$ is then proportional to

$$\tilde{J}(u,v) \sim \frac{\cos \frac{uL}{2}}{(\frac{\pi}{2})^2 - (\frac{uL}{2})^2} \quad \frac{\sin \frac{vW}{2}}{\frac{vW}{2}} \tag{4}$$

To obtain the eigenvalue equation, we superimpose the electric fields generated by the periodic array of strips and apply the boundary condition that the total electric field on a representative strip is zero. The n^{th} strip is characterized by an amplitude $e^{-j\beta n\Delta}$ and a displacement of $n\Delta$ in the z-direction. Therefore, the transform of its current distribution is

$$\tilde{J}_n = \tilde{J}\, e^{j(v-\beta)n\Delta} \tag{5}$$

and the total field is

$$\tilde{E} = \tilde{G}\,\tilde{J} \sum_{n=-\infty}^{\infty} e^{j(v-\beta)n\Delta} \tag{6}$$

The total E-field on any strip is now equated to zero in the Galerkin sense:

$$\int\int_{\text{strips}} E \cdot J \, dy \, dz = 0 \tag{7}$$

By Parseval's theorem, (7) is also expressible by

$$\int_{-\infty}^{\infty}\int \tilde{E} \cdot \tilde{J} \, du \, dv = 0 \tag{9}$$

Substituting (6) into (8), one obtains

$$\int_{-\infty}^{\infty}\int \tilde{G}(u,v)\ \tilde{J}^2(u,v) \sum_{n=-\infty}^{\infty} e^{j(v-\beta)\,n\Delta}\ du\, dv = 0 \tag{10}$$

Utilizing the identity

$$\sum_{n=-\infty}^{\infty} e^{j(v-\beta)\,n\Delta} = \frac{2\pi}{\Delta} \sum_{n=-\infty}^{\infty} \delta\left(v-\beta-n\,\frac{2\pi}{\Delta}\right) \tag{11}$$

one of the integrals is eliminated and (9) becomes

$$\sum_{n=-\infty}^{\infty} \int_{-\infty}^{\infty} \left[\tilde{G}(u,v)\ \tilde{J}^2(u,v)\right]_{v=\beta+\frac{2n\pi}{\Delta}}\ du = 0 \tag{12}$$

Equation (12) is the desired eigenvalue equation. The solution of complex β satisfying (12) yields the desired complex wave number for the leaky-wave antenna.

3. Results.

Equation (12) requires an integration along the real axis in the u-plane and a summation over all Floquet modes. Since all the constituents of (12) are symmetric with respect to real u, the integration need be carried out only along half of the u-axis. Moreover, there appears to be little or no contribution to the expression beyond $u = 2$ and $|n| = 2$.

The solution for β is obtained via a search procedure which seeks the zeroes of Eq. (12) within some numerical tolerance. The antenna under consideration had 29 strips with the following dimensions at the center frequency of $f_o = 80$ GHz (see Figure 1): $L = 0.8\lambda$, $T = 0.3667\lambda$, $W = 0.3387\lambda$, $\Delta = 0.6667\lambda$, and with $\varepsilon = 2.46$. The computed β for $f = 0.95f_o$, $1.05f_o$ and $1.1f_o$ was $-.31 - j.03$, $-.222 - j.05$, $-.13 - j.03$ and $-.05 - j.03$ respectively. These solutions account for main beam directions of 108°, 103°, 97.5° and 93° with respect to the z-axis, compared to the experimental values of 109°, 103° 98° and 92°. These values of β correspond to a backward wave ($n = -1$). The real part of the fundamental ($n = o$) β differs very little from that of an unloaded dielectric rod and can be predicted by approximate methods [1-3]. However, the imaginary part of β has not been analytically computed before for this structure. The experimental results, obtained by near-field probing techniques, yield $Im(\beta) = -.03$ which is in very good agreement with our theory. As seen from Figure 3, the measured and computed beam widths, of about 5°, also agree well with each other. The behavior of the experimental pattern in the side-lobe region is attributable to the radiation from the pattern feed region which was not modeled on the theoretical calculations.

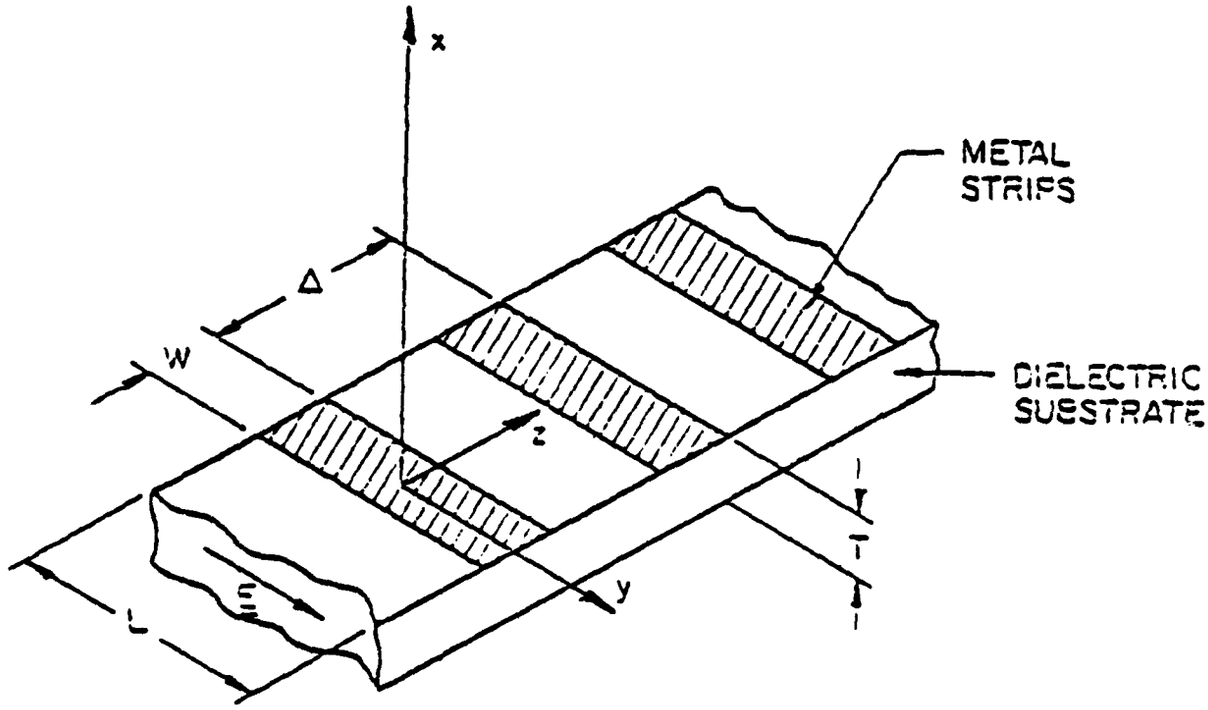

Figure 1. Leaky Wave Antenna Configuration.

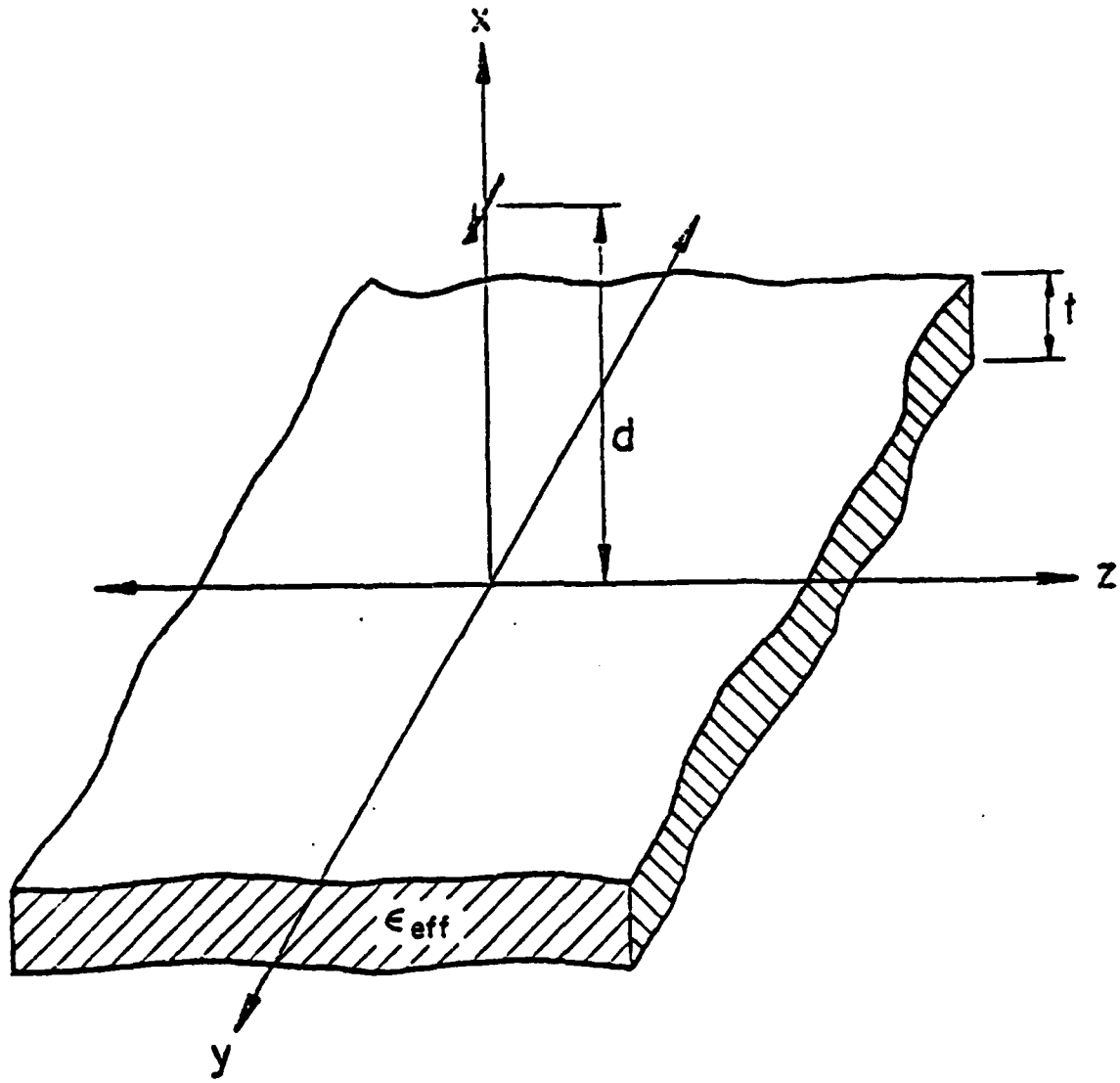

Figure 2. Geometry for the Construction of the Green's Function.

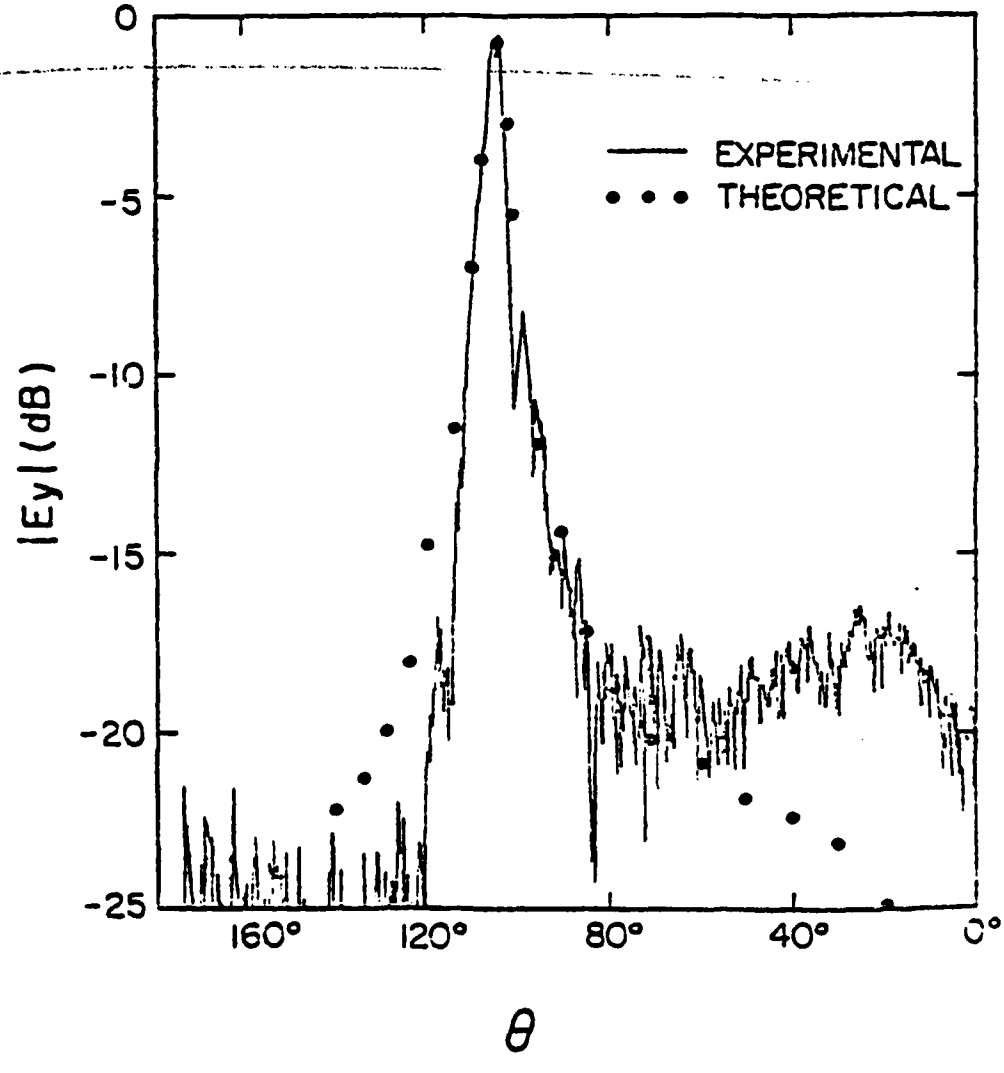

Figure 3. Computed and Measured Patterns of the Leaky Wave Antenna in the x-z plane.

References

[1] K. L. Klohn, R. E. Horn, H. Jacobs and E. Freibergs, "Silicon Waveguide Frequency Scanning Linear Array Antenna," IEEE Trans. Microwave Theory Tech., vol. MIT-26, pp. 764-773, October 1978.

[2] S. Kobayashi, R. Lampe, N. Deo and R. Mittra, "A Study of Millimeter-Wave Dielectric Antennas," 1979 AP-S International Symposium Digest, pp. 408-411, June 1979.

[3] K. Solbach, "E-Band Leaky-Wave Antenna Using Dielectric Image Line with Etched Radiating Elements," in 1979 MTT-S International Microwave Symposium Digest, pp. 214-216, April-May 1979.

[4] T. Tamir, "leaky-Wave Antennas," chapter 20 in: R. E. Collin and F. J. Zucker, Antenna Theory, Part II, McGraw-Hill, 1969, pp. 259-297.

[5] L. B. Felsen and N. Marcuvitz, Radiation and Scattering of Waves, chapter 2, Prentice-Hall, 1973.

[6] R. M. Knox and P. P. Toulios, "Integrated Circuits for the Millimeter Through Optical Frequency Range," in Proc. Symp. Submillimeter Waves (New York), March 31-April 2, 1970.

[7] W. V. McLevige, T. Itoh, R. Mittra, "New Waveguide Structures for Millimeter-Wave and Optical Integrated Circuits," IEEE Trans. Microwave Theory Tech., vol. MTT-23, pp. 788-794, October 1975.

[8] R. E. Collin, Field Theory of Guided Waves, chapter 11, McGraw-Hill, 1960.

APPENDIX C

RADIATION FROM AN OPEN-ENDED WAVEGUIDE WITH BEAM EQUALIZER - A SPECTRAL DOMAIN ANALYSIS

Wai Lee Ko, Vahraz Jamnejad, Raj Mittra, and Shung-Wu Lee*

ABSTRACT

A septum and an impedance matching post are used as a beam equalizer in an open-ended waveguide-feed for reflectors used in satellite communications systems. The performance of this design over a frequency band is evaluated using a spectral domain approach. The computed radiation patterns in the E- and H-planes, as well as the results for the impedance match, are presented in the paper.

*W. L. Ko, R. Mittra, and S. W. Lee are with the Electromagnetics Laboratory, Department of Electrical Engineering, University of Illinois, Urbana, IL 61801. V. Jamnejad was with the Electromagnetics Laboratory. He is now with JPL, 4800 Oak Grove Drive, Pasadena, CA 91103.

The work was supported by the Office of Naval Research, Contract N00014-75-C-0293.

I. Introduction

Rectangular waveguide array feeds for reflector antennas play an important role in the design of satellite communication systems. To make the radiation pattern more symmetric in the E- and H-planes of the feed, a beam equalizer is needed. The design used in this case is a septum placed across the mouth of the waveguide such that the aperture distribution is reshaped to satisfy the new boundary conditions imposed by the septum. Consequently, the H-plane radiation pattern is narrowed to approach the E-plane pattern, thereby achieving the beam equalizing effect. However, the introduction of such a septum creates an impedance mismatch problem for the feed. To alleviate this problem, a matching post is placed behind the septum so that the reflection back into the waveguide is minimized.

The performance of this design over the desired frequency band is evaluated using a spectral domain approach, or more specifically, Galerkin's method applied in the spectral domain [1]. The scattered fields on both sides of the beam equalizer are represented in terms of their Fourier transforms or spectra which can be related to the induced surface currents on the septum and the post. These unknown induced currents are expanded in terms of known basis functions and unknown coefficients. A matrix equation for the unknown coefficients is derived by applying the boundary conditions, and the moment method is then employed in the spectral domain to solve for these unknown coefficients, which in turn give the answer to the unknown scattered fields. The scattered fields for all modes obtained in this manner are then used to compute the reflection and transmission coefficients for each mode, propagating or attenuated. A tacit assumption made is that the scattered field on the open-ended side of the waveguide is the same as

that in an infinitely long waveguide containing the beam equalizer. In other words, the truncation effects of the waveguide are ignored in this analysis. The transmission coefficients are used to weight the radiation field due to each mode of waveguide and the superimposed radiation pattern is computed. The reflection coefficients are used to assess the impedance matching performance. Numerical results indicate that the E- and H-plane principally polarized patterns are equalized extremely well over the entire frequency band of operation and that the impedance matching is also quite satisfactory.

II. Analysis

The geometry of the waveguide with septum and post is shown in Figure 1. Since the cross-section of the post is very small, the post is modeled as a narrow strip to simplify the analysis. The incident field is propagating in the z-direction towards the post as shown schematically in Figure 1. There are surface currents induced on the septum and the post due to the incident field. The scattered fields radiated by these induced surface currents then propagate in both the z-direction and the -z-direction, giving rise to the transmitted and the reflected waves, respectively. In the following analysis, the truncation effects of the waveguide at z=0 are ignored, as though the post and septum were located in an infinite guide.

The incident field in the waveguide can be expressed in terms of TE and TM modes in the usual manner:

TE_{nm} modes:

$$E_x^i = jh_{nm} \frac{\omega\mu(\frac{m\pi}{b})}{k_c^2} \cos(\frac{n\pi}{a}x) \sin(\frac{m\pi}{b}y) \exp(-j\beta_{nm}z)$$

$$E_y^i = -jh_{nm} Z_{TE} \frac{\beta_{nm}(\frac{n\pi}{a})}{k_c^2} \sin(\frac{n\pi}{a} x) \cos(\frac{m\pi}{b} y) \exp(-j\beta_{nm} z)$$

$$E_z^i = 0$$

$$H_x^i = -E_y^i / Z_{TE}$$

$$H_y^i = E_x^i / Z_{TE}$$

$$H_z^i = h_{nm} \cos(\frac{n\pi}{a} x) \cos(\frac{m\pi}{b} y) \exp(-j\beta_{nm} z) \qquad (1a)$$

TM_{nm} modes:

$$E_x^i = -je_{nm} \frac{\beta_{nm}(\frac{n\pi}{a})}{k_c^2} \cos(\frac{n\pi}{a} x) \sin(\frac{m\pi}{b} y) \exp(-j\beta_{nm} z)$$

$$E_y^i = -j e_{nm} Z_{TM} \frac{\omega\varepsilon(\frac{m\pi}{b})}{k_c^2} \sin(\frac{n\pi}{a} x) \cos(\frac{m\pi}{b} y) \exp(-j\beta_{nm} z)$$

$$E_z^i = e_{nm} \sin(\frac{n\pi}{a} x) \sin(\frac{m\pi}{b} y) \exp(-j\beta_{nm} z)$$

$$H_x^i = -E_y^i / Z_{TM} \; ; \quad H_y^i = E_x^i / Z_{TM} \; ; \quad H_z^i = 0 \qquad (1b)$$

where $k_c^2 = (\frac{n\pi}{a})^2 + (\frac{m\pi}{b})^2$; $\beta^2_{nm} = k^2 - k_c^2$; $k^2 = \omega^2 \mu\varepsilon$

$$Z_{TE} = \omega\mu/\beta_{nm} \; ; \qquad Z_{TM} = \beta_{nm}/(\omega\varepsilon)$$

The scattered fields can be expressed in terms of their Fourier spectra, which are in turn related to the Fourier spectra of the induced surface currents. The Fourier spectra of the induced surface currents

are then solved for by the moment method applied in the transformed, i.e., the spectral domain. Specifically, Galerkin's method is used in the present analysis — the same basis functions are used as testing functions in the moment method. Upon solving the spectra of the induced surface currents, the scattered fields can be obtained in a straightforward manner. The analytic details follow.

Corresponding to each incident mode, the scattered fields E_x^s and E_z^s can be represented in the following form:

$$\begin{bmatrix} E_x^s \ (b/2 < y < b) \\ E_x^s \ (0 < y < b/2) \end{bmatrix} = \cos\left(\frac{n\pi}{a} x\right) \int_{-\infty}^{\infty} f_n(\alpha) \begin{bmatrix} \sin[\gamma_n(b-y)] \\ \sin \gamma_n y \end{bmatrix} \exp(-j\alpha z)d\alpha, \tag{2}$$

$$\begin{bmatrix} E_z^s \ (b/2 < y < b) \\ E_z^s \ (0 < y < b/2) \end{bmatrix} = \sin\left(\frac{n\pi}{a} x\right) \int_{-\infty}^{\infty} g_n(\alpha) \begin{bmatrix} \sin[\gamma_n(b-y)] \\ \sin \gamma_n y \end{bmatrix} \exp(-j\alpha z)d\alpha$$

where

$$\gamma_n = [k^2 - (\frac{n\pi}{a})^2 - \alpha^2]^{1/2} \tag{3}$$

and $f_n(\alpha)$, $g_n(\alpha)$ are the unknown Fourier spectra to be determined. The expression for E_y^s is then obtained from the Maxwell's equation $\nabla \cdot \vec{E} = 0$, giving

$$\begin{bmatrix} E_y^s \ (b/2 < y < b) \\ E_y^s \ (0 < y < b/2) \end{bmatrix} = \sin\left(\frac{n\pi}{a} x\right) \int_{-\infty}^{\infty} h_n(\alpha) \begin{bmatrix} \cos[\gamma_n(b-y)] \\ -\cos \gamma_n y \end{bmatrix} \exp(-j\alpha z)d\alpha \tag{4}$$

with

$$h_n(\alpha) = \frac{(\frac{n\pi}{a})\ f_n(\alpha) + j\alpha\ g_n(\alpha)}{\gamma_n} \tag{5}$$

Now that we have $\vec{E}$, we can find $\vec{H}$ by using the curl-of-$\vec{E}$ Maxwell's equation. However, in anticipation of relating the H-field with the induced surface currents on the septum and the strip, only the x- and the z- components of the H-field are computed, giving

$$\begin{bmatrix} H_x^s\ (b/2 < y < b) \\ \\ H_x^s\ (0 < y < b/2) \end{bmatrix} = \frac{-1}{j\omega\mu} \sin(\frac{n\pi}{a} x) \int_{-\infty}^{\infty} \exp(-j\alpha z)$$

$$\cdot \begin{bmatrix} [-\gamma_n\ g_n(\alpha) + j\alpha\ h_n(\alpha)] \cos [\gamma_n(b-y)] \\ \\ [\gamma_n\ g_n(\alpha) - j\alpha\ h_n(\alpha)] \cos \gamma_n\ y \end{bmatrix} d\alpha$$

$$\begin{bmatrix} H_z^s\ (b/2 < y < b) \\ \\ H_z^s\ (0 < y < b/2) \end{bmatrix} = \frac{-1}{j\omega\mu} \cos(\frac{n\pi}{a} x) \int_{-\infty}^{\infty} \exp(-j\alpha z)$$

$$\begin{bmatrix} [\gamma_n\ f_n(\alpha) + (\frac{n\pi}{a})\ h_n(\alpha)] \cos [\gamma_n(b-y)] \\ \\ [-\gamma_n\ f_n(\alpha) - (\frac{n\pi}{a})\ h_n(\alpha)] \cos \gamma_n\ y \end{bmatrix} d\alpha \tag{6}$$

The induced currents on the septum and the strip can also be expressed in terms of Fourier spectra. For each incident mode, we have

$$\begin{bmatrix} J_z\ (x, y = b/2,\ z) \\ J_x\ (x, y = b/2,\ z) \end{bmatrix} = \begin{bmatrix} \sin(\frac{n\pi}{a}\, x) \int_{-\infty}^{\infty} j_z(\alpha)\ \exp(-j\alpha z)\ d\alpha \\ \cos(\frac{n\pi}{a}\, x) \int_{-\infty}^{\infty} j_x(\alpha)\ \exp(-j\alpha z)\ d\alpha \end{bmatrix} \tag{7}$$

where $j_z(\alpha)$ and $j_x(\alpha)$ are Fourier spectra of the induced surface currents to be related to the spectra of the scattered H-field. This relationship is obtained by enforcing boundary conditions on the septum and the strip and can be written as

$$\begin{bmatrix} -H_x\ (y = \lim_{\varepsilon \to 0} (b/2 + \varepsilon)) + H_x\ (y = \lim_{\varepsilon \to 0} (b/2 - \varepsilon)) \\ H_z\ (y = \lim_{\varepsilon \to 0} (b/2 + \varepsilon)) - H_z\ (y = \lim_{\varepsilon \to 0} (b/2 - \varepsilon)) \end{bmatrix} = \begin{bmatrix} J_z \\ J_x \end{bmatrix} \tag{8}$$

where ε is a positive quantity.

Substitution of (6) and (7) into (8) leads to the following algebraic equations:

$$\begin{bmatrix} \frac{-2}{j\omega\mu} \cos(\frac{\gamma_n b}{2}) [\gamma_n\, g_n(\alpha) - j\alpha h_n(\alpha)] \\ \frac{-2}{j\omega\mu} \cos(\frac{\gamma_n b}{2}) [\gamma_n\, f_n(\alpha) + (\frac{n\pi}{a})\, h_n(\alpha)] \end{bmatrix} = \begin{bmatrix} j_z(\alpha) \\ j_x(\alpha) \end{bmatrix} \tag{9}$$

Substituting $h_n(\alpha)$ from (5) into (9) and manipulating the resulting equations leads to the following matrix equation for $f_n(\alpha)$ and $g_n(\alpha)$ in terms of the transform domain currents $j_x(\alpha)$ and $j_z(\alpha)$.

$$\begin{bmatrix} -j\alpha\left(\frac{n\pi}{a}\right) & k^2 - \frac{n^2\pi^2}{a^2} \\ k^2 - \alpha^2 & j\alpha\left(\frac{n\pi}{a}\right) \end{bmatrix} \begin{bmatrix} f_n(\alpha) \\ g_n(\alpha) \end{bmatrix} = \frac{-j\omega\mu\gamma_n}{2\cos\left(\frac{\gamma_n b}{2}\right)} \begin{bmatrix} j_z(\alpha) \\ j_x(\alpha) \end{bmatrix} \tag{10}$$

An inversion of (10) gives

$$\begin{bmatrix} f_n(\alpha) \\ g_n(\alpha) \end{bmatrix} = \frac{-j\omega\mu}{2k^2\gamma_n\cos\left(\frac{\gamma_n b}{2}\right)} \begin{bmatrix} -j\alpha\left(\frac{n\pi}{a}\right) & k^2 - \frac{n^2\pi^2}{a^2} \\ k^2 - \alpha^2 & j\alpha\left(\frac{n\pi}{a}\right) \end{bmatrix} \begin{bmatrix} j_z(\alpha) \\ j_x(\alpha) \end{bmatrix} \tag{11}$$

If the Fourier transforms of the currents $j_z(\alpha)$ and $j_x(\alpha)$ are known, we can obtain $f_n(\alpha)$ and $g_n(\alpha)$ from (11). Subsequently, (2), (4) and (6) can be used to derive the scattered fields by substituting for $f_n(\alpha)$ and $g_n(\alpha)$ in those expressions. The remaining task is to solve for the transform currents $j_z(\alpha)$ and $j_x(\alpha)$, using the Galerkin's method applied in the transform domain.

First we express the corresponding space domain currents in terms of a linear combination of a set of suitable basis functions with unknown coefficients.

$$\begin{bmatrix} J_x(x,z) \\ J_z(x,z) \end{bmatrix} = \begin{bmatrix} \cos\left(\frac{n\pi}{a}x\right) \left[U_c \sum_{i=1}^{I} A_i P_i(z) + U_t A_0 P_0(z)\right] \\ \sin\left(\frac{n\pi}{a}x\right) \left[U_c \sum_{\ell=1}^{L} B_\ell q_\ell(z)\right] \end{bmatrix}$$

$$= \begin{bmatrix} \cos\left(\frac{n\pi}{a}x\right) J_x(z) \\ \sin\left(\frac{n\pi}{a}x\right) J_z(z) \end{bmatrix} \qquad (12)$$

where U_c and U_t are truncation functions on the septum and the strip, respectively,

$$U_c = \begin{cases} 1 & -c<z<0, \\ 0 & \text{otherwise} \end{cases}$$

$$U_t = \begin{cases} 1 & -(c+d+t)<z<-(c+d) \\ 0 & \text{otherwise} \end{cases}$$

and $p_0(z)$, $p_i(z)$, and $q_\ell(z)$ are basis functions to be defined later.

Since the post is assumed to be of very small radius, we model it as a strip of width t, which is also small. Hence, only the x-directed current on the strip is expected to be significant. In (12), the unknowns to be evaluated are the coefficients A's and B's. From (7) and (12) it can be seen that

$$\begin{bmatrix} j_x(\alpha) \\ j_z(\alpha) \end{bmatrix} = \begin{bmatrix} \sum_{i=0}^{I} A_i P_i(\alpha) \\ \sum_{\ell=1}^{L} B_\ell Q_\ell(\alpha) \end{bmatrix} \qquad (13)$$

where

$$P_i(\alpha) = \frac{1}{2\pi} \int_{-c}^{0} p_i(z) \exp(j\alpha z)\, dz, \qquad i = 1, 2, \ldots, I$$

$$P_0(\alpha) = \frac{1}{2\pi} \int_{-(c+d+t)}^{-(c+d)} p_0(z) \exp(j\alpha z)\, dz$$

$$Q_\ell(\alpha) = \frac{1}{2\pi}\int_{-c}^{0} q_\ell(z)\ \exp(j\alpha z)\ dz,\ \ell = 1, 2, \ldots, L \tag{14}$$

Replacing (13) in (11), one obtains the expressions for the transform domain functions $f_n(\alpha)$ and $G_n(\alpha)$:

$$\begin{bmatrix} f_n(\alpha) \\ \\ g_n(\alpha) \end{bmatrix} = \frac{-j\omega u}{2k^2\gamma_n \cos\left(\frac{\gamma_n b}{2}\right)} \begin{bmatrix} \left(k^2 - \frac{n^2\pi^2}{a^2}\right)\left(\sum_{i=0}^{I} A_i P_i(\alpha)\right) - j\alpha\frac{n\pi}{a}\left(\sum_{\ell=1}^{L} B_\ell Q_\ell(\alpha)\right) \\ \\ j\alpha\frac{n\pi}{a}\left(\sum_{i=1}^{I} A_i P_i(\alpha)\right) + (k^2-\alpha^2)\left(\sum_{\ell=1}^{L} B_\ell Q_\ell(\alpha)\right) \end{bmatrix} \tag{15}$$

Substituting these expressions in (2), (4) and (6) we obtain the final results for the scattered fields in terms of the unknown coefficients A's and B's. In order to find these unknown coefficients, we enforce the boundary condition for the electric field on the septum and the strip, which requires the total tangential component of the electric field to be zero, i.e.,

$$\begin{bmatrix} E_x^s \\ \\ E_z^s \end{bmatrix} = \begin{bmatrix} -E_x^i \\ \\ -E_z^i \end{bmatrix} \quad \text{at } y = \frac{b}{2} \tag{16}$$

Using (1), (2), and (15) in (16) we derive the following equations for A's and B's.

$$\left[k^2 - \left(\frac{n\pi}{a}\right)^2\right]\sum_{i=0}^{I} A_i \int_{-\infty}^{\infty} \frac{1}{\gamma_n} \tan\left(\frac{\gamma_n b}{2}\right) P_i(\alpha)\ \exp(-j\alpha z)\ d\alpha$$

$$-j\frac{n\pi}{a}\sum_{\ell=1}^{L} B_\ell \int_{-\infty}^{\infty} \frac{\alpha}{\gamma_n} \tan\left(\frac{\gamma_n b}{2}\right) Q_\ell(\alpha)\ \exp(-j\alpha z)\ d\alpha$$

$$= \begin{cases} \dfrac{-2\frac{n\pi}{a}\beta_{nm}}{\omega\mu}\ \dfrac{k^2}{k_c^2}\ e_{nm}\sin(\frac{m\pi}{2})\ \exp\ (\mp j\beta_{nm}z), & \text{for TM modes.} \\ 2\frac{m\pi}{b}\ \dfrac{k^2}{k_c^2}\ h_{nm}\ \sin(\frac{m\pi}{2})\ \exp\ (\mp j\beta_{nm}z), & \text{for TE modes.} \end{cases}$$

$$j\frac{n\pi}{a}\sum_{i=0}^{I} A_i \int_{-\infty}^{\infty} \frac{\alpha}{\gamma_n}\ \tan\ (\frac{\gamma_n b}{2})\ P_i(\alpha)\ \exp\ (-j\alpha z)\ d\alpha$$

$$+ \sum_{\ell=1}^{L} B_\ell \int_{-\infty}^{\infty} \frac{(k^2-\alpha^2)}{\gamma_n}\ \tan\ (\frac{\gamma_n b}{2})Q_\ell(\alpha)\ \exp\ (-j\alpha z)\ d\alpha$$

$$= \begin{cases} \mp \dfrac{2jk^2}{\omega\mu}\ e_{nm}\ \sin\ (\frac{m\pi}{2})\ \exp\ (\mp j\beta_{nm}z), & \text{for TM modes} \\ 0 & \text{, for TE modes} \end{cases} \qquad (17)$$

Now multiply both sides of (17) by the basis functions $p_i(z)$ and $q_\ell(z)$ and integrate over z to obtain the following equations.

$$(k^2 - \frac{n^2\pi^2}{a^2})\sum_{i=0}^{I} A_i \int_{-\infty}^{\infty} \frac{1}{\gamma_n}\ \tan\ (\frac{\gamma_n b}{2})\ P_i(\alpha)\ P_{i'}^*(\alpha)\ d\alpha$$

$$- j\frac{n\pi}{a}\sum_{\ell=1}^{L} B_\ell \int_{-\infty}^{\infty} \frac{\alpha}{\gamma_n}\ \tan\ (\frac{\gamma_n b}{2})\ Q_\ell(\alpha)\ P_{i'}^*(\alpha)\ d\alpha$$

$$= \begin{cases} \dfrac{-2(\frac{n\pi}{a})\beta_{nm}}{\omega\mu} \quad \dfrac{k^2}{k_c^2}\, e_{nm} \sin\dfrac{m\pi}{2} \begin{bmatrix} P_i^*,\ (\beta_{nm}) \\ P_{i'},\ (\beta_{nm}) \end{bmatrix} & , i'=0,1,..,I \text{ for TM modes} \\ 2(\frac{m\pi}{b}) \quad \dfrac{k^2}{k_c^2}\, h_{nm} \sin\dfrac{m\pi}{2} \begin{bmatrix} P_i^*,\ (\beta_{nm}) \\ P_{i'},\ (\beta_{nm}) \end{bmatrix} & , i'=0,1,..,I \text{ for TE modes} \end{cases}$$

$$j\frac{n\pi}{a} \sum_{i=0}^{I} A_i \int_{-\infty}^{\infty} \frac{\alpha}{\gamma_n} \tan(\gamma_n \frac{b}{2})\, P_i(\alpha)\, Q_{\ell}^*,(\alpha)\, d\alpha$$

$$+ \sum_{\ell=1}^{L} B_{\ell} \int_{-\infty}^{\infty} \frac{(k^2-\alpha^2)}{\gamma_n} \tan(\frac{\gamma_n b}{2})\, Q_{\ell}(\alpha)\, Q_{\ell}^*,(\alpha)\, d\alpha$$

$$= \begin{cases} \begin{bmatrix} - \\ + \end{bmatrix} \dfrac{2jk^2}{\omega\mu}\, e_{nm} \sin\dfrac{m\pi}{2} \begin{bmatrix} Q_{\ell}^*,\ (\beta_{nm}) \\ Q_{\ell},\ (\beta_{nm}) \end{bmatrix} & , \ell'=1,2,\ldots,L \text{ for TM modes} \\ 0 & , \ell'=1,2,\ldots,L \text{ for TE modes} \end{cases} \qquad (18)$$

The upper quantities within the square bracket in (18) are associated with positive z incident modes, and the lower quantities are associated with negative z incident modes. Both cases are included because we are interested in the transmission coefficients as well as the reflection coefficients. The integrals are evaluated by numerical integration, and the resulting system of linear equations is solved as usual for the unknowns A's and B's by matrix inversion.

The choice of basis functions, i.e., the p's and q's, is based on previous experience and the consideration of the behavior of the currents at the edges of the septum and the strip. Only two terms for the expansion of the currents on the septum are retained, which are believed to be adequate for this analysis. The basis functions and their Fourier transforms are shown in Table 1.

Let us now consider the case of interest, namely, one in which the incident fields are TE_{0_m} modes. We have n=0, and the following relations:

$$\gamma_0^2 = k^2 - \alpha^2 \tag{19}$$

$$\beta_{0m}^2 = k^2 - \left(\frac{m\pi}{b}\right)^2 \tag{20}$$

When n=0, (18) can be simplified to the following

$$\sum_{i=0}^{2} A_i \int_{-\infty}^{\infty} \frac{\tan\left(\frac{\gamma_0 b}{2}\right)}{\frac{\gamma_0 b}{2}} P_i(\alpha)\, P_{i'}^*(\alpha)\, d\alpha$$

$$= \frac{4}{m\pi} \sin\left(\frac{m\pi}{2}\right) h_{0m} \begin{bmatrix} P_{i'}^*, (\beta_{0m}) \\ P_{i'}, (\beta_{0m}) \end{bmatrix}, \quad i'=0, 1, 2$$

$$\sum_{\ell=1}^{2} B_\ell \int_{-\infty}^{\infty} \gamma_0 \tan\left(\frac{\gamma_0 b}{2}\right) Q_\ell(\alpha)\, Q_{\ell'}^*(\alpha)\, d\alpha = 0, \quad \ell'=1,2 \tag{21}$$

The equations for A's and B's are uncoupled. Therefore, A's and B's can be solved for separately. The system of equations for B's is homogeneous,

which leads to the conclusion that all B's are zero. Consequently, there are no components of the current in the z direction either in the septum or the strip. In the following development, only the system of equations for A's is investigated. Observe that the solution of A's involves an inversion of a 3 x 3 matrix, which is an easy task for the computer. However, the evaluation of the matrix elements involves nine complex integrals to be numerically integrated. Since there are singularities in these integrals, we must examine the integrands carefully to make sure that the numerical integration is applied correctly to give accurate results in spite of the singularities. Therefore, it is useful to write the expressions appearing in the integrands of (21) in an explicit manner as follows:

$$P_0P_0^* = \frac{t^2}{16\pi} \exp\left[-2\left(\frac{t\alpha}{4}\right)^2\right]$$

$$P_1P_0^* = \frac{ct}{16\sqrt{\pi}} J_0\left(\frac{c\alpha}{2}\right) \exp\left[-\left(\frac{t\alpha}{4}\right)^2\right] \exp\left[j\alpha\left(\frac{c}{2} + d + \frac{t}{2}\right)\right]$$

$$P_0P_1^* = \frac{ct}{16\sqrt{\pi}} J_0\left(\frac{c\alpha}{2}\right) \exp\left[-\left(\frac{t\alpha}{4}\right)^2\right] \exp\left[-j\alpha\left(\frac{c}{2} + d + \frac{t}{2}\right)\right]$$

$$P_2P_0^* = j\frac{ct}{16\sqrt{\pi}} J_1\left(\frac{c\alpha}{2}\right) \exp\left[-\left(\frac{t\alpha}{4}\right)^2\right] \exp\left[j\alpha\left(\frac{c}{2} + d + \frac{t}{2}\right)\right]$$

$$P_0P_2^* = -j\frac{ct}{16\sqrt{\pi}} J_1\left(\frac{c\alpha}{2}\right) \exp\left[-\left(\frac{t\alpha}{4}\right)^2\right] \exp\left[-j\alpha\left(\frac{c}{2} + d + \frac{t}{2}\right)\right]$$

$$P_1P_1^* = \frac{c^2}{16} J_0^2\left(\frac{c\alpha}{2}\right)$$

$$P_2P_2^* = \frac{c^2}{16} J_1^2\left(\frac{c\alpha}{2}\right) \qquad (22)$$

Note that $P_1P_2^*$, $P_2P_1^*$, etc. are not of interest here because the corresponding integrands are odd and therefore the integrals involving them are identically zero. Now observe that the integrand in (21) contains a simple pole located at $\alpha = \beta_{01}$ on the path of integration for $0 < \alpha < \infty$, provided that the wave number satisfies the following condition:

$$\frac{\pi}{b} < k < 3\frac{\pi}{b} \tag{23}$$

This is the case when the incident field is the dominant, propagating mode in the waveguide. Introduction of some loss in the medium clarifies the position of the poles along the integration path, as shown in Fig. 2. Each of the integrals in (21) can be written in the following form

$$\int_{-\infty}^{\infty} F(\alpha)d\alpha = \int_{-\infty}^{-\beta_{01}} F(\alpha)d\alpha + \int_{-\beta_{01}}^{\beta_{01}} F(\alpha)d\alpha + \int_{\beta_{01}}^{\infty} F(\alpha)d\alpha + \pi j \text{ Res } (-\beta_{01})$$

$$- \pi j \text{ Res } (\beta_{01}) = \int_{-\infty}^{-2\beta_{01}} F(\alpha)d\alpha + \int_{-2\beta_{01}}^{0} F(\alpha)d\alpha$$

$$+ \int_{0}^{2\beta_{01}} F(\alpha)d\alpha + \int_{2\beta_{01}}^{\infty} F(\alpha)d\alpha + \pi j \text{ Res } (-\beta_{01}) - \pi j \text{ Res } (\beta_{01})$$

$$= \int_{-\infty}^{-2\beta_{01}} F(\alpha)d\alpha + \int_{-\beta_{01}}^{0} [F(-2\beta_{01} - \alpha) + F(\alpha)]\, d\alpha$$

$$+ \int_{0}^{\beta_{01}} [F(\alpha) + F(2\beta_{01} - \alpha)]\, d\alpha$$

$$+ \int_{2\beta_{01}}^{\infty} F(\alpha)d\alpha + \pi j \text{ Res } (-\beta_{01}) - \pi j \text{ Res } (\beta_{01}) \tag{24}$$

In the above equation, a bar across the integral sign means principal value integration. The method of foldover as shown makes the new integrand remain bounded at the singularity of the old integrand; hence, this new integral is easily evaluated by the numerical method. Also, since the integrand goes to zero rapidly as α becomes large, the integration limit ∞ can be replaced by a large number, e.g., $14\ \beta_{01}$. It should be noted that if the foldover method was not used, the integral could still be evaluated numerically, in some cases, but the integration limit ∞ must be replaced by a much larger number because of the heavy tail of the integrand, and doing so requires increased computer time and the results are less accurate. The residues given in (24) are easily calculated and are given by the general form

$$\text{Res}(\pm\beta_{01}) = \frac{4}{b^2(\pm\beta_{01})}\ P_i\ (\alpha)\ P^*_{i'}\ (\alpha)\ \Big|_{\alpha\ =\ \pm\beta_{01}}\ ,\ i,\ i' = 0,\ 1,\ 2$$

with $P_i\ (\alpha)\ P^*_{i'}\ (\alpha)$ given in (22).

(25)

Having discussed the evaluation of the matrix elements in detail, we can proceed to solve the matrix equation (21) to obtain the A's. Having found these A's, we compute $f_0(\alpha)$ from (15) and then calculate the scattered fields from (2). For n=0, both E^s_z and $E^s_y = 0$, and there is only E^s_x, which can be written as

$$\begin{bmatrix} E^s_x\ (\frac{b}{2} < y < b) \\ E^s_x\ (0 < y < \frac{b}{2}) \end{bmatrix} = \int_{-\infty}^{\infty} \frac{-j\omega\mu_0}{2\gamma_0 \cos\left(\frac{\gamma_0 b}{2}\right)} \begin{bmatrix} \sum_{i=0}^{2} A_i P_i\ (\alpha) \end{bmatrix} \begin{bmatrix} \sin\ [\gamma_0\ (b-y)] \\ \sin\ \gamma_0\ y \end{bmatrix}$$

$$\exp\ (-j\alpha z)\ d\alpha \qquad (26)$$

$$\text{where } \gamma_0 = \begin{cases} \sqrt{k^2 - \alpha^2} & \text{if} \quad k > |\alpha| \\ j\sqrt{\alpha^2 - k^2} & \text{if} \quad k < |\alpha| \end{cases}$$

Let us evaluate (26) at $y = \frac{b}{2}$,

$$E_x^s(y=\frac{b}{2}) = \frac{-jkbZ_0}{4} \left[\sum_{i=0}^{2} A_i \int_{-\infty}^{\infty} \frac{\tan \frac{\gamma_0 b}{2}}{\frac{\gamma_0 b}{2}} P_i(\alpha) \exp(-j\alpha z)\, d\alpha \right] \tag{27}$$

Since the scattered fields on both sides of the beam equalizer are given by (27), we can compute the transmission and reflection coefficients by normalizing these scattered fields to the incident field given in (1). The reflection coefficient R can be expressed as

$$R = \frac{E_x^s}{E_x^i} \Bigg|_{\substack{y=\frac{b}{2} \\ z<0}}$$

$$= \frac{-\pi \exp(j\beta_{01} z)}{4\, h_{01}} \sum_{i=0}^{2} A_i \left[2\pi j \sum_{m=1,3,5,\ldots} \text{Res}_i(\zeta_m) \right] \tag{28}$$

where the poles are given by

$$\zeta_1 = -\beta_{01} = -\sqrt{k^2 - (\tfrac{\pi}{b})^2} \quad ; \qquad \zeta_{m\geq 3} = j\sqrt{(\tfrac{m\pi}{b})^2 - k^2}$$

and the residues at these poles are given by

$$\text{Res}_i(\zeta_1) = \frac{4\, P_i(-\beta_{01}) \exp(jz\beta_{01})}{b^2\, (-\beta_{01})}$$

$$\text{Res}_i(\zeta_m) = \text{Res}_i(j\chi_m) = \frac{4\, P_i(j\chi_m)\, \exp(\chi_m z)}{b^2(j\chi_m)} \quad , \qquad m \geq 3$$

with $\chi_m = \sqrt{(\frac{m\pi}{b})^2 - k^2}$

$$P_0(j\chi_m) = \frac{t}{4\sqrt{\pi}} \exp\left[\chi_m(c+d+\frac{t}{2})\right] \exp\left[(\frac{t\chi_m}{4})^2\right]$$

$$P_1(j\chi_m) = \frac{c}{4} \exp\left(\frac{\chi_m c}{2}\right) I_0\left(\frac{c}{2}\chi_m\right)$$

$$P_2(j\chi_m) = \frac{jc}{4} \exp\left(\frac{\chi_m c}{2}\right) jI_1\left(\frac{c}{2}\chi_m\right)$$

and I_0, I_1 are modified Bessel functions of the first kind. In deriving (28), the integral in (27) has been evaluated by the residue theorem with the contour closed in the upper half of the α-plane. By the same token, the transmission coefficient T can also be obtained, except this time the contour is closed in the lower half of the α-plane.

$$T = \left.\frac{E_x^s}{E_x^i}\right|_{\substack{y=\frac{b}{2} \\ z>0}}$$

$$= \frac{-\pi \exp(j\beta_{01}z)}{4h_{01}} \sum_{i=0}^{2} A_i \left[-2\pi j \sum_{m=1,3,5,\ldots} \text{Res}_i(\zeta_m)\right] \qquad (29)$$

where the poles are given by

$$\zeta_1 = \beta_{01} = \sqrt{k^2 - (\frac{\pi}{b})^2}$$

$$\zeta_{m\geq 3} = -j\sqrt{(\frac{m\pi}{b})^2 - k^2}$$

and the residues at these poles are given by

$$\text{Res}_i(\zeta_1) = \frac{4\, P_i(\beta_{01})\, \exp\,(-j\beta_{01} z)}{b^2 \beta_{01}}$$

$$\text{Res}_i(\zeta_m) = \text{Res}_i(-j\chi_m) = \frac{4\, P_i(-j\chi_m)\, \exp\,(-\chi_m z)}{b^2(-j\chi_m)} \quad , \quad m \geq 3$$

with $\chi_m = \sqrt{(\frac{m\pi}{b})^2 - k^2}$

$$P_0\,(-j\chi_m) = \frac{t}{4\sqrt{\pi}}\, \exp\,[-\chi_m(c+d+\frac{t}{2})]\, \exp\,[(\frac{t\chi_m}{4})^2]$$

$$P_1\,(-j\chi_m) = \frac{c}{4}\, \exp\,(-\frac{\chi_m c}{2})\, I_0\,(\frac{c}{2}\chi_m)$$

$$P_2\,(-j\chi_m) = \frac{jc}{4}\, \exp\,(-\chi_m \frac{c}{2})\, [-jI_1\,(\frac{c}{2}\chi_m)]$$

and I_0, I_1 are modified Bessel functions of the first kind. Numerical results indicate that minimum reflection and maximum transmission can be achieved if the separation between the septum and the strip is 0.1 wavelength for the given dimensions in Fig. 1.

The radiation pattern of the waveguide feed with beam equalizer can now be computed in the following manner. First, the aperture field distribution in the plane containing the waveguide mouth is estimated by a superposition of the waveguide mode field at this plane with each mode being weighted by the corresponding transmission coefficients for the modes. Since the transmission coefficients have been evaluated at a different reference plane, it is necessary to refer these transmission coefficients back to the aperture plane. This is done by multiplying the transmission

coefficients by an appropriate correcting factor, which is a phase factor for a propagating mode and is an exponential factor for an attenuated mode. The radiation pattern is then obtained by the familiar Fourier transform relation between the far field and the aperture field. For TE_{nm} modes, the far fields are given by the following expressions [2]:

$$E_\theta = -\left(\frac{\mu}{\varepsilon}\right)^{1/2} \frac{(\pi ab)^2 \sin\theta}{2\lambda^3 r\, k_{nm}^2} \left[1 + \frac{\beta_{nm}}{k}\cos\theta + R\left(1 - \frac{\beta_{nm}}{k}\cos\theta\right)\right]$$

$$\cdot \left[\left(\frac{n\pi}{a}\sin\phi\right)^2 - \left(\frac{m\pi}{b}\cos\phi\right)^2\right] \Psi_{nm}(\theta,\phi)$$

$$E_\phi = -\left(\frac{\mu}{\varepsilon}\right)^{1/2} \frac{(\pi ab)^2 \sin\theta \sin\phi \cos\phi}{2\lambda^3 r}$$

$$\cdot \left[\cos\theta + \frac{\beta_{nm}}{k} + R\left(\cos\theta - \frac{\beta_{nm}}{k}\right)\right] \Psi_{nm}(\theta,\phi) \qquad (30)$$

with

$$\Psi_{nm}(\theta,\phi) = \left[\frac{\sin\left(\frac{\pi a}{\lambda}\sin\theta\cos\phi + \frac{n\pi}{2}\right)}{\left(\frac{\pi a}{\lambda}\sin\theta\cos\phi\right)^2 - \left(\frac{n\pi}{2}\right)^2}\right] \cdot \left[\frac{\sin\left(\frac{\pi b}{\lambda}\sin\theta\sin\phi + \frac{m\pi}{2}\right)}{\left(\frac{\pi b}{\lambda}\sin\theta\sin\phi\right)^2 - \left(\frac{m\pi}{2}\right)^2}\right]$$

$$\cdot \exp\left\{-j\left[kr - \frac{\pi}{\lambda}\sin\theta\,(a\cos\phi + b\sin\phi) - (n+m+1)\frac{\pi}{2}\right]\right\}$$

where (r,θ,ϕ) are the conventional right-handed spherical coordinates. The total radiation pattern is then obtained by a superposition of these individual mode patterns with the appropriate transmission coefficients referenced at the aperture plane. Computed patterns and numerical results are presented in the next section.

III. Computed Results

The performance of the square waveguide feed with beam equalizer whose dimensions are shown in Fig. 1 with $d = 0.1\lambda$ is evaluated over a frequency band of operation. The value for c has been chosen experimentally to be 0.25λ. The computed radiation patterns in the E- and H-planes are presented in Figure 3. The beam equalization is quite satisfactory over the entire band. The corresponding aperture field distributions are shown in Figure 4. Looking at these aperture distributions,[1] one can explain how the beam equalizer works. It goes as follows. The aperture distribution for the E-plane pattern is uniform which gives a familiar (sin x)/x type of pattern. The H-plane pattern is due to a cosine-taper type of aperture distribution if there is no beam equalizer present. Hence, the beamwidth is larger than that of the E-plane pattern for a square waveguide aperture. However, the introduction of the beam equalizer forces the H-plane aperture field to vanish at the center of the aperture, which makes the field distribution look more uniform. Hence, the main lobe of the H-plane pattern narrows to achieve the beam equalization effect in the E- and H-planes. The pattern is mainly determined by the septum; the post is present for

[1] These curves are generated using only the first three terms in the modal series expansion. While the boundary conditions at the waveguide walls are satisfied perfectly by definition of the modal functions, there appears to be a small residue of E_x at the septum in the middle of the waveguide. This residue is solely due to the truncation of an infinite series to a finite number of terms. Perfect cancellation can be approached when more and more terms are used in the series.

impedance matching. The computed reflection coefficients over the frequency band are shown in Table 2. If the post is absent, the reflection coefficients will be much larger than those shown in Table 2.

IV. Conclusions

A septum and an impedance matching post used as a beam equalizer in an open-ended waveguide-feed for reflectors used in satellite communications systems have been analyzed by using a spectral domain approach. The computed radiation patterns in the E- and H-planes, as well as the impedance match results, have been presented in the paper. The performance of the beam equalizer over the entire band of operating frequency has been evaluated. The results indicate that the E- and H-plane principally polarized patterns are equalized extremely well over the entire frequency band of operation and that the impedance matching is also satisfactory.

Acknowledgement

The authors are grateful to Dr. C. C. Han and Dr. Y. M. Hwang of Ford Aerospace Company for bringing the problem to their attention, and for helpful suggestions and technical guidance. This work was sponsored in part by Ford Aerospace and Communications Corporation and in part by Office of Naval Research under Grant N00014-75-C-0293.

References

[1] R. Mittra and T. S. Li, "A spectral domain approach to the numerical solution of electromagnetic scattering problems," AEÜ, vol. 29, pp. 217-222, 1975.

[2] S. Silver, Microwave Antenna Theory and Design, M.I.T. Radiation Laboratory Series, McGraw-Hill Company, New York, 1949.

Table 1. BASIS FUNCTIONS IN SPATIAL AND SPECTRAL DOMAINS

Spatial Domain	Spectral Domain
$p_0(z) = \exp\left[-\left(\frac{z+c+d+\frac{t}{2}}{\frac{t}{2}}\right)^2\right]$	$P_0(\alpha) = \frac{t}{4\sqrt{\pi}} \exp\left[-j\alpha\left(c+d+\frac{t}{2}\right)\right] \exp\left[-\left(\frac{t\alpha}{4}\right)^2\right]$
$p_1(z) = \frac{1}{\sqrt{1-\left(\frac{z+c/2}{c/2}\right)^2}}$	$P_1(\alpha) = \frac{c}{4} \exp\left(-j\alpha\frac{c}{2}\right) J_0\left(\frac{c\alpha}{2}\right)$
$p_2(z) = \frac{\frac{z+c/2}{c/2}}{\sqrt{1-\left(\frac{z+c/2}{c/2}\right)^2}}$	$P_2(\alpha) = \frac{jc}{4} \exp\left(-j\frac{\alpha c}{2}\right) J_1\left(\frac{c\alpha}{2}\right)$
$q_1(z) = \sqrt{1-\left(\frac{z+c/2}{c/2}\right)^2}$	$Q_1(\alpha) = \frac{c}{4} \exp\left(-j\frac{c\alpha}{2}\right) \frac{J_1\left(\frac{c\alpha}{2}\right)}{\frac{c\alpha}{2}}$
$q_2(z) = \frac{z+c/2}{c/2} \sqrt{1-\left(\frac{z+c/2}{c/2}\right)^2}$	$Q_2(\alpha) = \frac{jc}{4} \exp\left(-j\frac{c\alpha}{2}\right) \frac{J_2\left(\frac{c\alpha}{2}\right)}{\frac{c\alpha}{2}}$

J_0, J_1, and J_2 are Bessel functions of the first kind and of order zero, one, and two, correspondingly.

TABLE 2

REFLECTION COEFFICIENTS OVER THE FREQUENCY BAND

$d = 0.1\lambda$

Frequency (GHz)	Reflection coefficient R	VSWR = $\frac{1+\lvert R\rvert}{1-\lvert R\rvert}$
3.75	$0.2729/\underline{-130.25}°$	1.751
3.85	$0.1879/\underline{-134.90}°$	1.463
3.95	$0.1071/\underline{-142.02}°$	1.240
4.05	$0.0358/\underline{-167.87}°$	1.074
4.15	$0.0442/\underline{73.10}°$	1.092

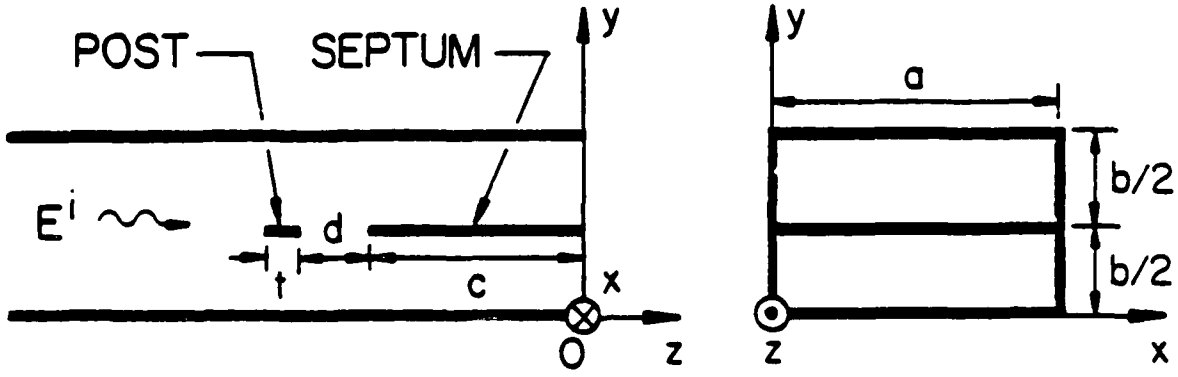

$a = 1.3\ \lambda$

$b = 1.3\ \lambda$

$c = 0.25\ \lambda$

d IS VARIABLE

$t = 0.062\ \lambda$

$f = 3.95$ GHz

$\lambda = 0.076$ m

Figure 1. Geometry of the waveguide with septum and post.

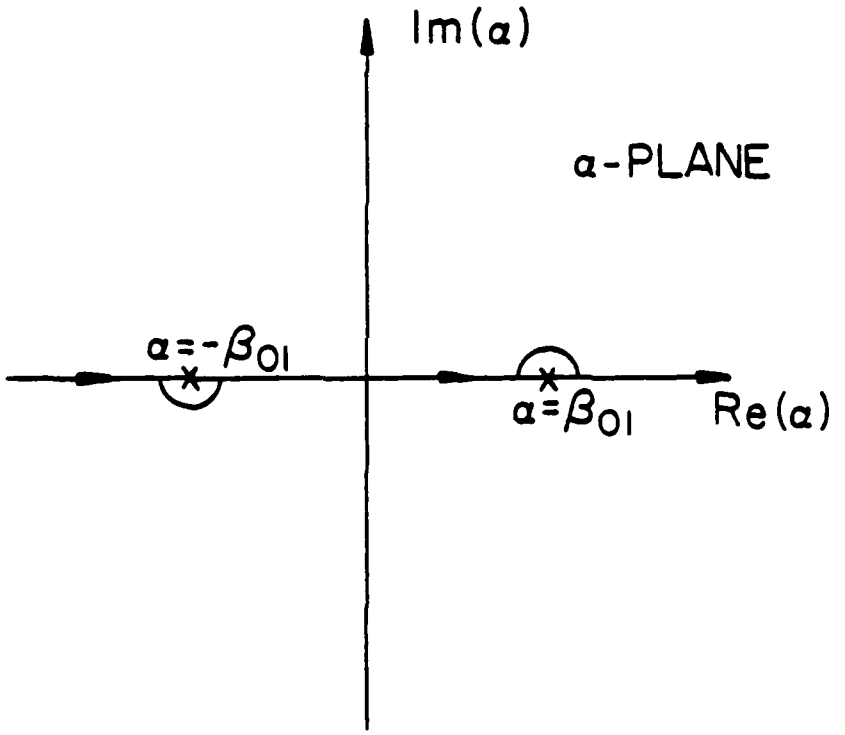

Figure 2. Location of poles in the integration path of integrals in Eq. (21).

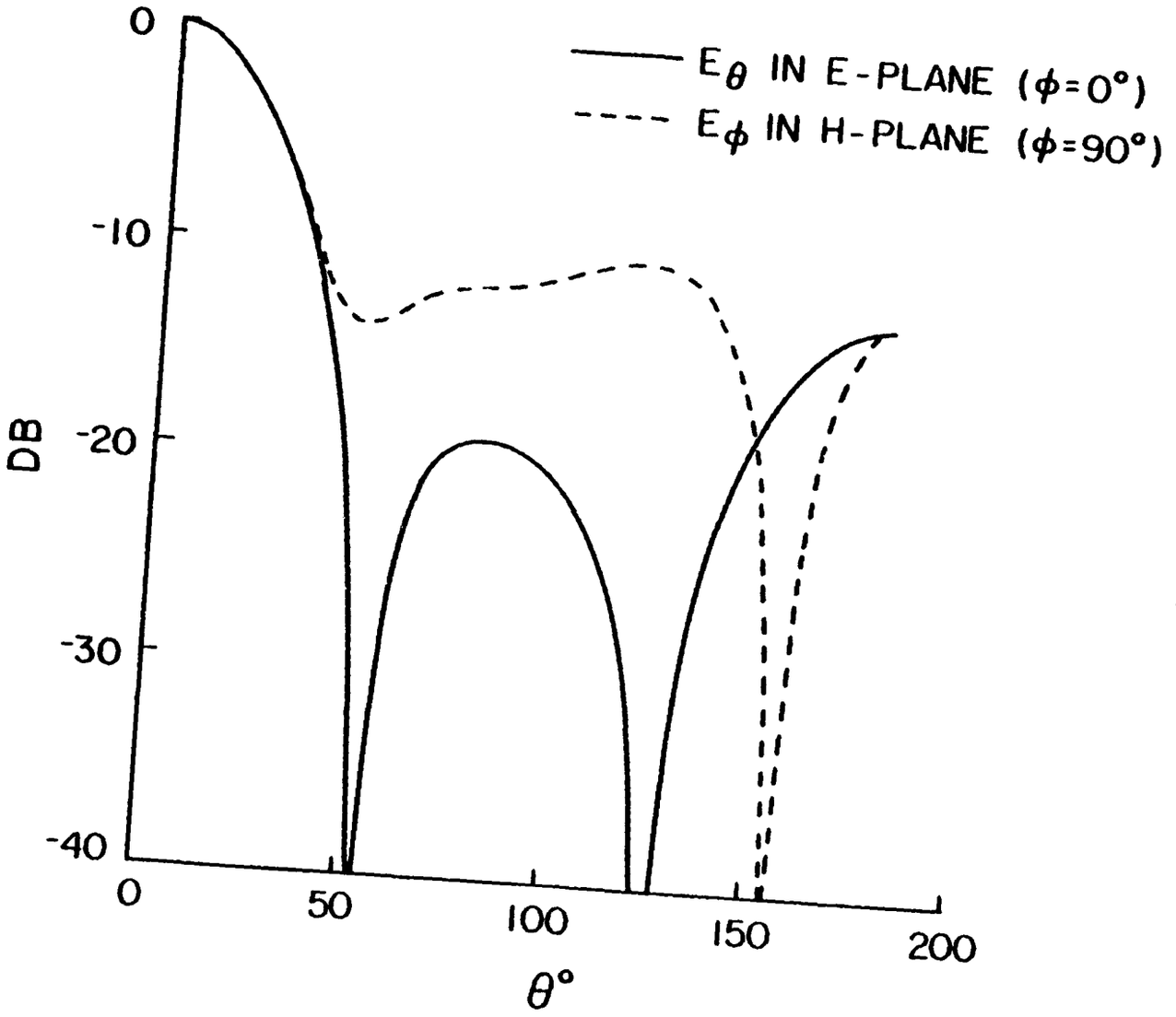

Figure 3(a). Radiation patterns in E- and H-planes at lower bandedge of a 10% center frequency band.

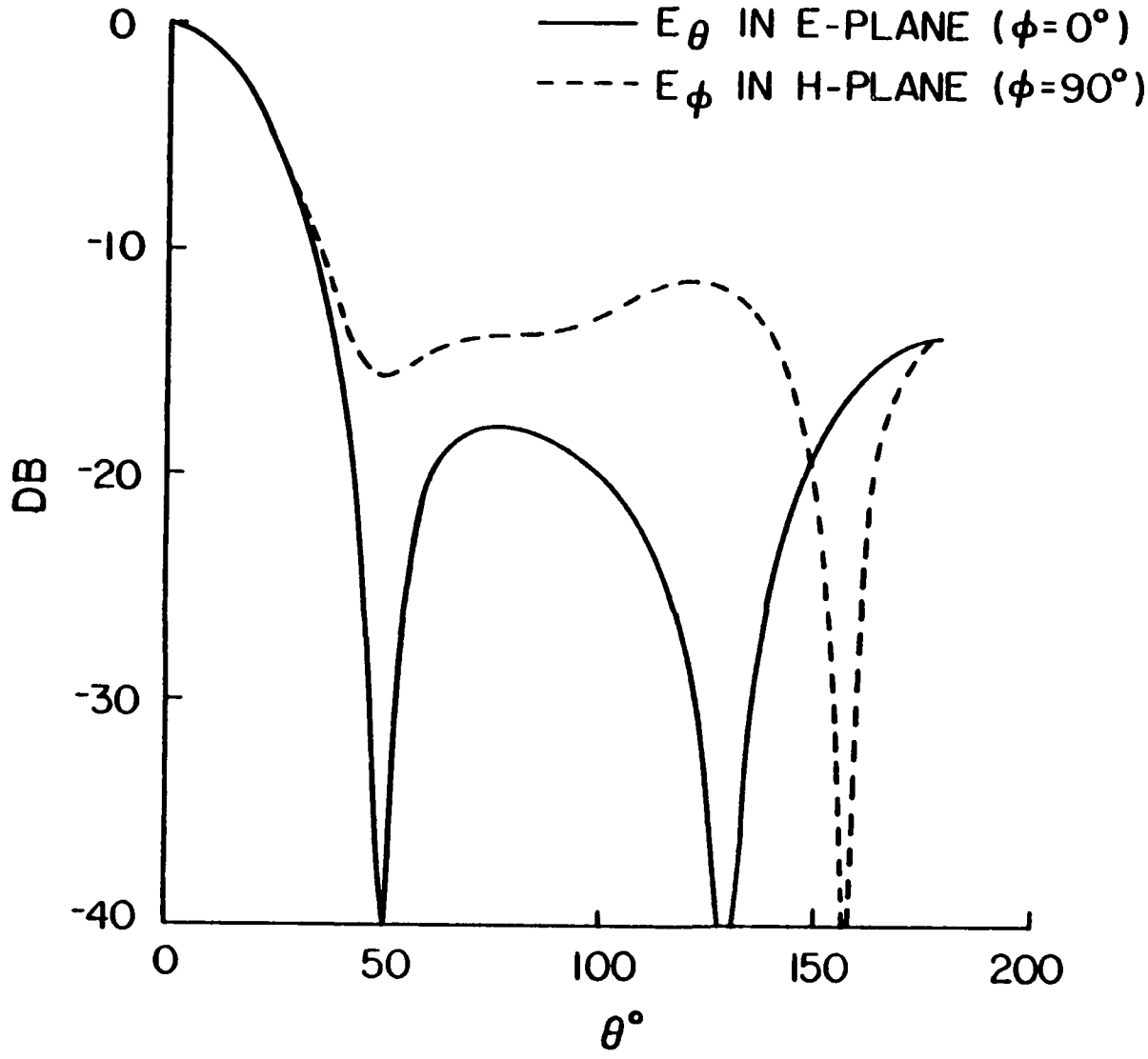

Figure 3(b). Radiation patterns in E- and H-planes at center frequency of a 10% center frequency band.

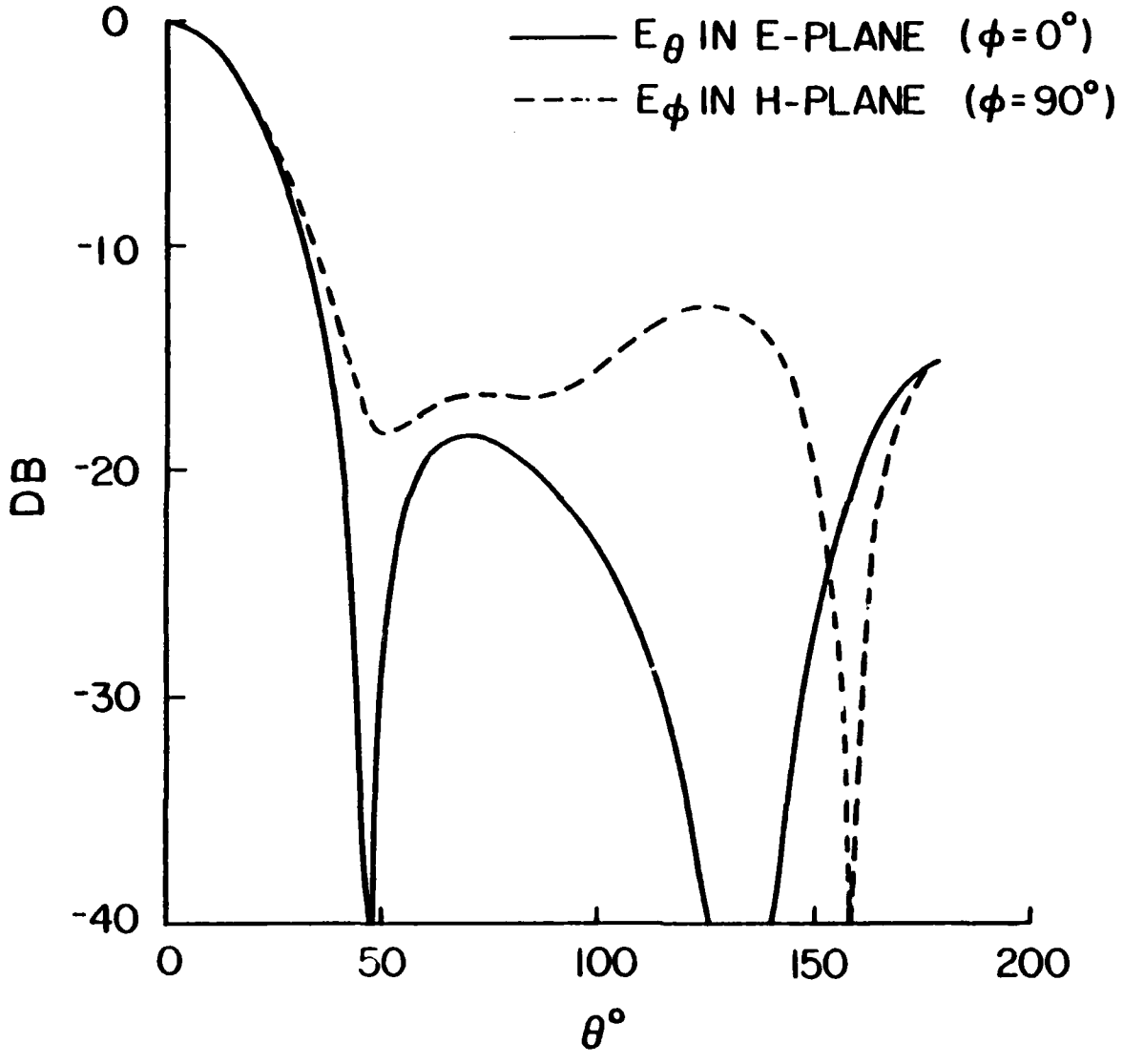

Figure 3(c). Radiation patterns in E- and H-planes at upper bandedge of a 10% center frequency band.

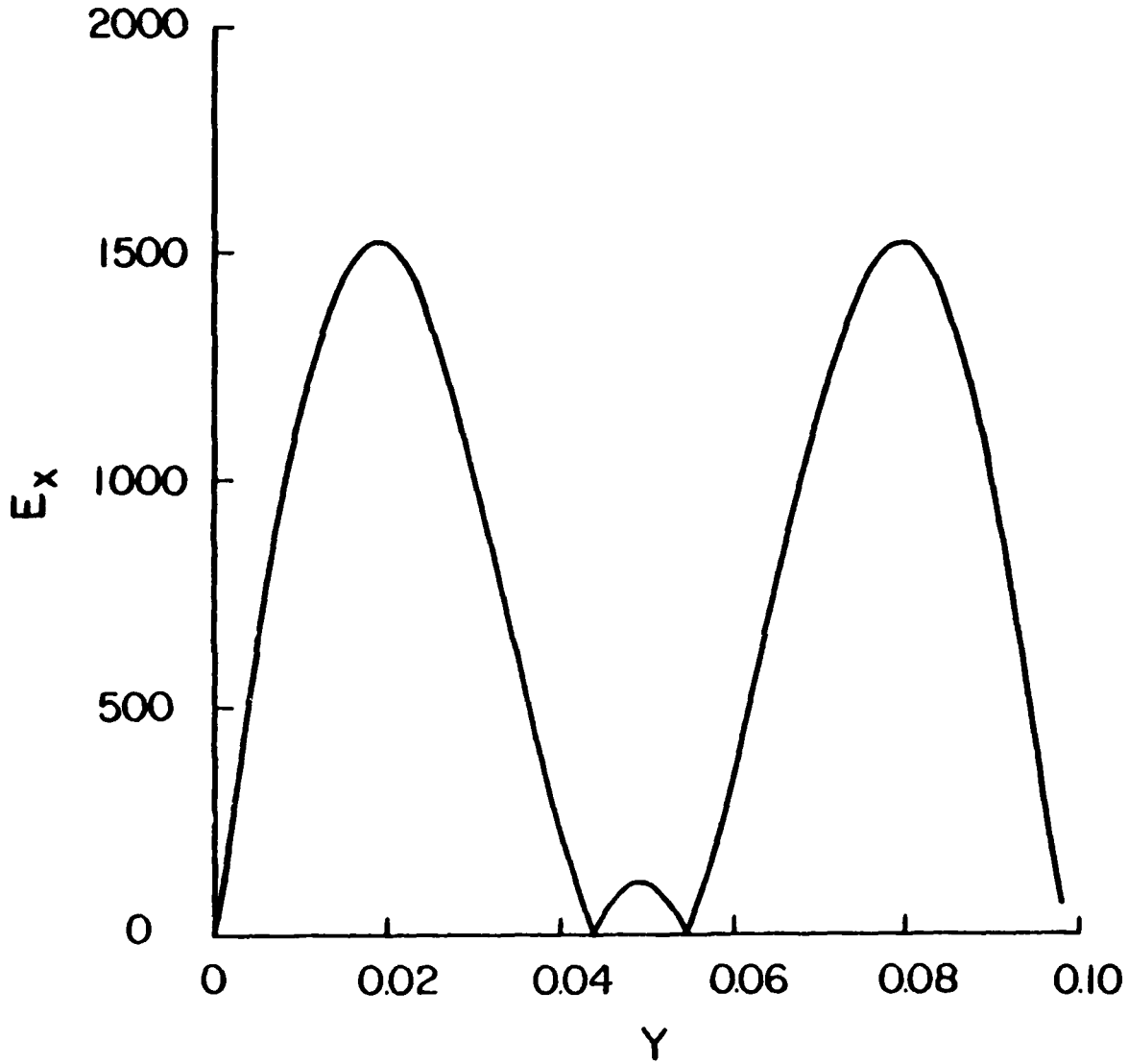

Figure 4(a). Aperture distribution at lower bandedge of a 10% center frequency band.

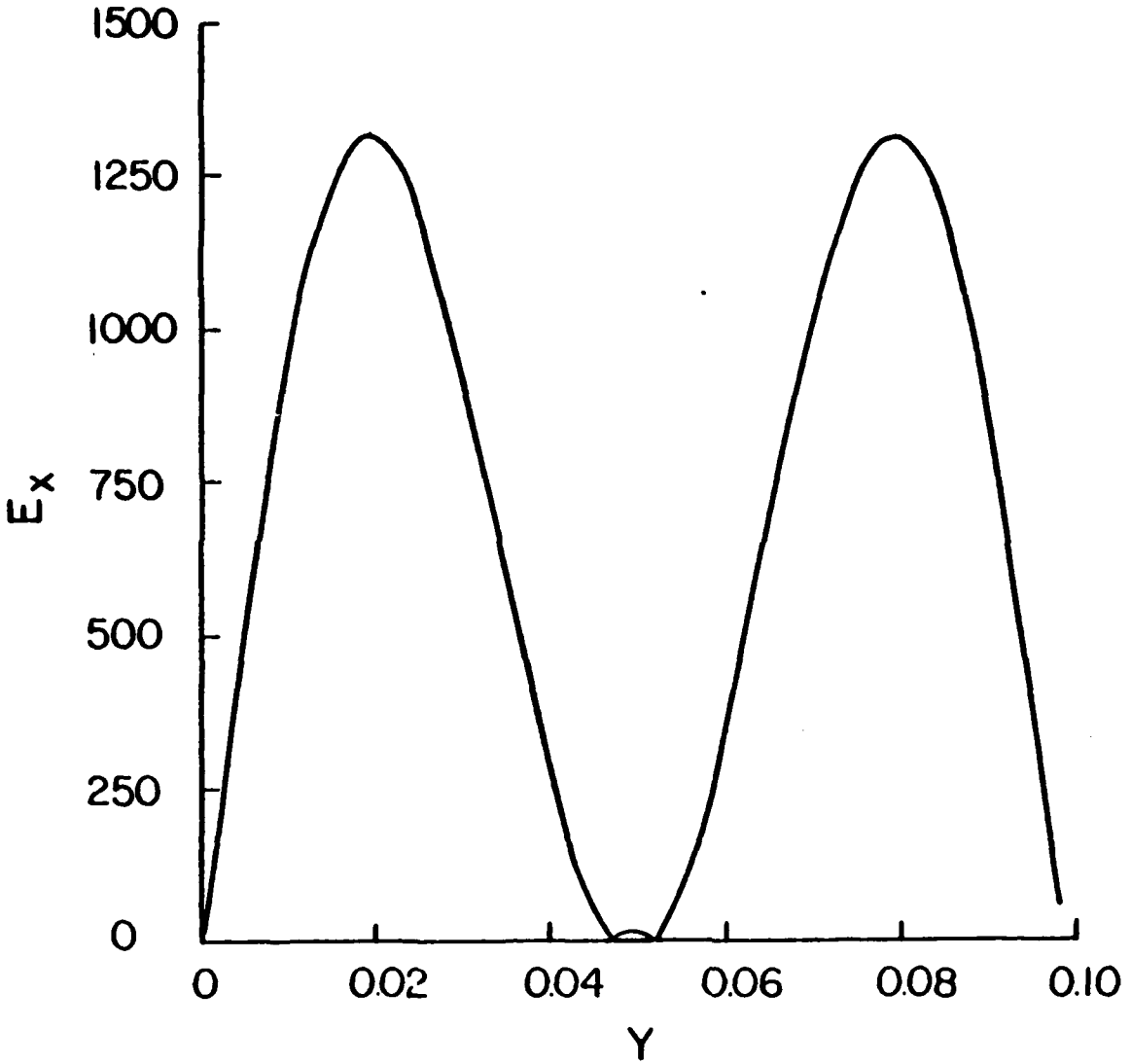

Figure 4(b). Aperture distribution at center frequency of a 10% center frequency band.

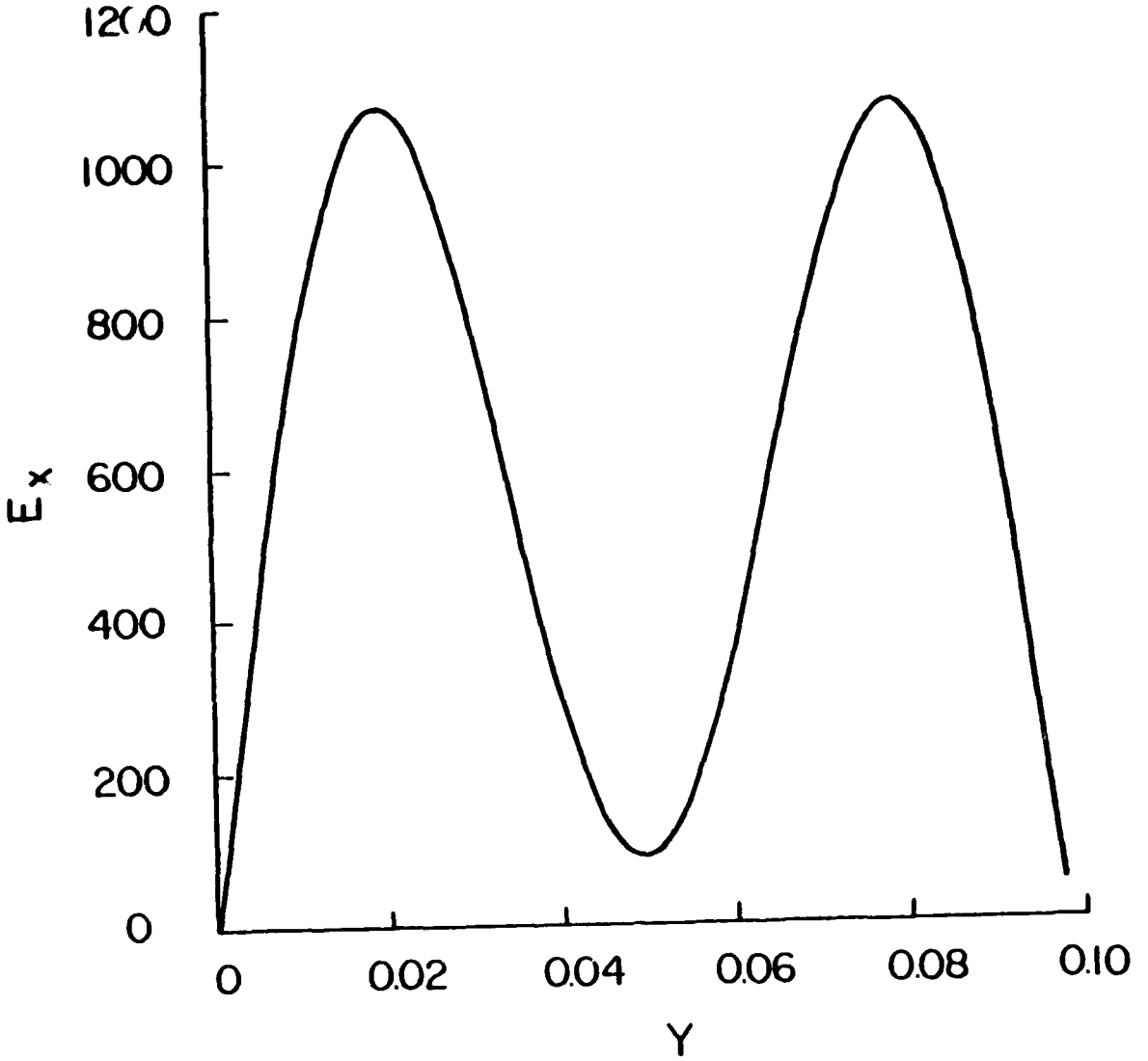

Figure 4(c). Aperture distribution at upper bandedge of a 10% center frequency band.

APPENDIX D

A SPECTRAL-ITERATION APPROACH FOR ANALYZING SCATTERING FROM FREQUENCY SELECTIVE SURFACES

by

CHICH-HSING TSAO

RAJ MITTRA

ABSTRACT

In this paper, we apply a novel technique, called the spectral-iteration approach, for analyzing the problem of scattering from periodically perforated screens which find useful applications as radomes, optical filters, artificial dielectrics, and so on. The formulation is carried out in the spectral domain where a set of algebraic equations is obtained directly for the spectral coefficients of the aperture field distribution (or the induced current density) rather than via an integral equation formulation. These equations are then solved simultaneously using an iterative procedure developed in this pape. that circumvents the need for matrix inversion. Because the matrix solution is avoided in the spectral approach, it is capable of handling large aperture sizes in a computationally efficient manner. The efficiency of computation results from the use of the FFT (Fast Fourier Transform) algorithm which is employed in the derivation of the algebraic equations and in the iteration procedure. A unique feature of the spectral-iteration approach is that it has a built-in boundary-condition check which provides a reliable indication of the accuracy of the solution. This paper also shows that the spectral domain technique can be applied to even a wider class of geometries, e.g., the step discontinuity in a waveguide.

The work was supported by the Office of Naval Research, Contract N00014-75-C-0293.

I. INTRODUCTION

Periodic structures such as arrays of conducting strips or periodically perforated screens which can be either free-standing or printed on dielectric substrates (see Fig. 1) have frequency selective properties, and find many applications as artificial dielectrics, optical and quasi-optical devices, and dichroic surfaces for antenna reflectors and radomes.

Conventionally, the problem of electromagnetic scattering from these periodic structures is attacked using the mode-matching procedure employed in conjunction with the method of moments. A description of this procedure can be found in a number of papers on the subject by Chen [1], Lee [2], and McPhedran and Maystre [3]. Though this method works quite well in the low-frequency region, it becomes prohibitively costly if not impractical at the high frequency region where the aperture size is one to two wavelengths, or larger, because the matrix size required for an accurate solution becomes prohibitively large and the numerical computation becomes extremely time-consuming and costly. The high frequency techniques, e.g., GTD, cannot be applied to circumvent the above difficulty either, because the complex geometrical configuration of the structure does not lend itself to the ray formalism of GTD. In this paper we introduce a new technique based on the spectral domain approach which provides an efficient and accurate solution to the grating problems described in this paper.

As a first step, the new approach begins with the formulation of the problem in terms of an integral equation in the transform domain. The standard procedure for deriving the integral equation for the unknown aperture field (or the induced current) is still followed; however, in the transform domain the convolution form of the integral equation becomes

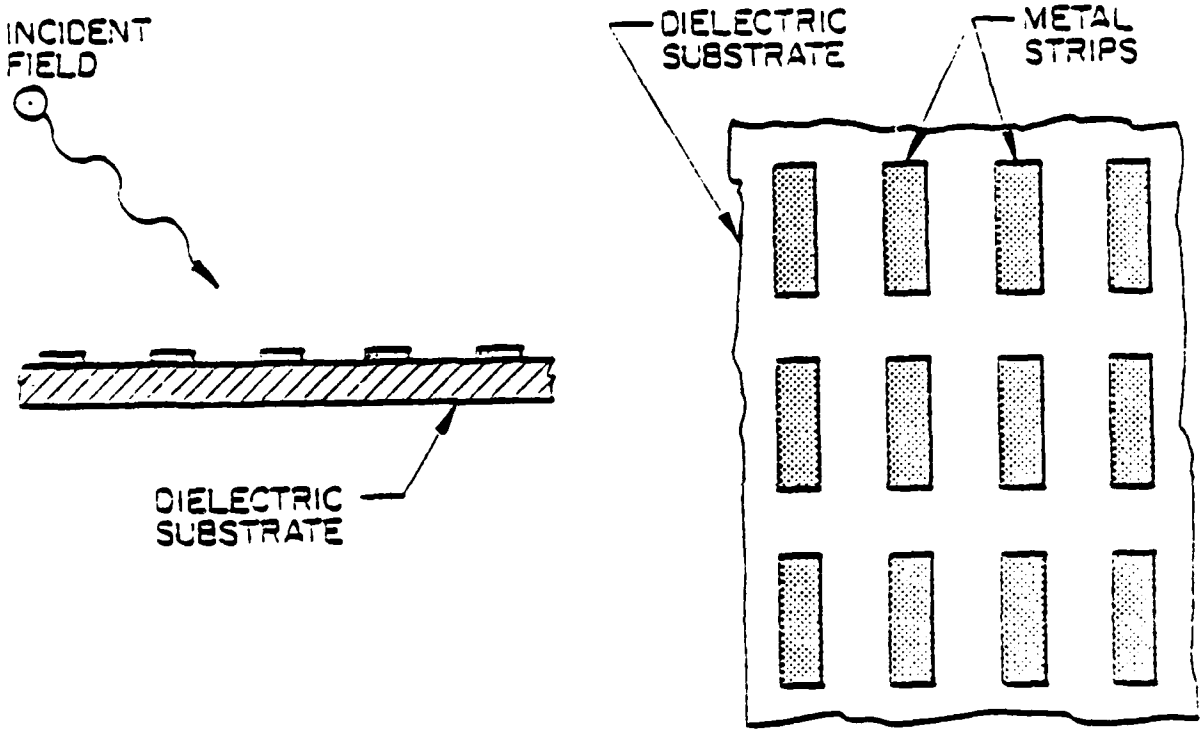

(a) Side view (b) Top view

Figure 1. Frequency Selective Surface.

an algebraic one. Furthermore, because of the periodic nature of the structure, the transform naturally takes the form of DFT (discrete Fourier transform) which can, in turn, be efficiently evaluated using the FFT (fast Fourier transform) algorithm. The transformed integral equation is subsequently solved, using an iterative procedure, simultaneously for the aperture field and the induced current. It is evident that the method avoids the time-consuming steps of evaluating the matrix elements and their subsequent inversion. More importantly, the problem of storing and handling over-sized matrices is circumvented even at high frequencies, where the number of unknowns can exceed the figure 2000. An added feature of the method is that a built-in step in the iterative procedure provides a convenient measure for the boundary condition check, a feature not readily available in conventional approaches. Finally, the convergence of the iterative procedure is enhanced by combining it with a variational approach in a manner explained later. For completeness, we mention that an approach similar to the present one has been used by Mittra and Ko [4] in studying the single-scatterer (as opposed to the periodic grating) problem. The above authors have used the GTD solution as the zeroth order approximate solution and have also employed an iterative procedure to generate the final solution. However, to-date this procedure has not been applied to the grating problems being considered in this paper.

In the next section, we present the formulation of the periodic grating problem. In Section 3, we describe the iterative procedure. In Section 4 we illustrate the application of the technique to a number of practical geometries. Finally, we demonstrate in Section 5 that the approach is useful for a class of closed-region problems, e.g., waveguide discontinuities. A brief summary of the paper is included in Section 6 and some conclusions are presented.

II. FORMULATION

For the sake of illustrating the spectral approach, we consider the problem of a uniform plane wave scattered from a free-standing periodically perforated conducting screen shown in Fig. 2. However, the method of solution is easily and conveniently extendable to the case of a screen on a dielectric substrate.

Due to the periodicity of the structure, the electric field on either side of the screen can be expanded in terms of the Floquet space harmonics. Using the $e^{j\omega t}$ time convention (suppressed), we can write

$$\begin{pmatrix} E_x \\ E_y \end{pmatrix} = \begin{pmatrix} E_x^i \\ E_y^i \end{pmatrix} + \sum_{m=-\infty}^{\infty} \sum_{n=-\infty}^{\infty} \begin{pmatrix} X_{mn}^+ \\ Y_{mn}^+ \end{pmatrix} \psi_{mn} e^{\gamma_{mn} z} \quad \text{for } z > 0,$$

and (1)

$$\begin{pmatrix} E_x \\ E_y \end{pmatrix} = \sum_{m=-\infty}^{\infty} \sum_{n=-\infty}^{\infty} \begin{pmatrix} X_{mn}^- \\ Y_{mn}^- \end{pmatrix} \psi_{mn} e^{-\gamma_{mn} z} \quad \text{for } z < 0$$

where $\vec{E}^i$ represents the incident field, (X_{mn}^+, Y_{mn}^+) and (X_{mn}^-, Y_{mn}^-) are the reflection and the transmission coefficients of the Floquet's harmonic modes, respectively and ψ_{mn}'s stand for the Floquet mode functions, given by

$$\psi_{mn} = \exp[j(u_{mo} x + v_{mn} y)]$$

where

$$u_{mo} = \frac{2\pi m}{a} - k \sin\theta \cos\phi \ ,$$

$$m,n = 0, \pm 1, \pm 2, \ \ldots$$

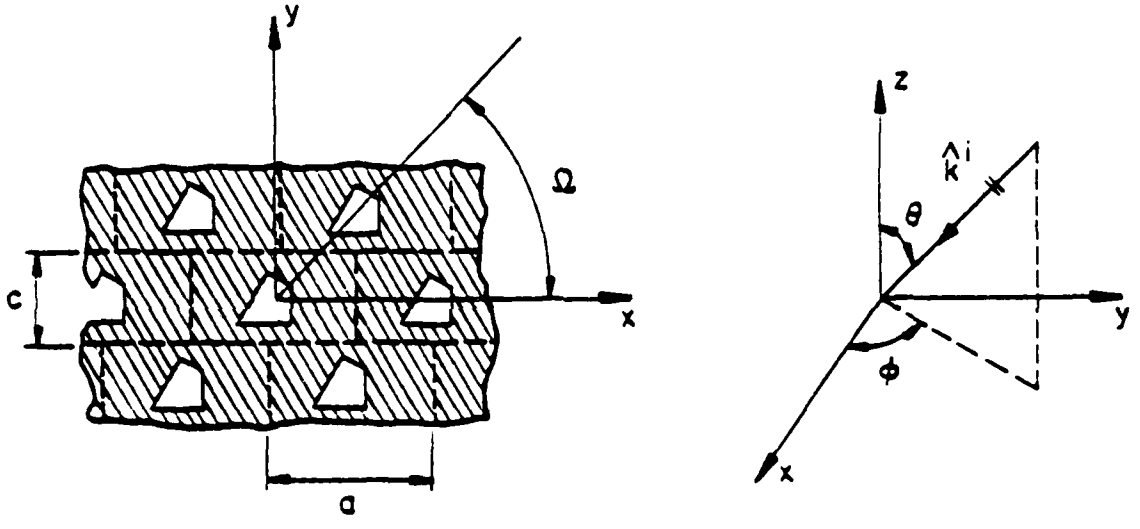

Figure 2. Free-standing, periodically perforated screen illuminated by a plane wave propagating in $\hat{k}^i$ direction.

$$v_{mn} = \frac{2\pi n}{c} - \frac{2\pi m}{a} \cot \Omega - k \sin \vartheta \sin \flat \ ,$$

and

$$\gamma_{mn} = \begin{cases} -j[k^2 - (u_{mo}^2 + v_{mn}^2)]^{1/2} & \text{if } k^2 > (u_{mo}^2 + v_{mn}^2) \\ -[(u_{mo}^2 + v_{mn}^2) - k^2]^{1/2} & \text{if } k^2 < (u_{mo}^2 + v_{mn}^2) \end{cases} .$$

The z-component of the E-field can be derived from (1) using the divergence theorem.

Enforcing the condition that the tangential field is continuous across the interface, we obtain

$$X_{mn}^{+} = X_{mn}^{-} \ , \ Y_{mn}^{+} = Y_{mn}^{-} \text{ when } m \neq 0 \text{ or } n \neq 0$$

and

$$X_{oo}^{+} + E_x^i = X_{oo}^{-} \ , \ Y_{oo}^{+} + E_y^i = Y_{oo}^{-} \ .$$

The H-field in the region $z > 0$ and $z < 0$ can be derived from Equation (1). Evaluating the H-field at $z = 0^{-}$ and $z = 0^{+}$, subtracting the expression for one from the other, and making use of the requirement that the tangential components be continuous across the aperture, one arrives at the equation:

$$\frac{1}{-j\omega\mu} \sum_{m=-\infty}^{\infty} \sum_{n=-\infty}^{\infty} \begin{pmatrix} A_{mn} & B_{mn} \\ C_{mn} & -A_{mn} \end{pmatrix} \begin{pmatrix} X_{mn}^{-} \\ Y_{mn}^{-} \end{pmatrix} \psi_{mn} = \begin{pmatrix} -H_x^i + \hat{\vartheta}\left(\frac{1}{2} J_y\right) \\ -H_y^i + \hat{\vartheta}\left(\frac{1}{-2} J_x\right) \end{pmatrix} \text{ for } z = 0 \qquad (2)$$

where $\vec{H}^i$ is the incident H-field,

$\vec{J}$ is the induced current on the surface,

$A_{mn} = u_{mo} \cdot v_{mn} / \gamma_{mn}$,

$B_{mn} = v_{mn}^2 / \gamma_{mn} - \gamma_{mn}$,

$C_{mn} = \gamma_{mn} - u_{mo}^2 / \gamma_{mn}$,

In (2) we have used the notation that for a function $f(\vec{r})$ defined on the $z = 0$ plane, where $\vec{r}$ is the position vector on that plane, the truncation operator ϑ is defined by

$$\vartheta(f(\vec{r})) = 0 \qquad \text{for } \vec{r} \text{ on the conducting surface}$$
$$= f(\vec{r}) \qquad \text{for } \vec{r} \text{ in the aperture}$$

and

$$\hat{\vartheta}(f(\vec{r})) = f(\vec{r}) - \vartheta(f(\vec{r})) \ .$$

The obvious identity $\hat{\vartheta}(\vec{J}) = \vec{J}$ and that $\hat{z} \times [\vec{H}(z = 0^+) - \vec{H}(z = 0^-)] = \vec{J}$ have also been used in deriving (2).

Unlike the integro-differential equation in the conventional method, which applies only in the aperture (or strip) region, (2) is valid over the entire surface. The price paid for extending the equation to the full range is the introduction of an extra unknown $\vec{J}$. However, as we will soon see, the additional unknown $\vec{J}$ can be solved for along with the aperture field using the iterative procedure discussed in the next section.

III. ITERATIVE PROCEDURE

The summation involved in (1) and (2) can be readily identified as the DFT operation. Let F be the operator representing the DFT, and let $\vec{\tilde{E}}_t$ represent the tangential electric field in the transformed domain. Identifying $(\tilde{X}_{mn}, \tilde{Y}_{mn})$ in (2) as the Fourier coefficients of $\vec{\tilde{E}}_t$, and writing $\tilde{G}$ for the matrix

$$\begin{pmatrix} A_{mn} & B_{mn} \\ C_{mn} & -A_{mn} \end{pmatrix}$$

we can write (2) symbolically as

$$F(\tilde{G}\cdot\vec{\tilde{E}}_t) = -\vec{\tilde{H}}_t^i + \hat{\vartheta}(\vec{J}) \quad , \tag{3}$$

where the subscript t indicates the tangential components, and it is understood that all the quantities are evaluated at $z = 0$.

If the induced current were available, the solution for $\vec{\tilde{E}}_t$ could be immediately obtained by invoking (3) and by using

$$\vec{\tilde{E}}_t = \tilde{G}^{-1}(F^{-1}(-\vec{\tilde{H}}_t^i + \hat{\vartheta}(\vec{J}))) \quad . \tag{4}$$

In practice, however, $\vec{J}$ is the unknown to be solved for, together with $\vec{\tilde{E}}_t$ and hence (4) cannot be used directly. Instead of using (4), a recursive relation between the $(n+1)^{th}$ approximate solution $\vec{\tilde{E}}_t^{(n+1)}$ and the n^{th} approximation $\vec{\tilde{E}}_t^{(n)}$ is now derived and the two unknowns $\vec{\tilde{E}}_t$ and $\vec{J}$ are solved for simultaneously using an iterative procedure.

To derive the recursion formula for $\vec{\tilde{E}}_t^{(n)}$, we begin with (3), which relates $\vec{J}^{(n)}$ and $\vec{\tilde{E}}^{(n)}$, and write

$$\hat{\vartheta}(\vec{J}^{(n)}) = F(\tilde{G}\cdot\vec{\tilde{E}}_t^{(n)}) + \vec{H}_t^i \quad . \tag{5}$$

Substituting (5) into (4), one obtains

$$\vec{\tilde{E}}_t^{(n+1)} = \tilde{G}^{-1}(F^{-1}(-\vec{H}_t^i + \hat{\vartheta}(F(\tilde{G}\cdot\vec{\tilde{E}}_t^{(n)}) + \vec{H}_t^i))) \quad . \tag{6}$$

Equation (6) is the desired recursive formula. Before inserting $\vec{E}_t^{(n)}$ into (5), we adjust its amplitude by multiplying with a scale factor K, computed according to the variation expression

$$K = \frac{\langle \vec{E}_t^{(n)}, -\vec{H}_t^i \rangle}{\langle \vec{E}_t^{(n)}, F(\tilde{G}\cdot\vec{\tilde{E}}_t^{(n)}) \rangle} \tag{7}$$

where $\langle f, g \rangle = \int_{\text{aperture}} f\cdot g\cdot da$.

Equation (7) is obtained by applying the one-term Galerkin's method to Equation (3) using $\vec{E}_t^{(n)}$ as the testing function. It is apparent that K = 1 when $\vec{E}_t^{(n)}$ is the exact solution. K, therefore, also provides an indication of the accuracy of the n^{th} iterated result in a weighted-average sense.

In the following we proceed to outline an iterative procedure for solving (6):

1. Begin with an initial estimate $\vec{E}_t^{(0)}$. The amplitude of $\vec{E}_t^{(0)}$ is to be properly adjusted using the scale factor K determined from Equation (7).
2. Compute $\vec{\tilde{E}}_t^{(0)}$, the discrete Fourier transform of $\vec{E}_t^{(0)}$. This step can be carried out efficiently using the FFT algorithm.
3. Compute $\tilde{G}\cdot\vec{\tilde{E}}_t^{(0)}$.

4. Obtain the DFT of $\bar{\bar{G}} \cdot \bar{\bar{E}}_t^{(0)}$ using FFT.

5. Subtract $-\bar{\bar{H}}_t^i$ from the result obtained from step 4. This gives the zeroth-order approximate solution $\bar{J}^{(0)}$. Generally, the approximate solution for $\bar{J}$ obtained in this step has non-zero values extending beyond the conducting surface. The satisfaction of the boundary condition for the induced current can thus be verified by checking how well the n^{th} approximation for the current $\bar{J}^{(n)}$ is confined to the conducting surface.

6. Add $-\bar{\bar{H}}_t^i$ to $\bar{J}^{(0)}$ obtained in the last step, and take the inverse DFT of the result using FFT.

7. Multiply $\bar{\bar{G}}^{-1}$ by the result obtained from step 6., obtaining $\bar{\bar{E}}_t^{(1)}$.

8. Take the inverse transform of $\bar{\bar{E}}_t^{(1)}$ to get $\bar{\bar{E}}_t^{(1)}$. The exact solution for $\bar{\bar{E}}_t$ should have zero value on the conducting surface. This criterion serves as a boundary condition check for the approximate solution $\bar{\bar{E}}_t^{(n)}$ obtained in this step.

9. Repeat the whole procedure, as necessary, using $\vartheta(\bar{\bar{E}}_t^{(1)})$ to generate the next higher-order solutions $\bar{J}^{(1)}$ and $\bar{\bar{E}}_t^{(2)}$ until convergence is achieved.

In the following two sections several examples are presented to illustrate the application of the technique described above.

IV. SCATTERING FROM GRATINGS AND GRIDS

Let us consider a free-standing, strip grating structure illuminated by a normally incident uniform plane wave as shown in Fig. 3. Let the incident E-field be polarized parallel to the edges of the strip (an H-wave).

The formulation for this problem is given by Equation (2). The iterative procedure discussed in Section III is applied to solve for the tangential aperture E-field, $\vec{E}_t$, and the induced current density, $\vec{J}$.

Figure 4a shows the incident E-field truncated in the aperture, which is used as the zeroth-order approximation for $\vec{E}_t$, i.e., $\vec{E}_t^{(0)} = \vartheta(\vec{E}_t^i)$. The $\vec{J}^{(0)}$ derived from $\vec{E}_t^{(0)}$ is shown in Fig. 5a. $\vec{J}^{(0)}$ has significant non-zero values extending into the aperture region. This could be expected because of the crude initial estimate made for $\vec{E}_t^{(0)}$. Figure 5b shows $\vec{J}^{(1)}$ obtained after one iteration. Observe the significant improvement achieved with just a single iteration even though the zeroth-order approximation for $\vec{E}_t^{(0)}$ was rather crude. Higher-order solutions for $\vec{E}_t^{(n)}$ and $\vec{J}^{(n)}$, obtained via further iterations, are shown, respectively, in Figures 4b to 4d and Figures 5b to 5d. The rapid convergence and the accuracy, which is verified by the boundary condition check of the solutions, are well-demonstrated in these figures. The induced current density $\vec{J}$ also shows the expected edge behavior, i.e., it becomes large at the edges as it should for the incident H-wave.

Figures 6 and 7 show the solutions for $\vec{E}_t$ and $\vec{J}$ obtained after four iterations when the gratings are illuminated by an obliquely incident plane wave with an incident angle $\vartheta = 30°$ and with the H-field polarized

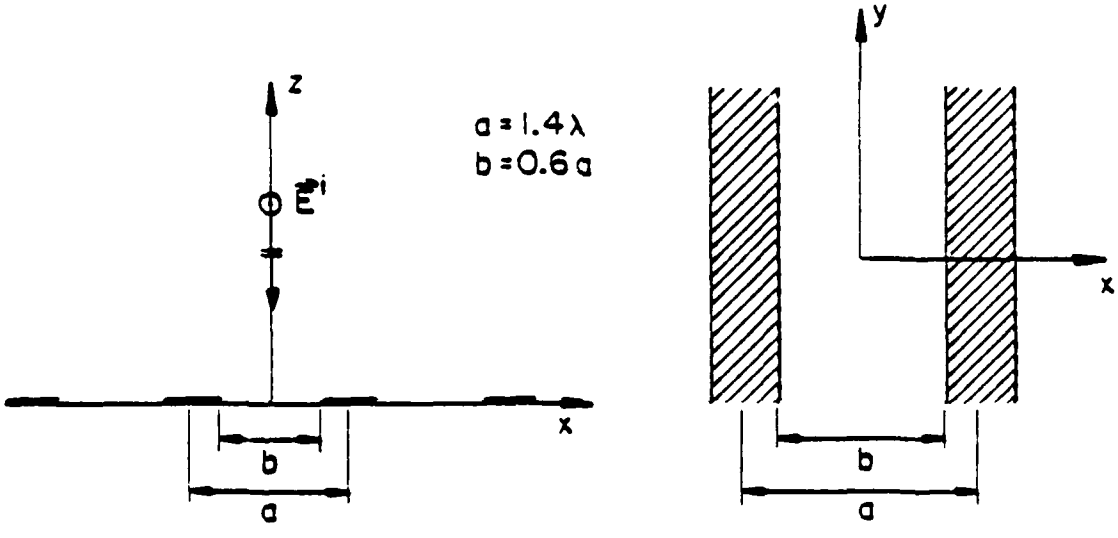

Figure 3. Free-standing grating illuminated by a normally incident H-wave.

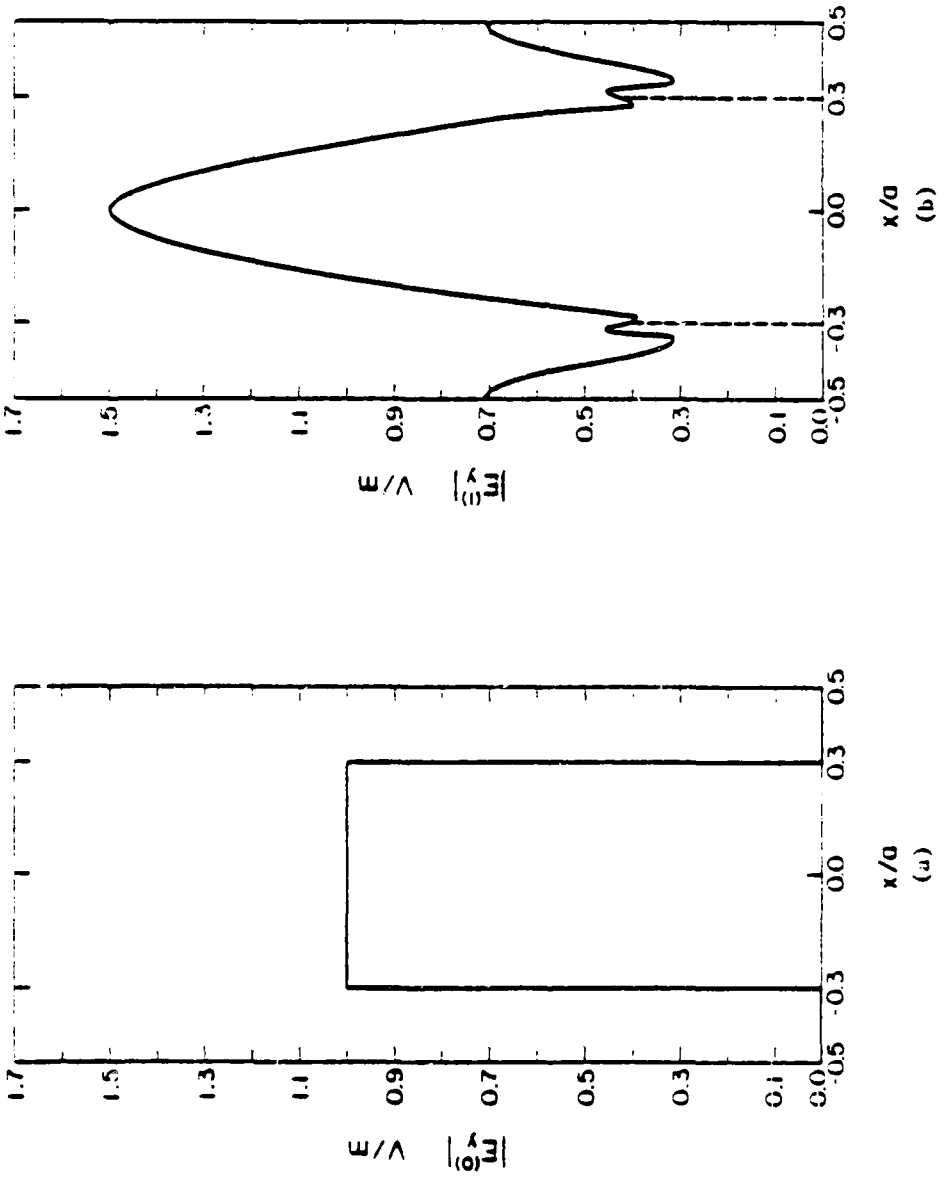

Figure 4. Magnitude of the aperture E-field distribution for the geometry shown in Figure 1, obtained via four consecutive iterations.

AD-A105 664 ILLINOIS UNIV AT URBANA ELECTROMAGNETICS LAB F/G 20/14
INVESTIGATION OF TRANSFORM TECHNIQUES FOR SOLVING ELECTROMAGNET--ETC(U)
APR 81 S W LEE, R MITTRA, W L KO N00014-75-C-0293
UNCLASSIFIED UIEM-81-3 NL

2 OF 2
AD A105664

END
DATE FILMED
11 81
DTIC

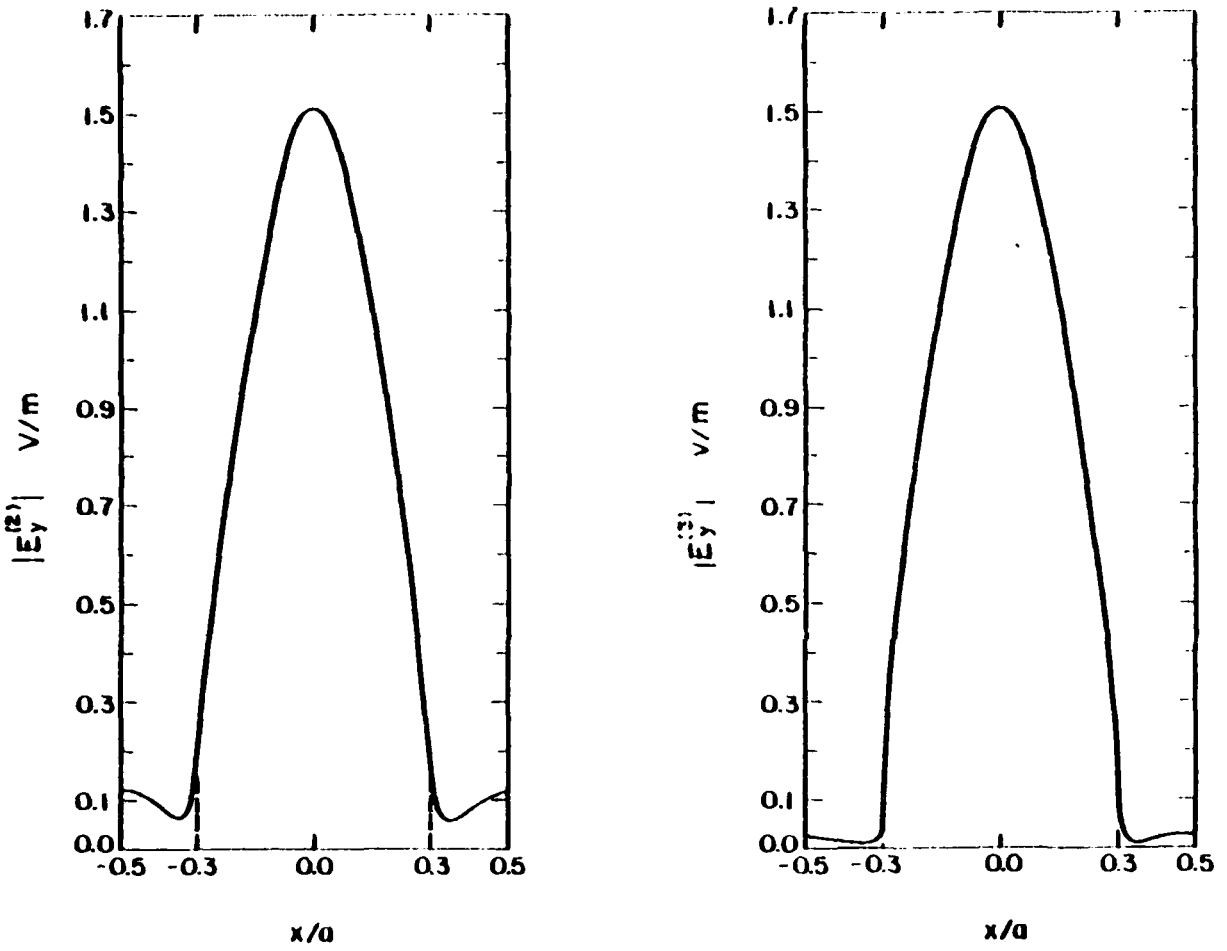

Figure 4. Magnitude of the aperture E-field distribution for the geometry shown in Figure 3, obtained via four consecutive iterations.

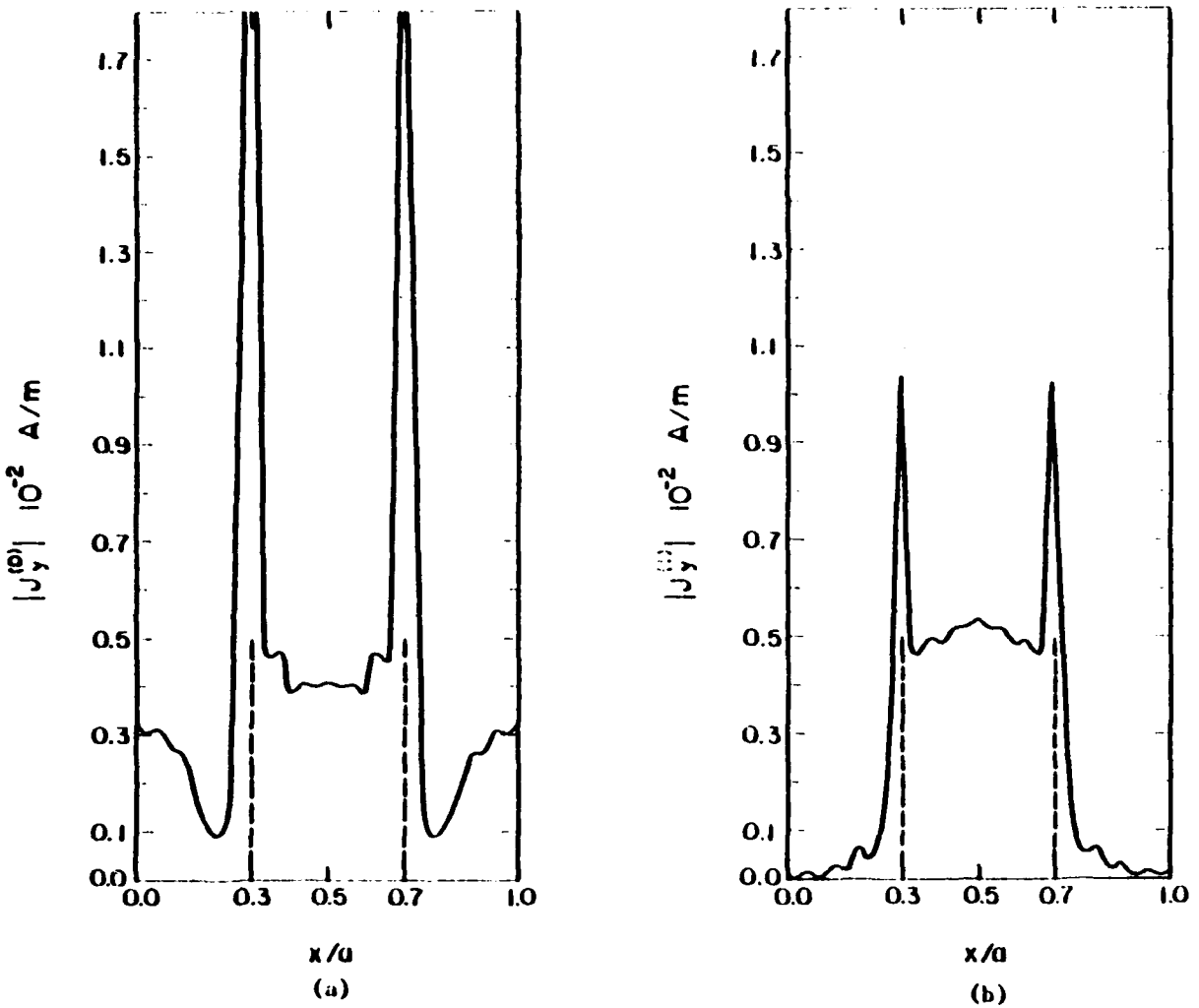

Figure 5. Magnitude of the induced current density distribution on the strip for the geometry in Figure 3, obtained via four consecutive iterations.

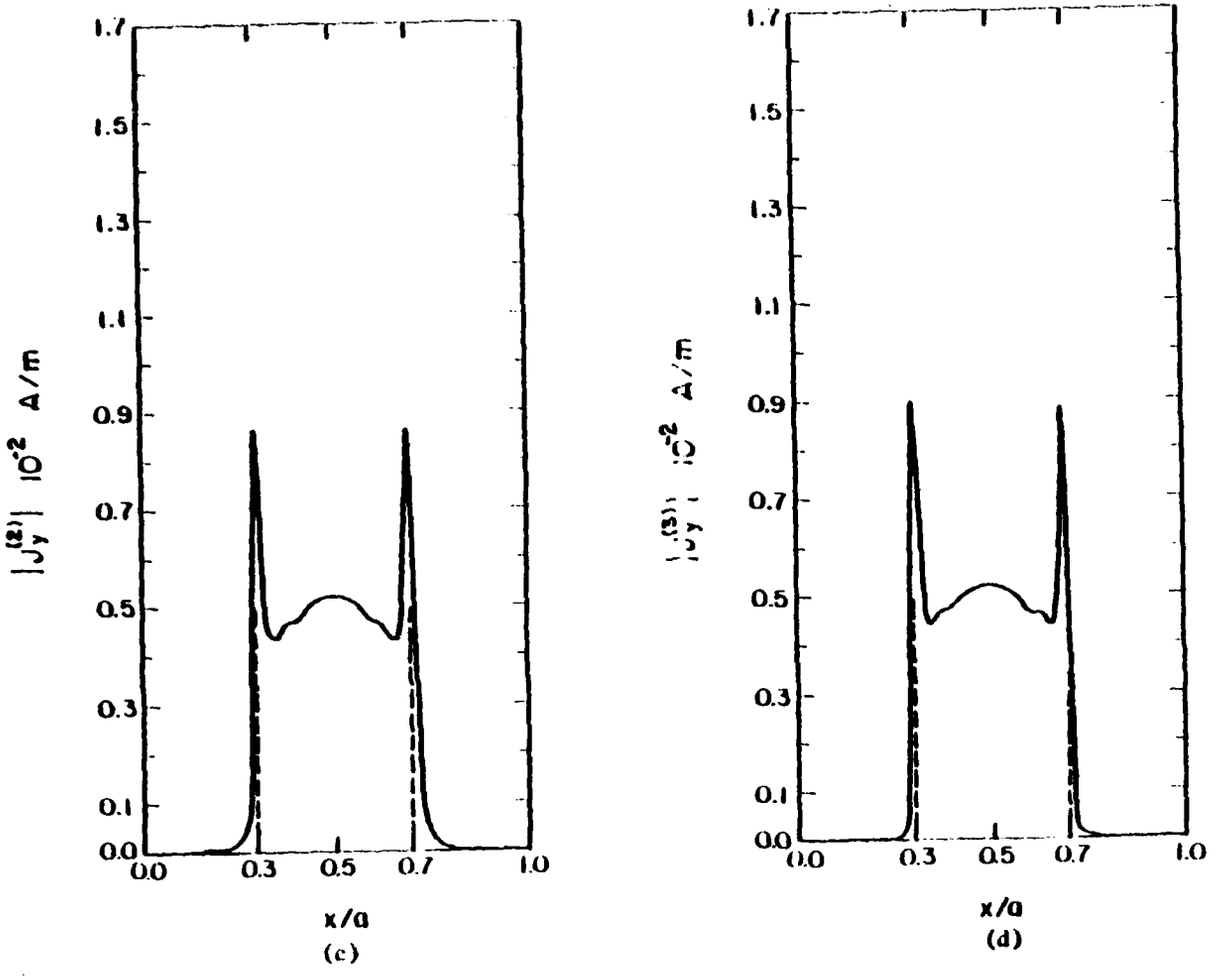

Figure 5. Magnitude of the induced current density distribution on the strip for the geometry in Figure 3, obtained via four consecutive iterations.

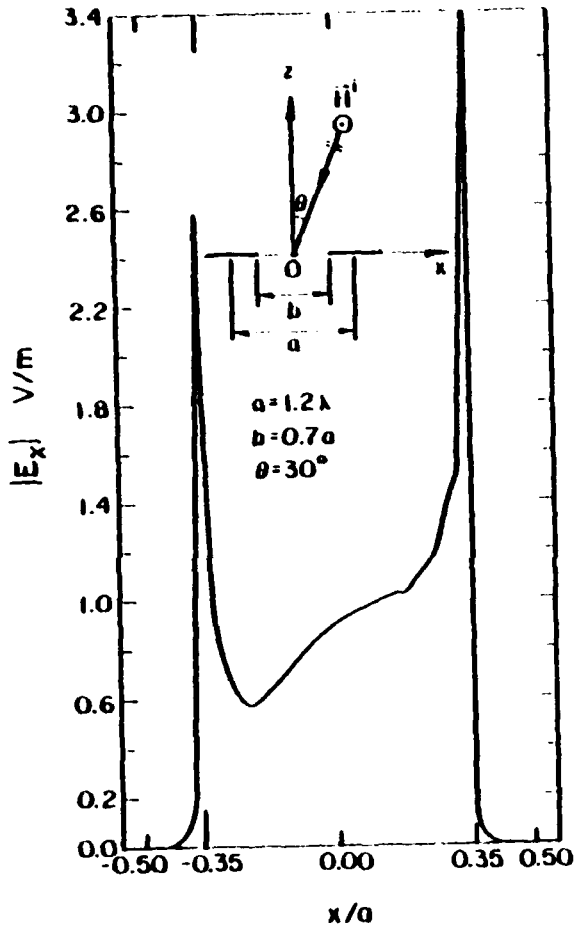

Figure 6. Magnitude of the aperture E-field distribution for a free-standing grating illuminated by an obliquely incident E-wave.

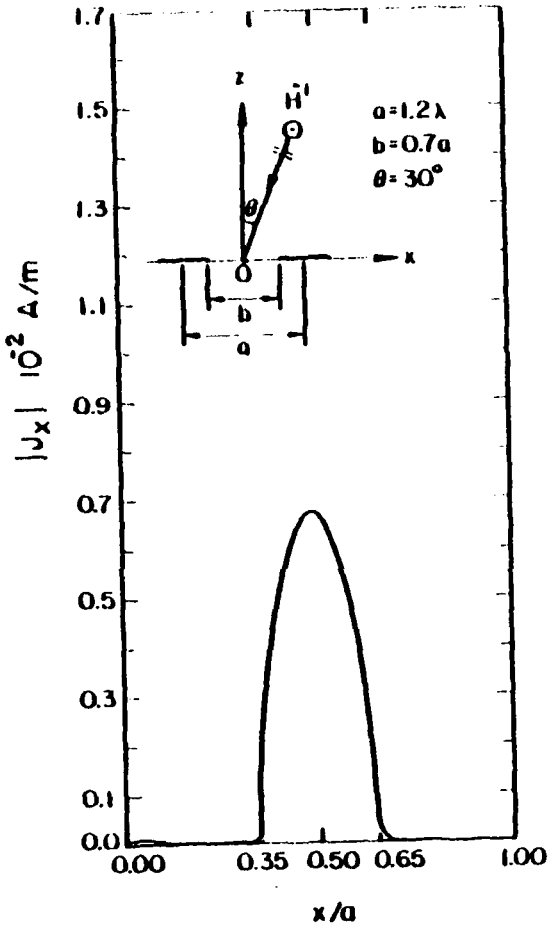

Figure 7. Magnitude of the induced current density distribution on the strips of a free-standing grating illuminated by an obliquely incident E-wave.

parallel to the edges of the strip (in the E-wave case). Again, the boundary conditions are satisfied extremely well by the results, and the aperture E-field also shows the expected edge behavior for the incident E-wave.

Next we consider the scattering from a free-standing conducting grid illuminated by a normally incident plane wave. The geometry of the problem is shown in Fig. 8. The aperture area is approximately $10\lambda^2$ whereas the cell area is about $44\lambda^2$. The initial approximation for $\vec{E}_a$ is still chosen to be the truncated incident field, and the dominant component of the tangential aperture E-field is shown when the incident E-field is polarized in the y-direction.

For all the computations in this section, 32 terms in the Floquet expansion functions are used in representing the unknown fields along each of the two dimensions. This leads to 2^{11} equivalent unknowns to be solved for. The computation time, however, required for deriving the solution is quite moderate (5 ~ 6 secs. of CPU time on the CDC Cyber 175 System). Clearly, any matrix method dealing with such a large number of unknowns will be totally impractical.

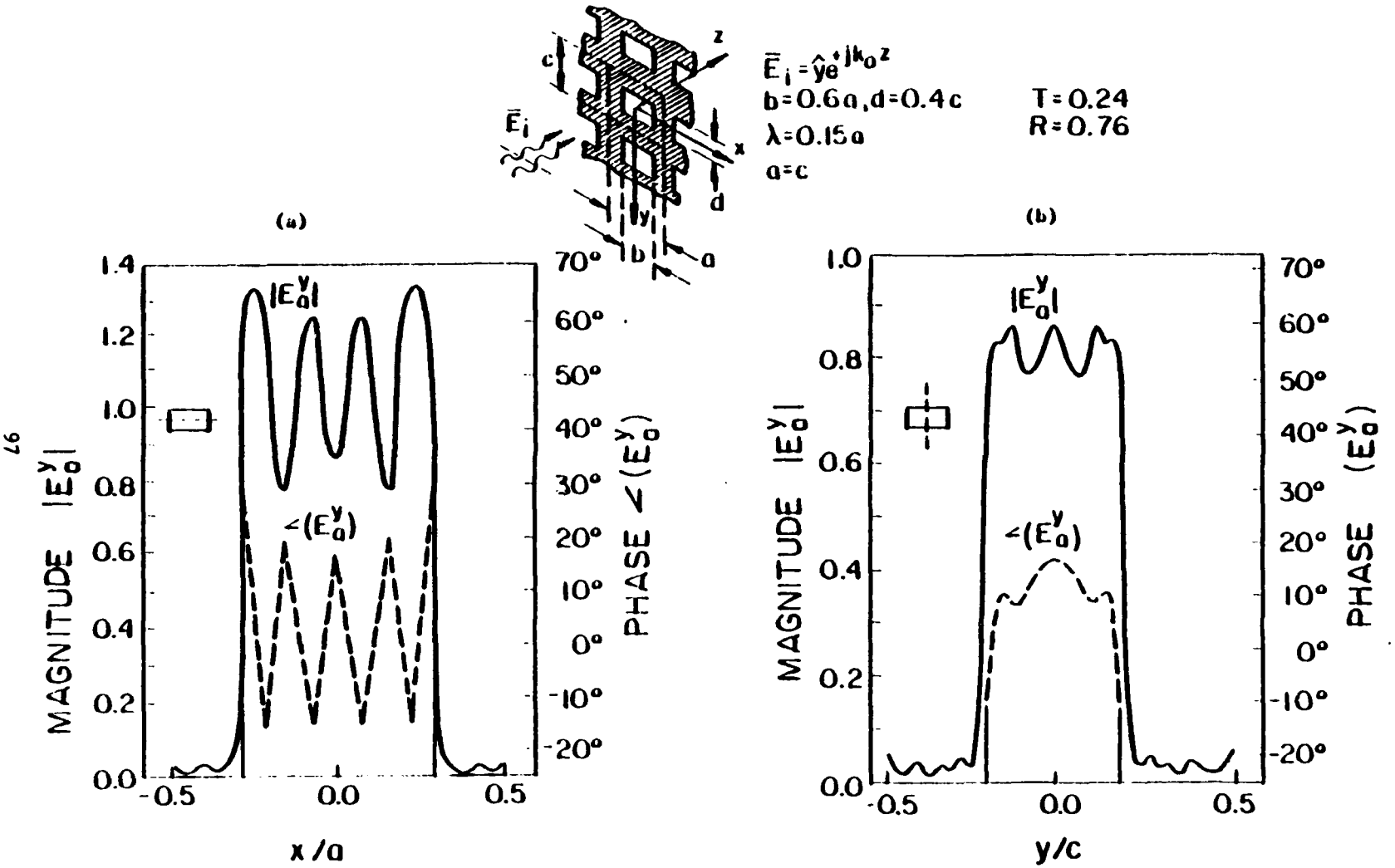

Figure 8. Distribution of the dominant component of E-field in the plane of a perforated screen with rectangular apertures. (a) E_y-field sampled along the x-axis; (b) E_y-field sampled along the y-axis.

V. GENERALIZATION TO TWO-REGION PROBLEMS

In this section, the iterative technique is further generalized to analyze a wider class of geometries. These geometries are characterized by the feature that they comprise a junction of two or more regions of dissimilar dimensions. An open-region type example is a corrugated surface which can be thought of as a junction of two regions, viz., the infinite half-space and a periodic array of short-circuited waveguides. For the sake of simplicity, a closed-region type problem - a step discontinuity in a parallel-plate waveguide - is considered in this section. The geometry is shown in Figure 9. The incident field is a TE mode wave. The formulation of this problem can be found in the literature. The integral equation is given by

$$\int_0^b E_y(x')K^-(x,x')dx' = \int_0^b E_y(x')K^+(x,x')dx' - 2H_x^i \qquad (8)$$

$$\text{for } 0 < x < b, \quad z = 0$$

where E_y is the unknown aperture E-field,

H_x^i is the incident H-field,

$$K^-(x,x') = \frac{1}{j\omega\mu} \sum_{m=-\infty}^{\infty} \gamma_m^- \sin\frac{m\pi}{a}x \sin\frac{m\pi}{a}x' ,$$

$$K^+(x,x') = \frac{1}{j\omega\mu} \sum_{m=-\infty}^{\infty} \gamma_m^+ \sin\frac{m\pi}{b}x \sin\frac{m\pi}{b}x' ,$$

$$\gamma_m^- = \begin{cases} j(k^2 - (\frac{m\pi}{a})^2)^{1/2} & \text{if } k^2 > (\frac{m\pi}{a})^2 , \\ ((\frac{m\pi}{a})^2 - k^2)^{1/2} & \text{if } k^2 < (\frac{m\pi}{a})^2 , \end{cases}$$

and

$$\gamma_m^+ = \begin{cases} -j(k^2 - (\frac{m\pi}{b})^2)^{1/2} & \text{if } k^2 > (\frac{m\pi}{b})^2 , \\ ((\frac{m\pi}{b})^2 - k^2)^{1/2} & \text{if } k^2 < (\frac{m\pi}{b})^2 . \end{cases}$$

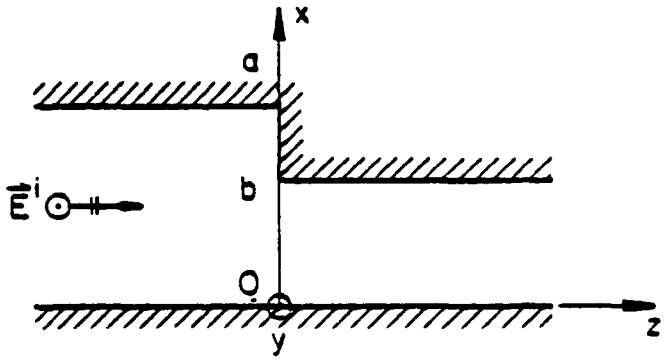

Figure 9. Step discontinuity in a parallel-plate waveguide with a TE incident wave.

Note that Equation (8) is defined in the region $0 < x < b$. To apply the iterative technique, it has to be extended to the full range $0 < x < a$. This is achieved by introducing an extra unknown function $J(x)$, and the extended equation takes the form

$$\int_0^a E_y(x')K^-(x,x)dx' = \int_0^a E_y(x')K^+(x,x')dx' + \theta(-2H_x^i) + \hat{\theta}(J(x)) \quad (9)$$

for $0 < x < a$

where for any function $f(x)$

$$\theta(f(x)) = f(x) \quad \text{if } 0 < x < b \ ,$$
$$= 0 \quad \text{if } b < x < a \ ,$$

and

$$\hat{\theta}(f(x)) = f(x) - \theta(f(x)) \ .$$

A recursion formula relating the $(n+1)^{th}$ order solution $E_y^{(n+1)}$ to the n^{th} solution $E_y^{(n)}$ can be derived via a procedure similar to that developed in Section III. The formula is

$$\int_0^a E_y^{(n+1)} \cdot K^- = \int_0^a E_y^{(n)}K^+ + \theta(-2H_x^i) + \hat{\theta}\left(\int_0^a E_y^{(n)}K^- - \int_0^a E_y^{(n)}K^+ - \theta(-2H_x^i)\right). \quad (10)$$

Equation (10) is now solved using an iterative procedure similar to that developed in Section III. The integrations in (10) can again be carried out using the FFT because of the characteristic nature of the kernels. Figure 10 shows the aperture E-field distribution at the discontinuity. The initial approximation for E_y is taken to be the incident field truncated in the aperture.

The result is obtained in three iterations with 32 expansion functions used in representing the unknown field. We note that the boundary condition on E_y, viz., that it vanishes at the edges, is satisfied by the iterated solution.

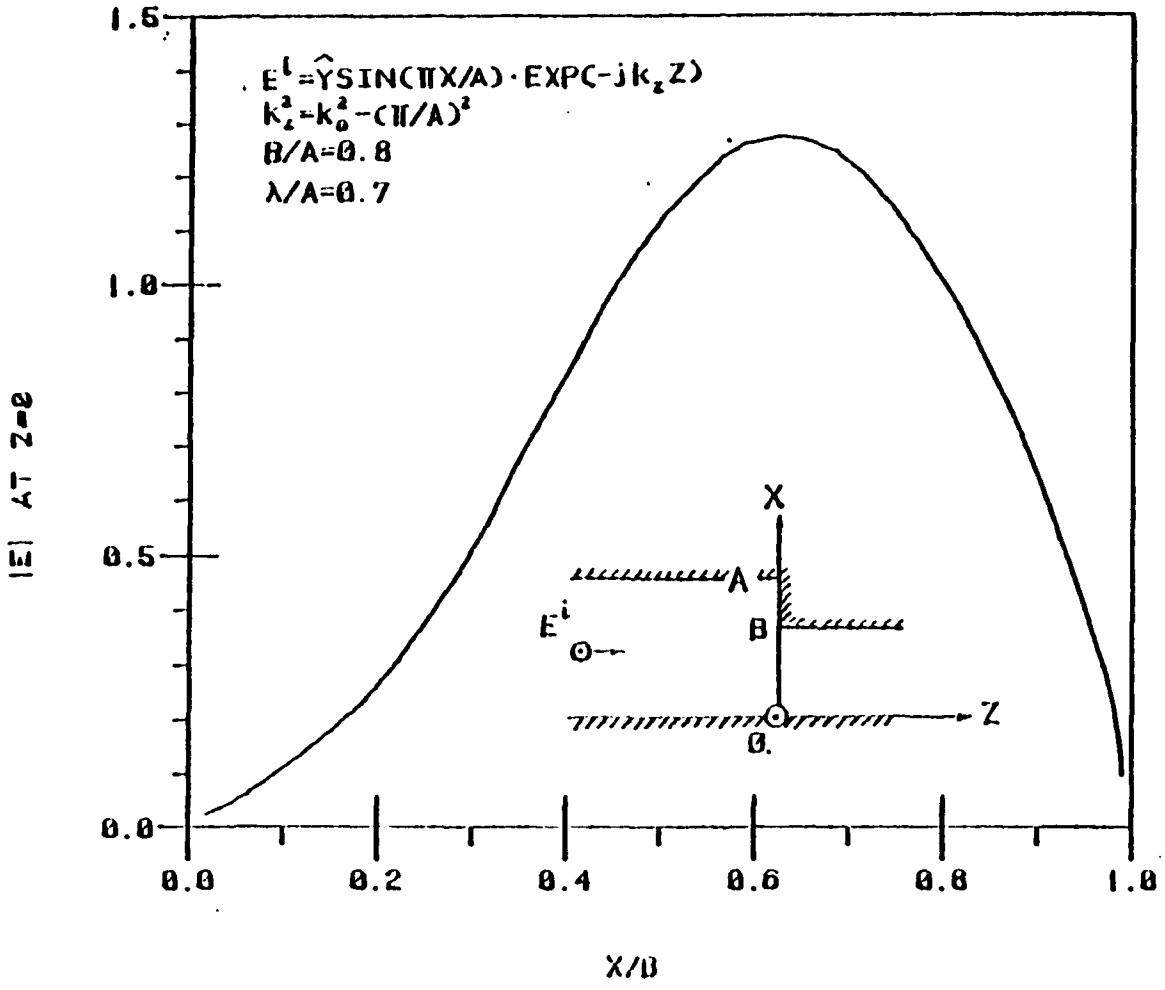

Figure 10. Magnitude of the E-field distribution at the step-discontinuity in a parallel-plate waveguide.

VI. CONCLUSION

In this paper, an iterative technique applied in the spectral domain has been employed to solve the problem of scattering from two-dimensional periodic structures. Applications of the technique have been illustrated using a number of examples. This spectral-iteration technique has been found to be very efficient for two reasons: (i) it is applied in the transform domain, where only algebraic operations instead of convolution integrations are involved, (ii) the use of the efficient FFT algorithm, which is employed to carry out the algebraic DFT, is natural to the procedure. The technique also has a built-in boundary condition check which verifies the accuracy of the iterated solution - an important feature not available in conventional methods. Furthermore, the induced current and the aperture field are solved for simultaneously which is another unique advantage not available in other methods. Finally, as mentioned earlier, this technique is particularly appealing in the high frequency analysis where the moment method has unsurmountable difficulties and other asymptotic techniques fail. Before closing, we would like to point out that at the lower end of the frequency scale the effect of mutual coupling among adjacent apertures (or conducting strips) becomes significant and the field distribution in the aperture begins to deviate substantially from the incident field. Consequently, it becomes difficult to choose a good initial approximation for the aperture field, particularly the cross-polarized component, such that a rapid convergence of the iteration process is ensured. Fortunately, however, an alternative method also developed by the authors [5] and called the Spectral-

Galerkin approach, has been found to be well-suited in the low frequency region. This approach is based on an application of the Galerkin's method in the spectral domain. It selects the proper expansion functions which are analytically Fourier transformable and which satisfy both the boundary and edge conditions for the unknown fields. It has been shown that the required matrix size is much smaller than in the conventional schemes and the numerical computation is very efficient.

REFERENCES

[1] C. C. Chen, "Transmission through a conducting screen perforated periodically with apertures," Microwave Theory and Techniques, vol. 18, no. 9, pp. 627-632, 1970.

[2] S. W. Lee, "Scattering by dielectric-loaded screen," IEEE Trans. Antennas Propagat., vol. 19, no. 5, pp. 656-665, 1971.

[3] R. C. McPhedran and D. Maystre, "On the theory and solar applications of inductive guides," Appl. Phys., vol. 14, pp. 1-20, 1977.

[4] W. L. Ko and R. Mittra, "A new approach based on a combination of integral equation and asymptotic techniques for solving electromagnetic scattering problems," IEEE Trans. Antennas Propagat., vol. 25, no. 2, 1977.

[5] C. H. Tsao and R. Mittra, "A Spectral-Galerkin analysis of the scattering from frequency selective surfaces," to be published.

APPENDIX E

A SPECTRAL-ITERATION TECHNIQUE FOR ANALYZING A CORRUGATED-SURFACE TWIST POLARIZER FOR SCANNING REFLECTOR ANTENNAS

R. Kastner and R. Mittra

ABSTRACT

In this paper we present an analysis of the corrugated-surface twist polarizer which finds application in the design of scanning reflector antennas. We employ the spectral-iteration technique, a novel procedure which combines the use of the Fourier transform method with an iterative procedure. The first step in the spectral-iteration method is the conversion of the original integral equation for the interface field into a form which is suitable for iteration using a method developed previously [5]-[7]. An important feature of the technique is that it takes advantage of the DFT type of kernel of the integral equation and evaluates the integral operators efficiently using the FFT algorithm. Thus, in contrast to the conventional techniques, e.g., the moment method, the spectral-iteration approach requires no matrix inversion and is capable of handling a large number of unknowns. Furthermore, the method has a built-in check on the satisfaction of the boundary conditions at each iteration.

The work was supported by the Office of Naval Research, Contract N00014-75-C-0293.

A SPECTRAL-ITERATION TECHNIQUE FOR ANALYZING A CORRUGATED-SURFACE TWIST POLARIZER FOR SCANNING REFLECTOR ANTENNAS

I. INTRODUCTION

This paper presents an analysis of the corrugated-surface twist polarizer, a device which is used to rotate the polarization plane of an incident wave by 90°. Such a polarizer finds applications in scanned reflector antenna systems (Fig. 1) where a rapid mechanical scanning is achieved by the movement of the passive, light-weight polarizer [1]. The feed horn radiates a horizontally polarized field, which is reflected from the "transflector" radome, comprising horizontal strips, onto the twist polarizer. The twist polarizer is so designed that upon reflection from the polarizer the horizontally polarized incident wave is changed into a vertically polarized reflected wave to which the radome is virtually transparent. Thus, the radome also serves as a collimating device and the antenna is compact and light weight.

A common type of twist polarizer comprises a set of thin metallic strips or wires placed on top of a dielectric substrate, which is approximately $\lambda/4$ thick and is backed by a ground plane [1], [2], [3], [8]. In this paper, we investigate the design of an alternative configuration which also can be used for rotating the plane of polarization of an incident wave, viz., the corrugated-surface polarizer. Its basic mechanism can be explained very simply [4] by noting that if the period of the grooves is sufficiently small compared to the wavelength, a plane wave polarized parallel to the grooves will be reflected essentially from the outer surface of the polarizer, while a vertically polarized wave will be reflected from the bottom of the grooves, which results in a differential phase delay corresponding to twice the groove depth.

Thus, if the incident field were polarized at 45° to the direction of the grooves, the horizontal and vertical components would have equal amplitudes and phases, and a phase difference of 180° will be produced by a groove depth of $\lambda/4$. Unfortunately, the cell size is typically not small at millimeter waves and the above result is not sufficiently accurate for designing the polarizer.

The spectral-iteration approach [5], [6], [7], presented herein, provides a method for efficient and accurate analysis of the corrugated twist polarizer. Unlike conventional moment-method and mode-matching techniques, the spectral iteration technique requires no matrix inversion and, consequently, large cells can be analyzed without any difficulty. Furthermore, the accuracy of the solution can be conveniently checked at each stage of the iteration. This is done by determining how well the solution satisfies the boundary conditions and by verifying the conservation of energy.

II. GENERAL FORMULATION

Let the corrugated-surface twist polarizer, shown in Figure 2, be illuminated by a plane wave with a wave-number β in the x-direction. Because of the periodic nature of the geometries, phase-shift walls with period a can be placed in the external region ($z > 0$) of the structure and the problem can be reduced to that of solving for the discontinuity between a waveguide with these phase-shift walls and the short-circuited, parallel-plate waveguide of width b in the interior region (see Fig. 3). In two cases, viz., the TE polarization (parallel to grooves) and the TM polarization (perpendicular to grooves) need to be solved for individually to obtain the differential phase shift between the two reflection coefficients. For an incident wave polarized at 45° to the direction of the grooves, the plane of polarization will be rotated by 90° if the differential phase shift between the two reflection coefficients is 180°.

The spectral-iteration approach for this problem is based on the fact that the Green's functions for both the external and internal regions are expressible in terms of Fourier-type series. Thus, in each of these two individual regions the integral operator that relates E- and H-fields is exactly invertible. Denoting the operator for the external region, which is a cell bounded by the phase-shift walls, by L_-, and the operator for the inner region by L_+, we have the general form

$$L_-\psi + L_+\psi = 2F^{inc} \tag{1}$$

in which F^{inc} corresponds to the electric field incident from the outer region and ψ is the unknown magnetic field in the aperture. (If, instead, the unknown is the electric field in the aperture, then F is replaced by the incident magnetic field.)

III. TM POLARIZATION

In order to illustrate the application of the spectral-iteration technique, we consider the case of the twist polarizer illuminated by a TM polarized wave. (The TE case is discussed later.) We choose ψ to be the unknown electric field in the aperture and derive the following integral equation via the usual formulating procedure of matching the interface fields.

$$\frac{1}{a}\sum_{n=-\infty}^{\infty}\int_0^a \frac{1}{\sqrt{k_o^2-(\beta+n\frac{2\pi}{a})^2}}\psi(x')e^{j(\beta+n\frac{2\pi}{a})x'}e^{-j(\beta+n\frac{2\pi}{a})x}dx' + H(x) = 2H^{inc}(x) \tag{2}$$

where

$$H(x) = \begin{cases} \frac{2}{b}\sum_{m=0}^{\infty}\int_0^b \frac{j}{\cot(\sqrt{k_o^2-(\frac{m\pi}{b})^2}\,d)}\frac{1}{\sqrt{k_o^2-(\frac{m\pi}{b})^2}}\psi(x')\cos\frac{m\pi}{b}x'\cos\frac{m\pi}{b}x dx', & 0\le x\le b \\ h(x) & b\le x\le a \end{cases} \tag{3}$$

and

$$H^{inc}(x) = \frac{e^{-j\beta x}}{\sqrt{k_o^2-\beta^2}} \tag{4}$$

$h(x)$ is the unknown magnetic field outside the aperture where the boundary condition on the conducting wall requires ψ to be identically zero. For the sake of convenience, we have suppressed the factor $-j\omega\mu$ in H and H^{inc}. Equation (2) is of the form of (1).

The operator corresponding to the external region

$$L_-(\cdot) = \frac{1}{a} \sum_{n=-\infty}^{\infty} \int_0^a \frac{1}{\sqrt{k_o^2 - (\beta + n\frac{2\pi}{a})^2}} e^{j(\beta+n\frac{2\pi}{a})(x'-x)} dx'(\cdot) \qquad (5)$$

is invertible in the range $0 \leq x \leq a$, whereas the inner operator

$$L_+(\cdot) = \frac{2}{b} \sum_{n=0}^{\infty} \frac{j}{\cot(\sqrt{k_o^2 - (\frac{m\pi}{b})^2}\, d)} \frac{1}{\sqrt{k_o^2 - (\frac{m\pi}{b})^2}} \cos\frac{m\pi}{b} x' \cos\frac{m\pi}{b} x\, dx'(\cdot) \qquad (6)$$

has the same property in the range $0 \leq x \leq b$.

The iterative procedure for solving (2) will now be given:

1. Assume an initial $\psi(x)$, such that $\psi(x) = 0$ in the range $b \leq x \leq a$.
2. Evaluate $L_-(\psi)$ in the range $0 \leq x \leq a$ via a two-step FFT.
3. Compute $2H^{inc} - L_-\psi$ to obtain H.
4. Evaluate $L_+^{-1}(H)$ using a two-step cosine FFT transform over the portion $0 \leq x \leq b$ to obtain the next estimate for ψ in the aperture.
5. Add zeros over $b < x < a$ and return to step 2.

It is evident that the procedure requires the evaluation of L_-^{-1}, which in turn requires multiplication by the factor $\cot(\sqrt{k_o^2 - (\frac{m\pi}{b})^2}\, d)$. This factor becomes small in the neighborhood of $d = \lambda/4$ and for $m = 0$ and, hence, presents no difficulties in implementing the iteration procedure. Had we chosen ψ to be the electric field, a similar iteration procedure would have required the multiplication by the factor

$\tan(\sqrt{k_o^2 - (\frac{m\pi}{b})^2}\, d)$ and the process would have diverged. Thus, it is important to choose the proper unknown for ψ when using the iteration procedure.

The reflection coefficient is computed at each step of the iteration, and convergence is achieved when its absolute value tends to 1. Since a reflection coefficient close to +1 is expected, a uniform distribution may be chosen as an initial guess. It is found that, even with this initial choice, convergence is attained within three or four iterations.

IV. TE POLARIZATION

In this case, the magnetic field distribution is chosen as the unknown $\psi(x)$. We have the following integral equation:

$$\frac{1}{a}\sum_{n=-\infty}^{\infty}\int_0^b \frac{1}{\sqrt{k_o^2-(\beta+n\frac{2\pi}{a})^2}}\,\psi(x')\,e^{j(\beta+n\frac{2\pi}{a})x'}\,e^{-j(\beta+n\frac{2\pi}{a})x}\,dx' + E(x) = 2E^{inc}(x) \tag{7}$$

with

$$E(x) = \begin{cases} \dfrac{2}{b}\displaystyle\sum_{m=1}^{\infty}\int_0^b \frac{j\,\tan\left(\sqrt{k_o^2-(\frac{m\pi}{b})^2}\,d\right)}{\sqrt{k_o^2-(\frac{m\pi}{b})^2}}\,\psi(x')\,\sin\frac{m\pi}{b}x'\,\sin\frac{m\pi}{b}x & 0 \le x \le b \\ 0 & b < x < a \end{cases} \tag{8}$$

and

$$E^{inc}(x) = \frac{e^{-j\beta x}}{\sqrt{k_o^2-\beta^2}} \tag{9}$$

where a factor $j\omega\epsilon$ has been suppressed from E and E^{inc}. Next we redefine L_- and L_+ in a manner analogous to Equations (5) and (6), and outline the iterative procedure for solving (7) in the following:

1. Start with an initial guess for ψ (e.g., a uniform distribution with a corresponding reflection coefficient of -1).
2. Compute $L_+(\psi)$ over $0 \le x \le b$ by a two-step FFT sine transform.
3. Add zeros over $b < x < a$ to obtain E over the entire range $0 \le x \le a$ and evaluate $2E^{inc} - E$.
4. Compute L_-^{-1} of the last result over $0 \le x \le a$ and obtain the next estimate for $\psi(x)$.
5. Go to step 2.

For the TE case being considered here, step 2 requires the evaluation of $L_+(\psi)$, as opposed to the computation of $L_+^-(\psi)$ in the TM case. The evaluation of L_-, in turn, requires a multiplication by $\tan \sqrt{k_o^2 - (\frac{m\pi}{b})^2}\, d$. However, this does not pose a problem since the term $m = 0$, which diverges in the neighborhood of $d = \lambda/4$, is excluded in the sine transform. The convergence in the TE case is also attained with a very few iterations.

The use of the FFT procedure, combined with the small number of iterations needed to attain convergence, result in a considerable saving of computation time as compared to the conventional mode-matching and moment-method techniques which require a matrix inversion. Furthermore, the method can handle unit cells which are either large or small. Naturally, a larger cell size necessitates the use of an increased number of samples so that a typical sampling interval of about $\lambda/25$ is maintained, and the selection of a wider interval may slow down the convergence. Thus, for a given program that has fixed dimensions of FFT vectors, i.e., a fixed number of samples, there is an effective limit to which the frequency can be increased. However, if the primary quantity of interest is the reflection coefficient, the detailed information derived from a fine sampling of the aperture is not needed and a smaller number of samples is sufficient. A technique for improving the convergence for such a case is described in the next section.

V. SPEEDING UP THE CONVERGENCE

It should be noted that often the main difference between the approximate ψ derived after a few iterations and the exact solution is a complex factor. One can partly compensate for this difference by multiplying ψ at every iteration with the variational factor x, where

$$X = \frac{\langle \psi, 2F^{inc} \rangle}{\langle \psi, L\Psi \rangle} \tag{10}$$

F is defined in Equation (1) and $L = L_- + L_+$. The factor X, which tends to unity as ψ approaches the correct value, can be regarded as another measure of convergence. Although the use of X is of little help when the convergence is good, the incorporation of this variational factor does improve the convergence quite significantly for an undersampled ψ. More importantly, it also helps to achieve convergence for an otherwise divergent case when the variational factor is not used. This is demonstrated in Table 1.

TABLE 1. CONVERGENCE RATES, TE INCIDENCE, 25 SAMPLES

Cell size (wavelengths)	No. of iterations without variational factor	No. of iterations with variational factor
.9 and below	4	3
1.1	19	7
1.3	Divergent	13

VI. RESULTS

A corrugated-surface twist polarizer was constructed and experimentally tested. Its duty ratio b/a was 0.5, with a = 21 mm, or 0.6λ at the center frequency of 8.5 GHz, and d = 7.62 mm or 0.216λ. A comparison between the computed and measured axial ratios at various frequencies is presented in Fig. 4 for an incidence angle of 5°. Agreement between computations and measurements appears to be very good, despite an uncertainty of about ±1° in the measurement setup and a slight inclination of the plane of incidence relative to the direction of periodicity. Interestingly, when the frequency is increased beyond the grating-lobe bound of about $d/\lambda \simeq 1$ (not shown in Fig. 4), the computation predicts a sudden change in the axial ratio and the reflection coefficient, whose magnitude is no longer equal to one. The loss of reflected energy in the fundamental space harmonic is obviously accounted for by a second space harmonic, or a grating lobe.

ACKNOWLEDGEMENT

The authors are thankful to their colleague Ross Lampe for providing the experimental data for the twist reflector that were used to compare to the theoretical results derived in this paper.

REFERENCES

1. O. B. Kesler, W. F. Montgomery and C. C. Liu, "A millimeter-wave scanning antenna for radar application," Proc. 1979 Antenna Applications Symposium, Robert Allerton Park, Monticello, IL.
2. E. O. Houseman, Jr., "A millimeter wave polarization twist antenna," Proc. IEEE 1978 AP-S Int'l. Symposium, Washington, D.C., pp. 51-53.
3. D. K. Waineo and J. F. Konieczny, "Millimeter wave monopulse antenna with rapid scan capability," Proc. IEEE 1979 AP-S Int'l. Symposium, Seattle, WA, pp. 477-480.
4. W. B. Offutt, L. K. DeSize and W. H. Yale, "Methods of Obtaining Circular Polarization," Sec. 17.7, Antenna Engineering Handbook, (J. Jasik, (Ed.)). New York: McGraw-Hill, 1961.
5. W. L. Ko and R. Mittra, "A new approach based on a combination of integral equation and asymptotic techniques for solving electromagnetic scattering problems," IEEE Trans. Antennas Propagat., Vol. AP-25, No. 2, pp. 187-197, March 1977.
6. R. Mittra and A. Tsao, "Solving a class of open and closed discontinuity problems without matrix inversion," Proc. 1980 URSI Symposium, Quebec, Canada, p. 89.
7. R. Mittra and A. Tsao, "A spectral-iteration approach for analyzing scattering from frequency selective surfaces," to be published.
8. J. D. Hanfling, G. Jerinic and L. R. Lewis, "Twisterflector design using E-type and H-type modes," to be published in AP-S Transactions.

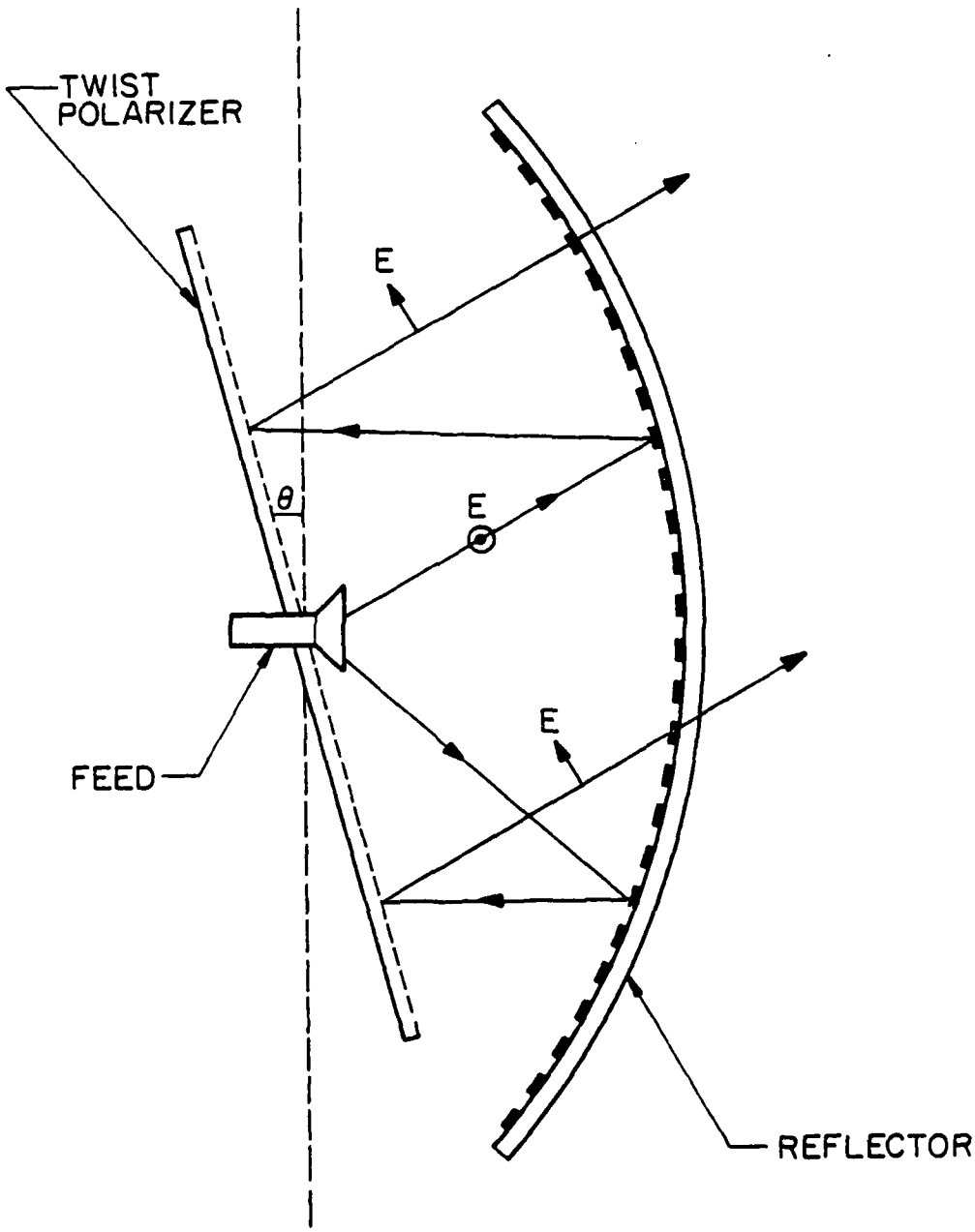

Figure 1. Twist Reflector Antenna System

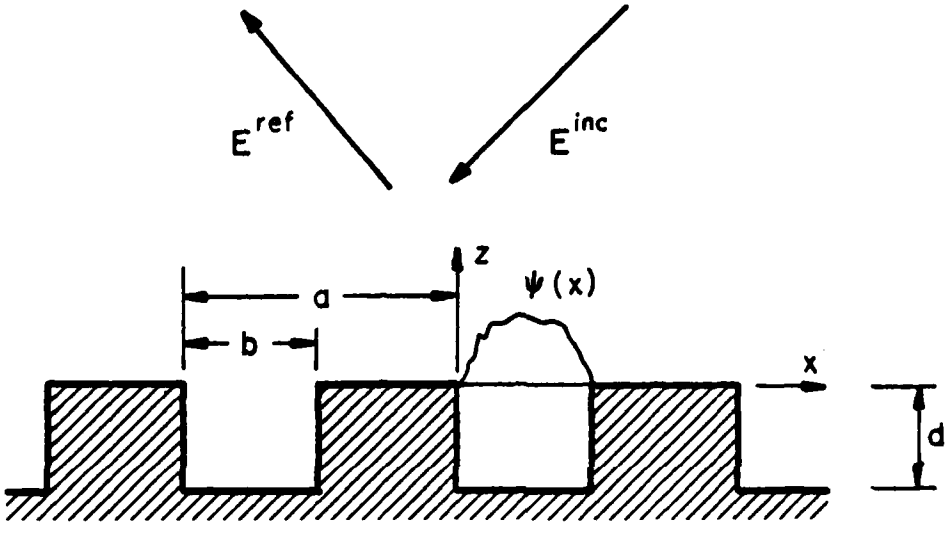

Figure 2. Corrugated Surface Configuration

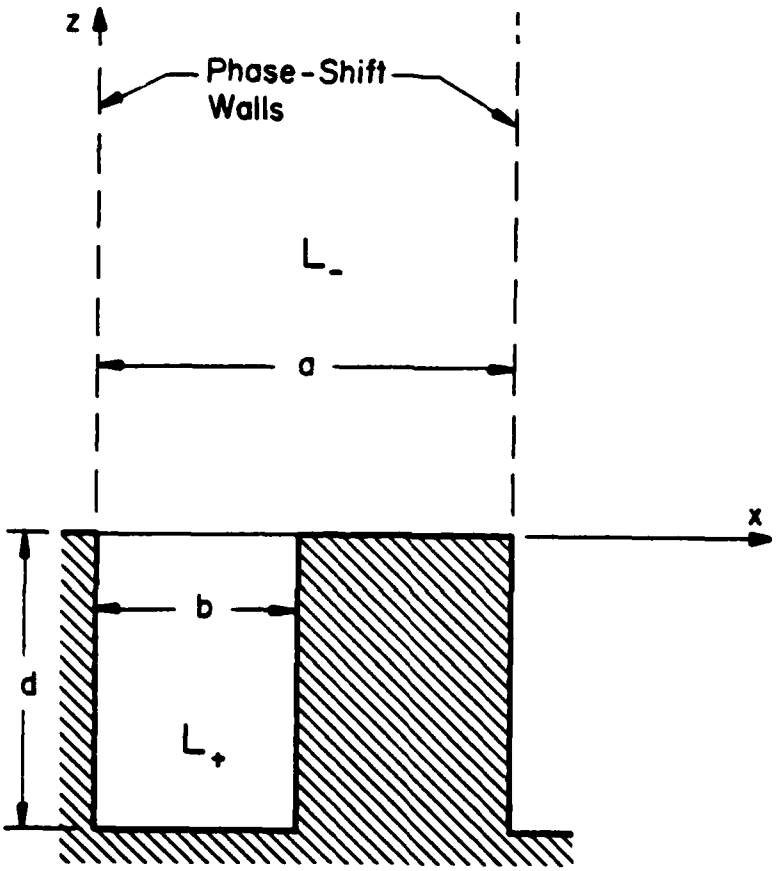

Figure 3. A Unit Cell of Corrugated Surface

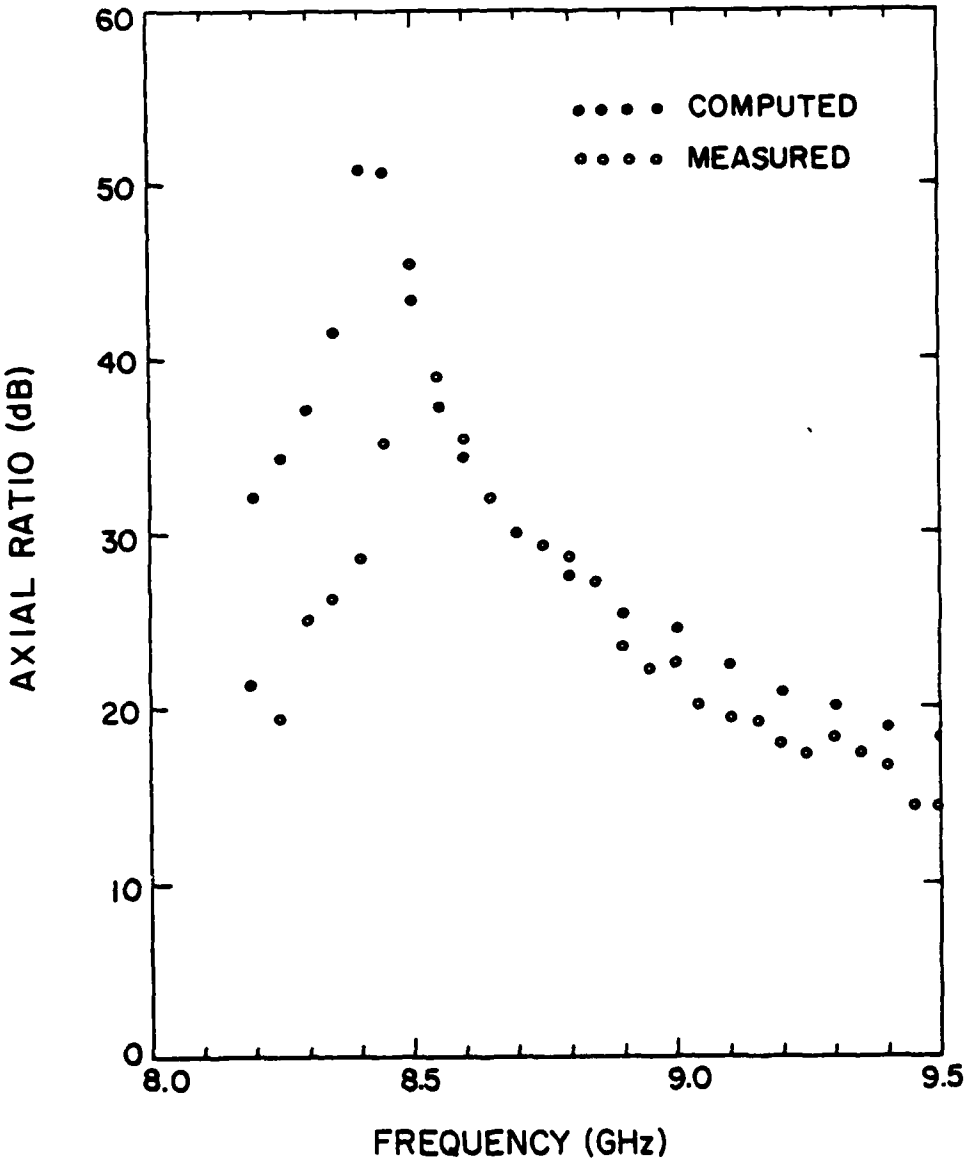

Figure 4. Twist Polarizer Performance


DATE
ILME